Effervescent Atomization of Suspensions in a Gaseous Cross Flow

Amr Abdelaziz Mostafa Saleh

A thesis

in

the Department

of

Mechanical and Industrial Engineering

Presented in Partial Fulfillment of the Requirements
for the Degree of Doctor of Philosophy (Mechanical Engineering)
Concordia University
Montreal, Quebec, Canada

December 2016

Concordia University
School of Graduate Studies

This is to certify that the thesis prepared

By: AMR ABDELAZIZ MOSTAFA SALEH

Entitled: Effervescent Atomization of Suspensions in a Gaseous Cross Flow

and submitted in partial fulfillment of the requirements for the degree of

Doctor of Philosophy (Mechanical Engineering)

Complies with the regulations of the University and meets the accepted standards with respect to originality and quality.

Signed by the final examining committee:

Dr. _____ Chair

Dr. Nasser Ashgriz _____ External Examiner

Dr. M. Reza Soleymani _____ External to Program

Dr. Christian Moreau _____ Examiner

Dr. Lyes Kadem _____ Examiner

Dr. Ali Dolatabadi _____ Thesis Supervisor

Approved by _____

Dr. Ali. Dolatabadi, Ph.D. Program Director
PhD. Program Director,
Department of Mechanical and Industrial Engineering

_____ _____

Dean of Faculty

Abstract

Effervescent Atomization of Suspensions in a Gaseous Cross Flow

Amr Abdelaziz Mostafa Saleh, Ph.D.

Concordia University, 2016

Atomization of liquids (pure liquids and suspensions) plays an important role in numerous industrial fields and applications. One of the main important applications is in thermal spraying processes which is the primary motivation for this study. The main trend in thermal spray processes is to coat with sub-micron and nano sized particles due to the superior performance of fine microstructured coatings. Recently, thermal spraying processes are using the suspension spraying technique. The breakup of a suspension in the atomization process differs from that of a pure liquid by the influence of the suspended particles on the fragmentation kinetics. In suspension spraying process, different types of atomizers are used but clogging problems can occur due to the suspension properties. Effervescent atomizers have shown to be a good alternative to the conventional atomizers to solve clogging issue when liquids with large variety of viscosity and density such as suspensions are atomized.

In this study, effervescent atomization of suspensions in a crossflow of air is investigated experimentally. The tests have been performed at different liquid-to-gas momentum flux ratios (q) and different gas to liquid ratios (GLR). Hydrophilic and hydrophobic particles are used in the experiments. Shadowgraphy and image processing have been used in order to capture the penetration height of the spray. New correlations have been developed to predict the spray penetration height of suspensions in case the non-aerated liquid jet (GLR= 0) and for the aerated liquid jet (GLR $\neq$ 0).

Moreover, suspensions properties such as viscosity and surface tension have a crucial effect on the atomization process. Because the atomization process and droplet formation occur in a very short timescale of the order of milliseconds, it is necessary to analyze the rapid change of the affecting suspension properties related to this timescale especially surface tension. Therefore, the time changing (dynamic) surface tension is more appropriate to be analyzed than static surface tension. In this work, the dynamic surface tension of suspensions is investigated using a combined analytical and experimental approach based on the physics governing the oscillation of elliptical jets. The dynamic surface tension of suspensions liquids in the timescale of milliseconds is calculated. The effect of the dynamic surface tension of suspension on its atomization process has been analyzed.

Acknowledgements

First and foremost, I thank ALLAH (God), for having made everything possible by giving me strength and courage to do this work. We have no knowledge except whatever he has taught us. He is the all-knowing, the all wise.

I would like to express my deepest gratitude to my supervisor, Dr. Ali Dolatabadi for his valuable guidance, support and patience during the entire course of this work. I have been very lucky to have a supervisor like him.

I would also like to thank my committee members, Dr. C. Moreau, Dr. L. Kadem and Dr. Soleymani for their helpful comments.

I would like to express the deep appreciation to Dr. Ghobad Amini for his vulnerable help in many aspects of my research. I would say, the success of this thesis would not have been possible without him.

Special thanks have to go to Dr. Fadel Ben Ettouil and Dr. Hany Gomaa for their continuous support. I would like to take the opportunity to thank my colleague, Tarek Ghoneimy for his help during my work.

I am also indebted to my colleagues in my research group, for their support, collaboration, friendship, discussions, and insightful feedback. Particularly, Mehdi jadidi, Ali Nozari, Mohammed Reza Attarzadeh, Alex Laroche and Dr. Shahin Amiri.

Finally, I would like to thank my country, Egypt, for funding and supporting my research.

Dedication

To my mother, who gave me everything……

Contents

List of Figures

List of Tables

Nomenclature

C	*Particles concentration (% per weight)*
D_h	*Duct hydraulic diameter (m)*
d	*Nozzle diameter (m)*
g	*Gravity acceleration (m/s^2)*
l	*Nozzle length (m)*
m	*Mass (kg)*
Oh	*Ohnesorge number ($\mu_l/\sqrt{\rho_l d\sigma}$)*
Q	*Flow rate (m^3/s)*
q	*Liquid-to-gas momentum flux ratio ($\rho_l u_l^2/\rho_g u_g^2$)*
R	*Radius of oscillating jet*
Re	*Reynolds number ($\rho_l u_l d/\mu_l$)*
T	*Surface age (s)*
t	*Time (s)*
u	*Jet average velocity (m/s)*
V	*Volume (m^3)*
We	*Weber number ($\rho_l u_l^2 d/\sigma_l$)*

Greek letters:

α	*Volume fraction*
ε	*Gas to liquid density ratio* (ρ_g / ρ_l)
ϕ	*Elliptical semi axis (m)*
λ	*Wavelength (m)*
μ	*Dynamic viscosity (kg/s.m)*
ρ	*Density (kg/m3)*
σ	*Surface tension (N/m)*

Subscripts:

1	*major semi axis property of elliptical jet*
2	*minor semi axis property of elliptical jet*
av	*Average*
g	*Gas property*
l	*Liquid property*
max	*Maximum*
min	*Minimum*
p	*Particles property*
st	*Static*
w	*Water*

List of Abbreviations

CMC	Critical micelle concentration
CWS	Coal water slurry
GLR	Gas to Liquid mass flow ratio ($\dot{m_g}/\dot{m_l}$)
PDPA	Phase Doppler Particle Analyzer
PIV	Particle Image Velocimetry
SMD	Sauter Mean Diameter

Chapter 1

Introduction

1.1 Background and Motivation

The process of liquid atomization plays an important role in numerous industrial branches, for example, in chemical, mechanical, aerospace, and civil engineering as well as in material science and metallurgy, food processing, pharmaceuticals, agriculture, environmental protection and medicine. The atomization of liquids in a gaseous crossflow is a very effective process in applications such as in propulsion systems (ramjets, scramjets), cooling and agricultural sprays. One of the applications of the liquid jet in cross flow is in thermal spraying processes which is the main motivation for this work. Thermal spraying is a process in which molten and semi-molten particles are deposited on a substrate as schematically shown in figure (1-1). Because the particles are molten or solid and sufficiently fast in a stream of gas, they can plastically deform while impacting on the substrate which results in the formation of well adhere and dense coatings. Particle temperature and velocity are increased by entering hot jets and flames. Various thermal

spray techniques are extensively used in industry to generate different types of coatings such as thermal barrier, wear resistance, and corrosion resistance. As a result, these techniques are widely used to coat piston rings and cylinder bores in automotive industry, rolls and blades in pulp and paper industry, ball and gate valves in process industry, turbine sections and landing gears in aerospace industry, and power plant boilers in power generation industry [1].

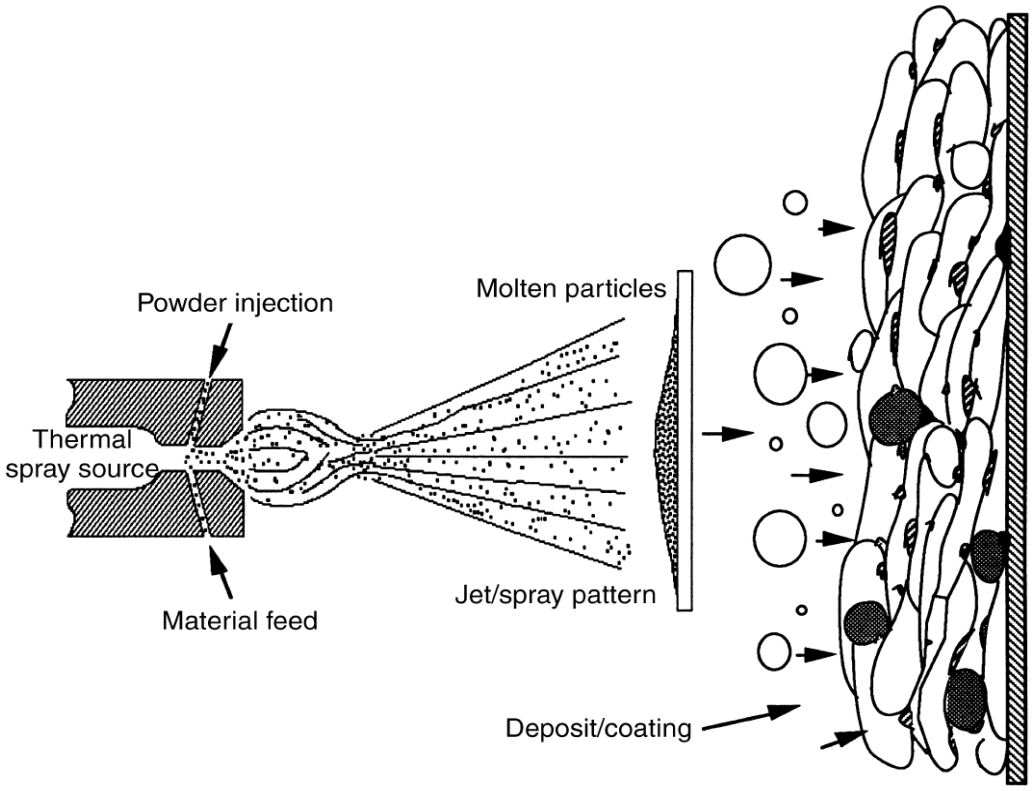

Figure 1-1: Schematic of a typical thermal spray process and coating formation [2].

The main trend of thermal spray processes is to coat with sub-micron and nano sized particles due to the superior performance of fine microstructured coatings. However, there are two main reasons that make coatings with fine particles very difficult. First, feeding submicron and nano

particles into the gas flow is a very difficult process because particles usually form agglomerates which result in clogging the feed lines. Second, sub-micron and nano particles strongly follow the gas phase streamlines (i.e. fine particles decelerate and get diverted by the flow in the stagnation region near the substrate). Spraying suspension of fine solid particles has been known as one of the best techniques to solve these problems related to coating with nano and sub-micron sized particles. In general, suspension atomization is considered one of the important special cases of atomization processes which has its specific properties and characteristics. A suspension is a combination of fine solid particles (usually in the range 500nm-5μm) and a solvent such as water or alcohol (e.g. ethanol) but suspensions could also form from two liquids or even a solid or liquid in a gas. An important criterion to identify a suspension is that the components can separate over time and the particles do not dissolve in the fluid which can result in agglomeration. Therefore, most of the times, a proper chemical stabilizers or surfactants are added to the suspension to prevent particles agglomerations and sedimentations [3]. The fine microstructured coatings produced by the suspension spraying process provide various unique properties, such as remarkable wear resistance, enhanced catalytic behavior, superior thermal insulation and thermal shock resistance. Moreover, superhydrophobic surfaces can be produced by the suspension spraying technique [3].

In current systems of suspension plasma spraying, suspension is injected into the jet or flame using mechanical injection methods, instead of powder injection as shown in figure (1-2). After fine droplets are produced, the liquid (both solvent and surfactant) evaporation becomes dominant. Because of liquid atomization and evaporation, the flame temperature decreases and only the solid particles or their agglomerations remain in the field. The particles are heated up and become molten by the flame and accelerated toward the substrate as shown in figure (1-3) [3].

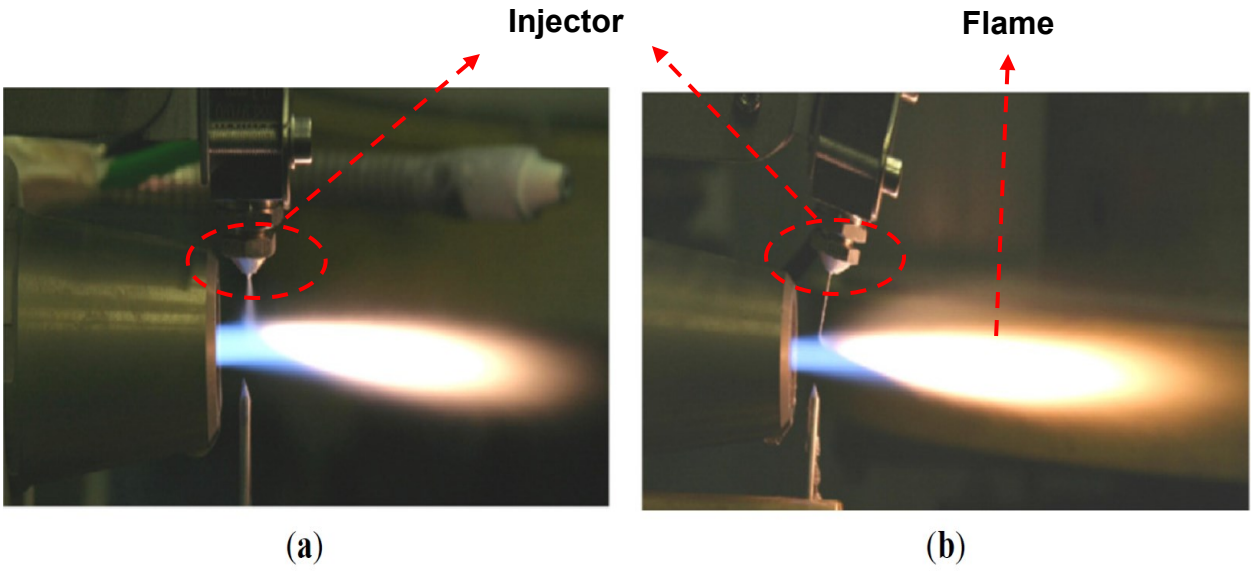

Figure 1-2: Suspension injection into a plasma plume; (a) pre-atomized jet and (b) continuous jet [4].

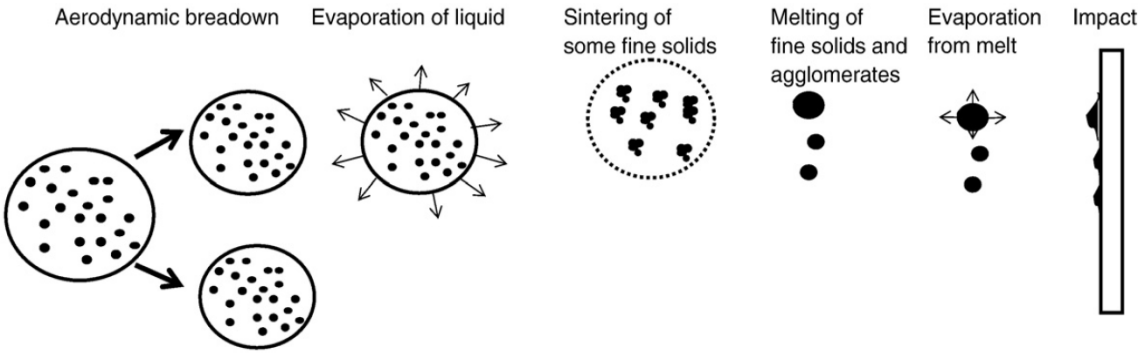

Figure 1-3: Evolution of a suspension droplet in the high temperature jet or flame [3].

Apparently, suspensions with high momentum flux result in an intense flame cooling and consequently solid particles may not be eventually molten. On the other hand, if the suspension momentum flux is too low it may not penetrate into the flame. This causes that most of the particles are not molten and do not have enough kinetic energy upon impacting on a substrate [5]. Moreover, the concentration of suspended solid particles in liquid may vary from one case to another depending on the application, thus the physical properties of the suspension do not remain unchanged. This will affect the spray characteristics, the size and distribution of the sprayed droplets in plasma field which consequently affect the coating quality. For example, production of larger droplets, with normally higher number density of suspended nanoparticles which evaporate in plasma field, results in agglomeration of nanoparticles and formation of large micron-sized particles. As a result of this agglomeration, the coating characteristics will be adversely influenced. In addition, the type of suspension atomizer results in different outcome for spray patterns (for example, the outlet orifice diameter size affects the resultant droplets sizes distributions). Moreover, operating conditions such as air injection pressure in a twin fluid atomizer can influence the droplets size within the spray [6].

As a conclusion, it is obvious that the coating quality obtained by the suspension spraying technique depends heavily on the atomization process and spray characteristics specifically the suspension droplet size and suspension penetration through the plasma jet [7, 8]. Consequently, suspension properties mainly viscosity and surface tension should be well characterized due to their dominant effect on the atomization process [8]. Therefore, in order to achieve the desired properties of the final product, the suspension plasma spraying should have a controllable and repeatable atomization process under different operating conditions and various particle concentrations [9, 10].

1.2 General Concepts of Atomization Process

The instability and breakup of liquid jets into drops which is referred to as atomization has been a subject of interest since the early nineteenth century due to its broad natural and industrial applications. The main objective of the atomization process is to increase gas-liquid interface. Any exchange process (heat, mass, or momentum) within the gas-liquid boundary directly influenced by the size of the exchange surface. The contact area of this gas-liquid interface in a spray system is related to the sum of the surfaces of all individual droplets. As a result of increasing the interface area, the heat and mass transfer between the liquid and gas phases increase. As in diesel engines for example, the combustion rate is controlled by the effective vaporization of the fuel which is directly related to the atomization process of liquid fuel [11, 12].

Generally, the atomization can be defined as a process in which a liquid jet or sheet is disintegrated and converted into drops by the kinetic energy of the liquid, or by the influence of high velocity air or gas exposure or as a consequence of applying external mechanical energy through a rotating or vibrating device [13]. Basically, atomization can be represented as a disruption of the surface tension integrating role by the effect of internal and external forces. In the absence of these disruptive forces, surface tension tries to pull the liquid into a sphere form to provide the minimum surface energy. Liquid viscosity resists any change in system geometry by exerting a stabilizing effect. On the other hand, aerodynamic forces acting on the liquid surface tries to increase the disruption process by applying an external force to distort the bulk liquid. When the magnitude of disruptive force exceeds the consolidating surface tension force, breakup of liquid jet happens. There are several parameters that have critical effects on the process of atomization. These parameters include, but not limited to, the internal geometry of the atomizer, jet surface waves, turbulence, velocity profile at the atomizer exit, the properties of the medium

into which the liquid is discharged, and the physical properties of the liquid itself such as density, viscosity and surface tension [13].

The atomization process is often accomplished by many types of atomizers that inject liquid streams with sufficient energy to provide sufficient breakup into droplets. To select the appropriate atomizer type for a specific application, many factors such as the desired droplet size, the spray shape, operating conditions and the properties of the liquid should be taken into account. Based on the required energy for spray formation, the common atomizer types used in industry are categorized into pressure atomizer, rotary atomizer, electrostatic, ultrasonic atomizer and twin-fluid atomizer [11, 13].

In the pressure atomizer, a pressurized liquid is discharged through a small opening at high speeds into gas atmosphere. The energy required for atomization is carried by the liquid itself, and the pressure energy is converted into kinetic energy. This type of atomization is typically used for low viscosity liquids. There are some limitations associated with this type of atomizers such as; large droplet size resulted in the spray, low mass flow rate as well as the need for pressurizing the liquid which may be difficult to get in some cases [11]. In the rotary atomizer, the liquid is introduced into a center of a high speed rotating surface. Due to the action of the centrifugal force, the liquid moves radially outward and is ejected at high speed from the rim of the surface and disintegrates into droplets. In this atomizer type, the energy used for atomization is the external mechanical energy required to rotate the surface. By using rotating surfaces with vanes or channels, probable slippage between liquid and solid surface can be avoided. In electrostatic atomizer, an electrical charge is used to accelerate liquid in an electric field results in an accelerating tiny liquid jet which further breaks into fine droplets at the tip in small quantities. The ultrasonic atomizer

utilizes the acoustic energy generated by a transducer or a piezoceramic element which produces acoustic waves necessary for liquid disintegration and spray formation [11, 13, 14].

In twin-fluid atomizer, the liquid stream is exposed to a high velocity gas stream and this two phase interaction results in the breakup of liquid phase and spray formation. Twin fluid atomizers can operate at low flowrates and low injection pressures and utilized in many applications including humidification, combustion, cooling, thermal spray coating and spray drying. Based on the way of mixing of the two-phase flow and the atomizing gas flowrate, these atomizers are categorized into air-blast, air-assist and effervescent atomizers. In air-blast and air-assist atomizers, air at very high velocity is introduced into already established jet or sheet of liquid before the discharge orifice. Both of these atomizers have many similarities and the main difference between them is that air-blast atomizer consumes a higher volume of the atomizing gas than air-assist. The main disadvantage of these two atomizers is the higher amount of the gas introduced into the atomized liquid which results in some practical limitations [6, 13-15]. In effervescent atomizer, the gas at low velocity is injected into the liquid flow upstream the discharge orifice resulting in bubbly flow which provides a high quality atomization. This atomizer is used in gas turbines combustors, boilers, spraying of viscoelastic liquids in addition to atomization of liquids with suspended nanoparticles [13, 14]. A schematic drawing of a typical twin-fluid atomizer is illustrated in figure (1-4).

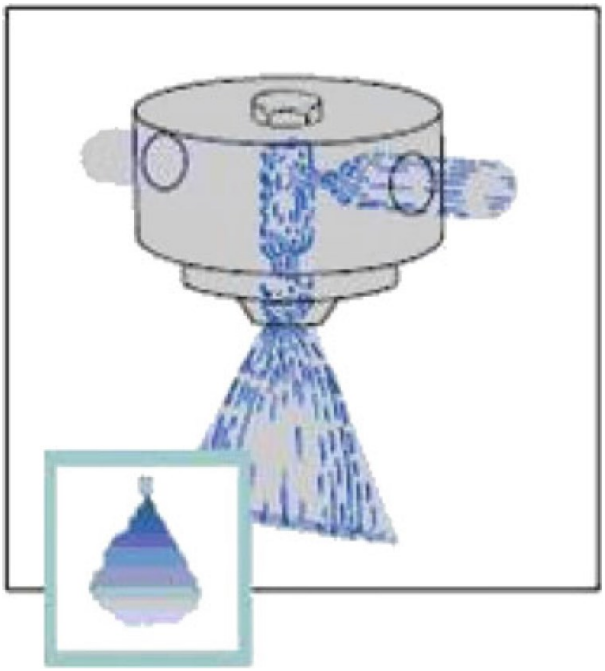

Figure 1-4: Schematic of a twin fluid atomizer [14].

1.3 Dynamic Surface Tension

Generally, atomization process and droplet formation occur in a very short time, of the order of milliseconds [16, 17] and one of the main dominant parameters on the atomization process is the surface tension [13, 14, 18]. When a sudden expansion of the surface of a solution, as in the atomization process, takes place, a portion of the bulk solution is brought to the surface. This freshly created surface, at the instant of its formation, may have different concentrations of its components than the bulk solution. Therefore, the surface tension of this new surface may have a different value than its value which is observed when the surface layer has enough time to come into equilibrium with the bulk solution [19]. The pure dynamic surface tension is defined as the tension founded at the instant of creation of the surface which corresponds to a surface of zero age while the static surface tension corresponds to equilibrium between the bulk solution and the

surface. Based on the nature of solution components and dissolved molecules, it is proven by experiments that the static surface tension needs time to reach and this time ranges from several milliseconds to several hours [20]. Between the initial state of the newly created surface and the final equilibrium state, the surface passes through a series of intermediate states which are related to a series of intermediate surface tensions. Therefore, dynamic surface tension can be defined as the non-equilibrium transient value of the surface tension measured before equilibrium is attained. As a consequence, it is a function of time or age of the surface. On the other hand, the static surface tension refers to the surface tension measured after the surface has reached equilibrium [20].

To have a better clarification, in case of pure liquids such as water, there are no other components or dissolved molecules therefore, the surface tension does not change with time so it is called static or equilibrium surface tension. On the other hand, by adding a surfactant or suspended solid particles (or both such as the suspensions used in thermal spray processes), the surface tension can be variable depending on the additives and operating conditions [21]. A clear effect on surface tension can be found if a surfactant is added to the solution. A surfactant molecule has two distinct parts; a hydrophilic dipolar head and a hydrophobic nonpolar tail. Surfactant molecules adsorbed at a liquid surface constitute a monolayer, retaining the aqueous hydrophilic head contact while avoiding contact between water and the hydrophobic tail [19, 22] , as shown in figure (1-5). Surfactants have the ability to accumulate at freshly created interfaces. However, they need a finite time for the adsorption on the interface until surface equilibrium is reestablished. The presence of surfactant on the interface affects the dynamic surface tension of the fluid. When the surface is fresh, surface tension is almost equal to that of the solvent or base liquid. As the adsorption rate increases, surface tension decreases to the equilibrium value over a certain time, which is required to saturate the interface with surfactant molecules [22].

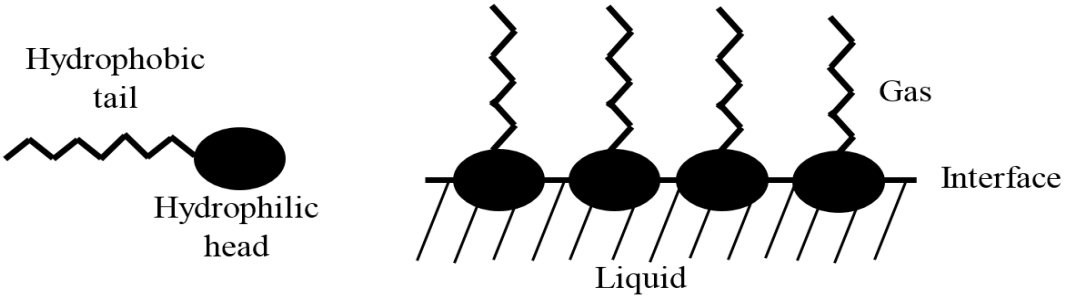

Figure 1-5: Surface structure in case of a surfactant added.

Moreover, it is found that the solid particles in suspension liquid can change the equilibrium surface tension with time, depending on the particle wettability [17]. In addition, surfactants are usually added to the suspension liquids to have a good dispersion of the suspended particles and hence avoid agglomeration and prevent sedimentation as illustrated in figure (1-6). Therefore, for suspensions, it is found that the time changing (dynamic) surface tension is more appropriate to be investigated than static surface tension [17, 23].

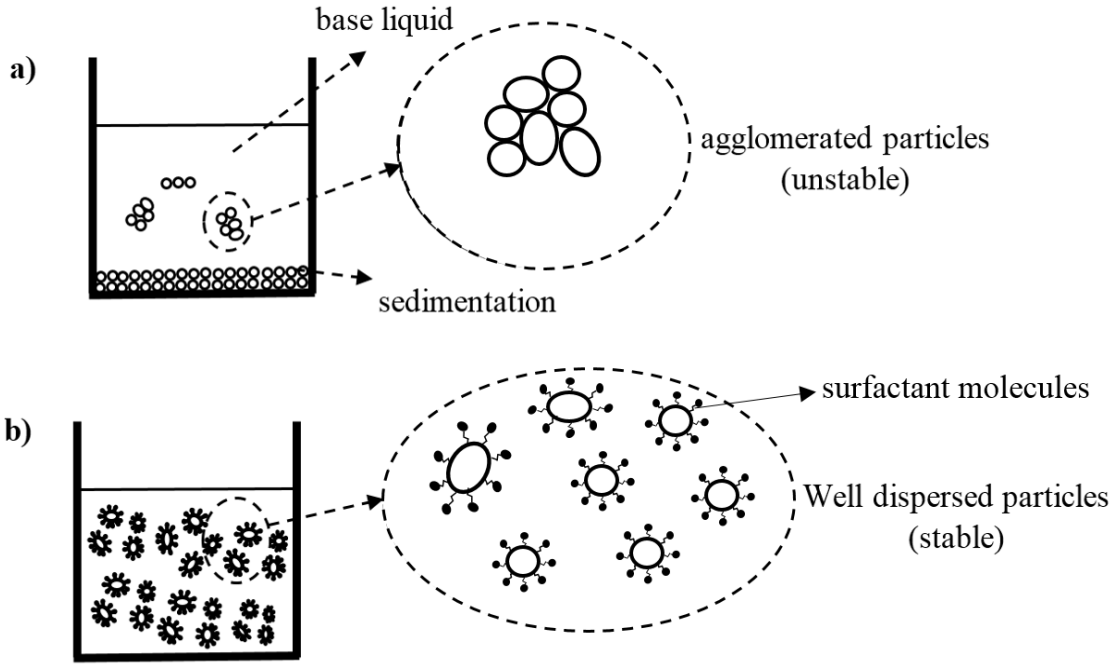

Figure 1-6: Schematic of suspended particles in a liquid;
(a) without a surfactant and (b) with a surfactant.

Consequently, analyzing dynamic surface tension of suspension can be a critical factor for understanding suspension atomization process in addition to controlling and predicting its characteristics which influence the quality of coating.

1.4 Objectives

In suspension thermal spraying processes, it is critical to predict the suspension atomization characteristics in order to control the quality of final product mainly the coating structure. For obtaining a high quality coating, the suspended solid particles should penetrate to the center of the plasma plume where the heat and momentum fluxes are maximum. On the other hand, if the solid particles are not capable of penetrating well and reach a proper penetration height into the flame, most of these particles are not molten. Consequently, they will not have enough kinetic energy upon impacting on a substrate to form a well-adhered coating. In addition, selection of the type of suspension atomizer is influential whether it is simple, such as plain cylindrical atomizers, or more complicated, such as twin-fluid atomizers (e.g., effervescent) [8]. Moreover, the suspension properties, mainly the surface tension, are not well characterized and have many discrepancies. This study aims to investigate the effervescent atomization of suspensions in a cross flow of air. Several spray characteristics such as, spray trajectory and penetration height are analyzed. The present study is implemented in cold conditions for momentum flux ratios close to that used in plasma conditions. The obtained results will help us to provide better knowledge and prediction when working in practical plasma spray conditions. Furthermore, the dynamic surface tension is measured to investigate its influence on the process of suspension atomization in cross flow. In order to achieve these objectives, the following steps are carried out:

1- Performing experimental investigation of the effervescent atomization of suspensions in air cross flow at different momentum flux ratios (q) and different gas to liquid ratio (GLR) and visualization of the flow by using shadowgraphy.
2- Analyzing the different spray characteristics such as spray penetration height and trajectory.
3- Investigating of the suspension dynamic surface tension based on a combined analytical and experimental study.
4- Analyzing the effect of the measured dynamic surface tension of suspension on its atomization process.

1.5 Thesis Layout

Chapter 2: reviews the literature related to the effervescent atomization of suspensions in a cross flow of gas. Due to the insufficient data, the literature review is presented by reviewing the literature relevant to the atomization of liquids in a cross flow and that of the effervescent atomization. In addition, the studies related to suspensions properties and atomization are reviewed.

Chapter 3: presents an experimental investigation of effervescent atomization of suspension liquids. Different types of suspended solid particles at different concentrations are tested. Experiments have been performed at different liquid-to-gas momentum flux ratios (q) and different gas to liquid ratios (GLR). Shadowgraphy and image processing are utilized to detect and measure spray penetration heights. New correlations for predicting spray penetration heights have been proposed.

Chapter 4: introduces an investigation of the suspension dynamic surface tension and its effect on atomization process based on the oscillating elliptical jet technique using a combined analytical and experimental study. Shadowgraphy and image processing are used to capture the images while a mathematical model is used to deduce the dynamic surface tension.

Chapter 5: summarizes the conclusions of the research and provides some suggestions for future work.

Chapter 2

Literature Review

In this thesis, atomization of suspensions in cross flow using an effervescent atomizer is investigated experimentally. This chapter introduces the literature review associated to effervescent atomization into a cross flow of gas. The review presents the literature related to liquid jet breakup in cross flow and effervescent atomization, since this work can be considered as a combination of both. Furthermore, suspension properties related to this work is introduced.

2.1 Atomization of Liquids in Cross Flow

The breakup of a liquid jet injected through a nozzle into a gas has been a subject of interest since the early nineteenth century. An early mathematical analysis was carried out by Lord Rayleigh to predict the conditions necessary to cause the collapse of a liquid jet issuing at low velocity [24, 25]. In honor of his thorough and fundamental study, the capillary instabilities and their effects on the liquid jet breakup were named after him. A more general theory for

disintegration at low jet velocities was developed by Weber who extended Rayleigh's analysis to include the effect of liquid viscosity on liquid jet breakup. Basically, he defined a map of liquid jet breakup, using the ratio of inertia to surface tension force, which since then has been called the Weber number [14]. Taylor performed an extensive study on the shear effect, especially at high velocities. He showed that the density of the ambient gas has a profound effect on the mechanism and type of jet breakup [14]. The number of studies following the above pioneering works are very large due to the increasing wide applications of the jet breakup processes. These studies have shown that there are several parameters that critically influence the atomization process. These parameters include the internal geometry of the atomizer, the jet velocity profile and turbulence at the atomizer exit, and the properties of both liquid and gas. Reitz and Bracco [26] performed a comprehensive study with the aid of experiments that provided a thorough discussion of the possible mechanisms which jet breakup has been attributed to. They concluded that a combination of factors contribute to the breakup process and not a specified single mechanism is always the reason.

In general, there are three forces acting on the liquid that dominate the breakup process as concluded by Sirignano and Mehring [18]. These forces are inertia force, surface tension force and viscous force. Consequently, the atomization process is governed by the following non-dimensional groups; Reynolds number ($Re = \rho LV / \mu$) and Weber number ($We = \rho LV^2/\sigma$). Another number commonly used is the Ohnesorge number, which is a combination of *Re* and *We*, defined as ($Oh = We^{0.5}/Re$) [18].

2.1.1 Fundamentals of Liquid Jet Breakup in Cross Flow

Recently, atomization of liquid jet in a cross flow of gas has been widely studied because of its dominant role in many applications (e.g. turbine engines, ram jets, cooling, thermal spraying, etc.). In the interest of understanding the atomization process of liquid jet in cross flow, several experimental studies have been conducted using several techniques to study its main characteristics. In general, the study of liquid jets has been usually performed by visualization techniques and image collection such as high-speed imaging, pulsed shadowgraphy and Mie scattering data obtained by slicing the spray with a laser sheet [27]. Detailed explanation of these techniques can be found in reference [11].

A general understanding of the jet breakup process in a cross flow of gas is deduced from experimental observations by some researchers as Wu et al. [28]. As shown in figure (2-1), the jet exits the orifice as a column with an initially round cylindrical cross-section. Then, the dynamic force of the cross flow causes the jet to flatten and bend in the cross flow direction. The spray field produced by a jet in crossflow can be divided into three regions: intact liquid column region, ligaments region, and droplets region [8, 28]. In the liquid column region, the instabilities are developed and result in the formation of ligaments and droplets. At the windward surface, the wave's amplitude increases along the jet column until breakup occurs at one of the wave troughs [8, 29]. This breakup that occurs at the wave trough, but not at every trough, leads to the formation of short jet segments, named ligaments. This breakup is referred to as the column breakup [28]. The column breakup point is defined as the location where the liquid column stops to exist [14]. The further breakup of ligaments into smaller droplets is defined as the secondary breakup [8]. Furthermore, surface waves with short wavelength appear on the leeward surface of the liquid jet. The interaction between these waves and the dynamic pressure of the crossflow results in stripping

droplets from the leeward surface, which is known as surface breakup. Generally, droplets resulted from surface breakup are smaller than those produced from ligaments [28].

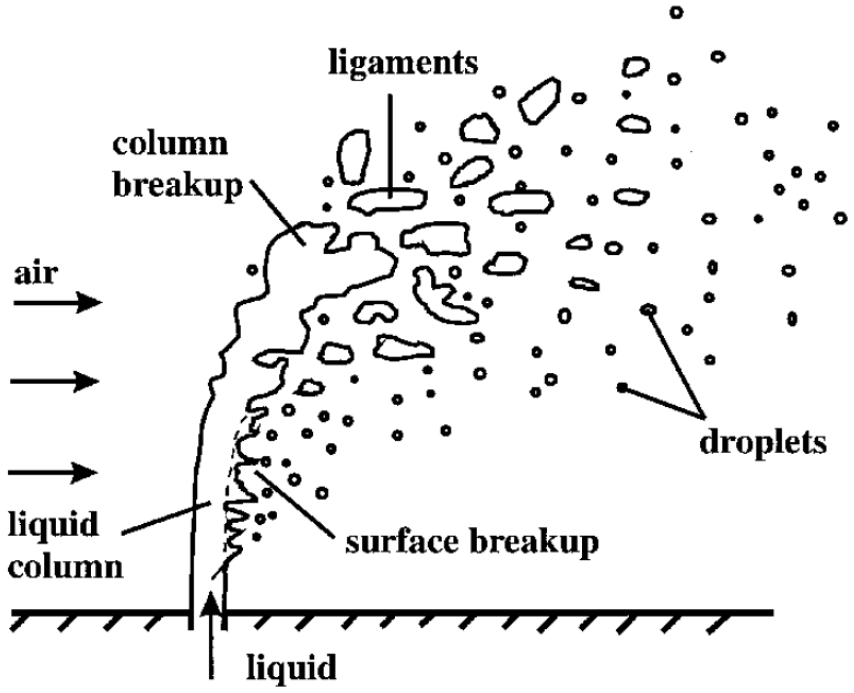

Figure 2-1: Jet breakup regions in a gaseous cross flow [28].

Basically, there are many parameters that influence the liquid jet crossflow phenomenon such as density, viscosity, and velocity of both phases, surface tension, duct hydraulic diameter (D_h), and nozzle diameter (d) [8, 27]. Based on these parameters, the atomization process in a gaseous cross flow is governed by the following non-dimensional groups:

a- Reynolds no. of the gaseous cross flow:

$$Re_g = \frac{\rho_g u_g D_h}{\mu_g} \qquad (2.1)$$

b- Reynolds no. of the liquid jet:

$$Re_l = \frac{\rho_l u_l d}{\mu_l} \tag{2.2}$$

c- Liquid-to-gas momentum flux ratio:

$$q = \frac{\rho_l u_l^2}{\rho_g u_g^2} \tag{2.3}$$

d- Weber no. of the gaseous cross flow:

$$We_g = \frac{\rho_g u_g^2 d}{\sigma_l} \tag{2.4}$$

e- Weber no. of the liquid jet:

$$We_l = \frac{\rho_l u_l^2 d}{\sigma_l} \tag{2.5}$$

f- Density ratio:

$$\varepsilon = \frac{\rho_g}{\rho_l} \tag{2.6}$$

A breakup map for liquid jets in crossflow, based on the gas Weber number, is proposed by Sallam et al. [30] to show different breakup regimes in crossflow. As shown in figure (2-2), the breakup processes of liquid jet in cross flow can be divided into the following different regimes [30, 31]:

a- Column breakup happens when the aerodynamic forces are higher than viscous and surface tension forces and results in the breakup of the jet to the same diameter size droplets.

b- Bag breakup occurs when the jet is stretched into a thin bag shape such as two rims with entraining air into its pocket. In this regime, the bag pocket suddenly explodes when the air pressure force inside the bag becomes higher than the surface tension force.

c- Multimode regime: a transitional regime between the bag and shear breakup regimes where a part of the jet remains intact and rest of the jet breaks up due to surface waves.

d- Shear mode: the jet column deforms and ligaments/fine droplets strip off the jet column side.

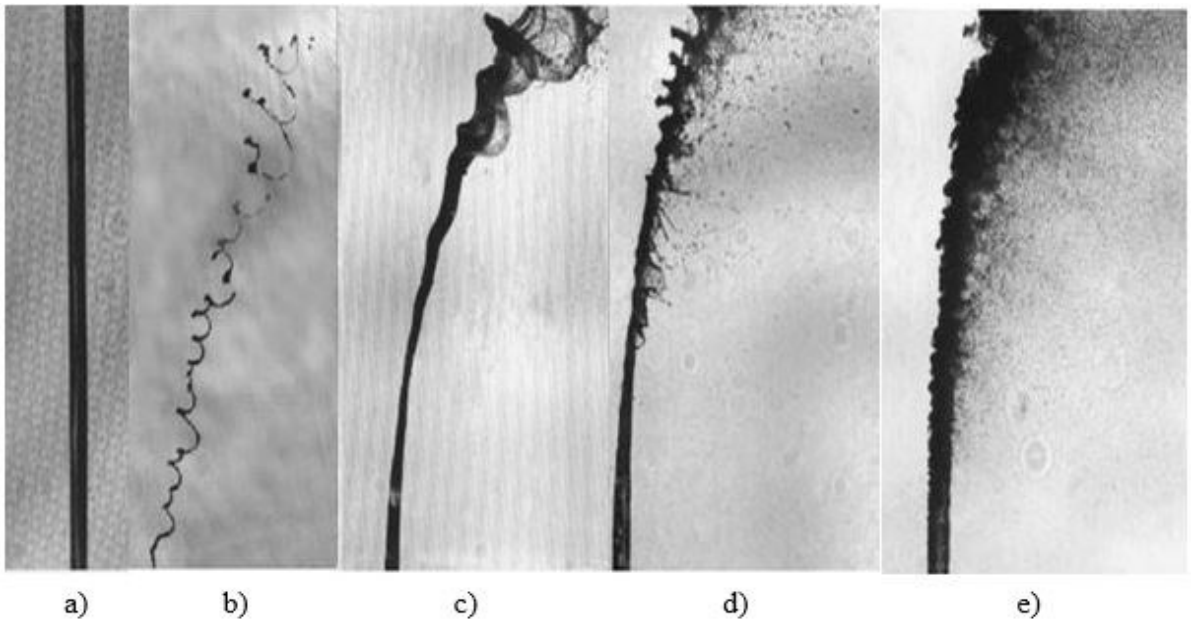

Figure 2-2: Breakup processes of liquid jets in a gaseous crossflow [30];
(a) no breakup, (b) column breakup, (c) bag breakup, (d) multimode breakup, and (e) shear breakup.

Table (2-1) summarizes the criteria based on gas Weber no. corresponding to all of the atomization regimes [30].

Table 2-1: Breakup regimes in cross flow based on gas Weber no. criteria [30].

Disintegration regime	***Weber* number Criteria**
Column	$We_g < 4$
Bag	$4 < We_g < 30$
Multi-mode	$30 < We_g < 110$
Shear	$We_g > 110$

Jet penetration or trajectory has attracted considerable attention due to their influence in many processes such as thermal spraying. Jet penetration of liquid jet in a cross flow is one of important parameters that indicates how well the injected liquid can mix with the air. Several studies investigated the spray penetration and trajectory [28, 29, 32-37]. One of the important studies of penetration of water jet in cross flow has been performed by Schetz and Padhye [38]. They worked experimentally on the effect of liquid-to-gas momentum flux ratio on the length of jet column breakup [38]. From the analysis of the results of these studies, it was found that there is a dependency of the jet penetration on the liquid-to-gas momentum ratio [29, 33, 36]. Spray penetration, spray width and spray cross-sectional area increase with increasing of the momentum flux ratio [28, 33, 35, 37]. It could be concluded that the momentum flux ratio has a great influence on the spray penetration and can be considered a key parameter in characterization of the crossflow injection process, both for liquid and gas jets [14, 27].

Considerable number of empirical correlations had been proposed to predict the trajectory of a liquid jet injected into a gaseous crossflow by many researchers. Generally, in most of these correlations, the jet trajectory of a liquid jet in a crossflow is a function of the liquid-to-gas

momentum flux ratio and the normalized distance from the injector in the cross flow direction. However, other parameters have been combined in the empirical correlations by several investigators such as Weber number, liquid to water viscosity ratio, pressure, Reynolds number and temperature [39]. Although there have been numerous correlations developed to describe this important topic, significant discrepancies exist among the resultant values and there is no universal correlation that is capable of predicting the jet trajectory over a wide range of conditions [8, 39]. These discrepancies may be attributed to the wide range of the variables such as liquid properties, crossflow conditions, the different measurement techniques as well as difficulties in defining the boundaries of the liquid jets [39, 40]. An extensive review of most of these correlations can be found in the works of No [39], Birouk et al.[40], Ashgriz [41] and Mashayek et al.[42]. Some popular correlations for jet penetration in subsonic cross flow based on different parameters are summarized as follows:

- Inamura et al. [39]:

$$\frac{y}{d} = (1.18 + 0.24d)q^{0.36} \ln\left[1 + (1.56 + 0.48d)\left(\frac{x}{d}\right)\right] \quad (2.7)$$

- Chen et al. [33]:

$$\frac{y}{d} = 9.91q^{0.44}\left[1 - e^{-\left(\frac{x}{d}\right)/13.1}\right]\left[1 + 1.67e^{-\left(\frac{x}{d}\right)/4.77}\right]\left[1 + 1.06e^{-\left(\frac{x}{d}\right)/0.86}\right] \quad (2.8)$$

- Wu et al. [28]:

$$\frac{y}{d} = 1.37q^{0.5}\left(\frac{x}{d}\right)^{0.5} \quad (2.9)$$

- Becker et al. [29]:

$$\frac{y}{d} = 1.48q^{0.42} \ln\left[1 + 3.56\left(\frac{x}{d}\right)\right] \quad (2.10)$$

- Stenzler et al. [35]:

$$\frac{y}{d} = 3.354q^{0.42}\left(\frac{x}{d}\right)^{0.391} (We)^{-0.088}\left(\frac{\mu_l}{\mu_w}\right)^{-0.027} \quad (2.11)$$

- Eslamian et al. [43]:

$$\frac{y}{d} = 0.191q^{0.30}\left(\frac{x}{d}\right)^{0.43} (We)^{-0.128}(Re_g)^{0.12}\,(Re_l)^{0.14} \quad (2.12)$$

- Bellofiore et al. [39]:

$$\frac{y}{d} = 0.909q^{0.476}\left(\frac{x}{d}\right)^{0.35} (We)^{-0.128}(Re_g)^{0.135} \quad (2.13)$$

Drop sizes after the breakup is another important parameter and should be investigated because of its crucial effect on different applications [28, 44]. Several experimental studies have been carried out for investigating this parameter [28, 29, 36-38, 45-48]. The results of these studies showed the effect of the air velocity and consequently the momentum flux ratio on the droplet diameter. It was found that the largest droplets were found in the spray core for low momentum flux ratio and at the periphery region for high momentum flux ratios [28, 36-38, 48]. The mean droplet size were found to decrease with increasing velocity of the gas cross flow [29, 45, 47, 48]. Generally, it can be concluded that the strongest dependence of mean droplet size is on velocity of the gaseous cross flow.

Another important factor is the effect of liquid properties on the spray characteristics. Generally, it can be concluded that the jet penetration decreases by increasing the liquid viscosity

due to increase of the drag force on the jet [35, 49]. Regarding surface tension, no significant effect on jet penetration was observed, although decrease in surface tension increases the wavelength and wave amplitude which intensifies the jet breakup process. Moreover, disintegration processes were faster and drop sizes were smaller for liquids with smaller surface tension values [46, 50]. Moreover, increasing Weber number of gas results in decrease of the average droplet size; consequently, the overall spray penetration decreases because smaller droplets decelerate faster [8].

2.2 Effervescent Atomizers

Effervescent atomization or "aerated-liquid atomization" is a special form of the twin-fluid atomization which was developed by Lefebvre and his colleagues in 1980s [51]. In this atomization technique, a small amount of gas is injected into a liquid stream. This results in a two-phase bubble-liquid flow inside the atomizer and then the resultant two-phase flow is discharged through the atomizer orifice [52]. By the presence of bubbles inside the liquid flow, the atomization process is improved due to decreasing of the liquid fraction passing through the exit orifice. As this bubbly flow exits the orifice and due to the pressure drops, the bubbles expand leading to ligaments formation. Due to the effect of further bubble expansion in addition to the effect of liquid velocity, these ligaments are broken to small droplets [14].

The effervescent atomizer has several advantages over other common atomizers. The main advantage is that good atomization can be achieved even at low injection pressures and low gas flowrates compared to those required by other twin-fluid atomizers. For any given injection pressure, smaller drop sizes can be obtained than those produced by other types of atomizers. Additionally, it has an exit orifice with larger diameter than other types of atomizers having similar

flowrates. This results in solving clogging problems and helps in atomization of liquids with impurities or suspended particles. Furthermore, good atomization performance can be obtained for various liquid types and liquid physical properties, which means that fluids with complex physical properties, such as viscous solutions, suspensions and non-Newtonian can be handled with this atomizer. Moreover, an effervescent atomizer provides reliability and simplicity which results in easy maintenance and low cost operation. The main drawback of effervescent atomizers, as the same as other types of twin-fluid atomizers, is the need to have a supply of pressurized gas. However, this requirement can be met easily, since the effervescent atomizer operates at low gas pressures and low gas flow rates [13, 15, 52, 53].

Effervescent atomizers are utilized in several applications such as gas turbines, boilers, internal combustion engines, furnace, burners and atomization of viscoelastic liquids as well as atomization of liquids containing suspended nanoparticles [14]. A typical effervescent atomizer has four main components; gas inlet, liquid inlet, a mixing chamber, and an exit orifice as shown in figure (2-3) [52]. Liquid is supplied to the atomizer through a port and flows down inside a perforated central tube to the exit orifice. The gas, which is at a pressure slightly higher than that of the liquid, is injected into the liquid stream through the holes in the aerator tube and generates bubbles. The generated bubbly flow moves downstream and then exits the orifice. Due to a high-pressure drop at the exit orifice, the gas expands suddenly and forms small droplets [14, 15, 52].

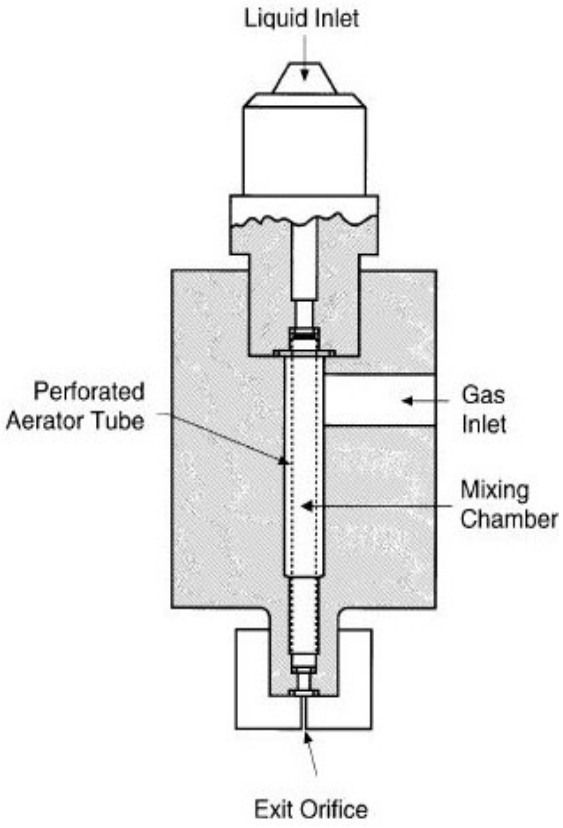

Figure 2-3: Schematic of a typical effervescent atomizer [52].

The two-phase flow inside the effervescent atomizer has been classified into three main regimes; bubbly flow, slug flow, and annular flow. The bubbly flow is generated at low gas to liquid mass flow rates ratio (GLR). In the bubbly flow, the liquid is the continuous phase while the gas forms the discrete phase, i.e. small individual or coalesced bubbles are dispersed inside the liquid stream. With increasing GLR, the size of bubbles increases and reaches the size of the inner diameter of the mixing chamber then the bubbly flow changes to slug flow. Due to the presence of larger bubbles approaching the exit orifice, the slug flow results in significant spray pulsation and unsteadiness. With a further increase in GLR, the internal flow changes to the annular flow regime at which gas flows in the center of mixing chamber while surrounded by an annular film of liquid on the wall of the mixing chamber. Compared to the other internal flow regimes, the

annular flow regime results in the smallest size of spray droplets. However, the annular flow requires a high flow rate of gas as well as the instability of the internal two-phase flow which are considered as its main drawbacks [15, 52]. Figure (2-4) illustrates the flow regimes inside the effervescent atomizer.

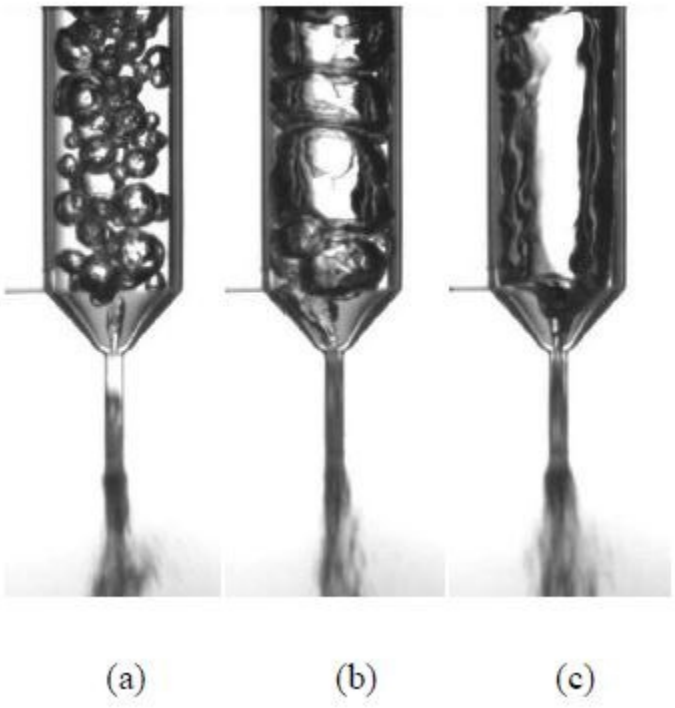

Figure 2-4:The flow regimes inside the effervescent atomizer [15];
(a) bubbly flow, (b) slug flow, and (c) annular flow.

The behavior of the effervescent atomization process and consequently the characteristics of the resulting spray are influenced by many parameters. The main parameters include the atomizer geometry, operating conditions and the physical properties of gas and liquid [6, 15, 52] as follows:

a- Atomizer geometry

The two-phase flow structure is influenced by the internal geometry of the atomizer resulting in affecting the atomizer performance. Many parameters such as the size and number of aerator

holes, discharge orifice diameter, length to diameter ratio (*l/d*) of the discharge orifice, as well as the mixing zone length were investigated by several researchers to analyze their effects on spray characteristics mainly droplet size.

The number and size of aeration holes are found to influence the bubble size and consequently the spray droplet size. Sovani et al. [52] and Wang et al. [54] found that using an aerator tube with multiple holes instead of a single hole with the same equivalent area leads to a narrower droplet size distribution. Several researchers such as Roesler et al. [55], Wang et al. [54] and Lefebvre et al. [51, 56] investigated the effect of the discharge orifice diameter on the droplet size. They found that using different orifice diameters results in a negligible difference in the resultant droplet size which means that atomization performance is insensitive to this parameter [52]. Chin et al. [57] and Sovani et al.[52] found that droplet size is decreasing with reducing length to diameter ratio (*l/d*) of the discharge orifice which can be considered a significant parameter in influencing the atomization performance. Mostafa et al. [58] and Jedelsky [59] concluded that the radial distribution of the droplet size and velocity depends on the mixing zone length.

b- Operating conditions

The main operating conditions that significantly affect the characteristics of resultant spray are GLR and injection pressure which are investigated by several researchers [52, 59, 60]. By using high-speed imaging, Huang et al. [61] investigated the influences of gas and liquid flow rates on the internal two-phase flow and spray droplet size. They found that increasing the water flow rate and/or decreasing the injection pressure (i.e. lower gas flow rate) results in increasing the droplet mean diameter and decreasing the mean droplet velocity. Additionally, Jedelsky et al. [59] found

that an increase in the injection pressure and/or GLR leads to decreasing the droplet mean diameter. They also observed that the droplets have higher mean diameter and lower velocity at the edge of spray. Lefebvre et al. [51] and Sovani et al. [52] measured the resultant droplet size at low and high injection pressure ranges. They found that the mean droplet size is reduced by increasing the injection pressure. Also, it is concluded that the droplet mean velocity increase with increasing the injection pressure and GLR. This conclusion is attributed to increasing aerodynamic drag force exerted by the larger mass of atomizing gas on droplets making them moving faster [52].

To summarize the effect of injection pressure and GLR on resultant droplet size, it can be concluded that increasing the injection pressure reduces the droplet size and consequently enhances the atomization performance. Additionally, the effect of change in injection pressure is more obvious at low injection pressures than at high injection pressures [52]. Moreover, GLR plays a dominant role in the spray mean droplets size. Most of the experimental studies show that increasing GLR results in decreasing droplet size. Furthermore, the mean droplet size can be represented as a nonlinear function of GLR as shown in figure (2-6) [52]. However, with increasing GLR, the flow regime changes from bubbly to slug flow that causes the instability and pulsation of spray which are not desirable features in most of the applications. Further increase in GLR generates the annular flow regime which produces the smallest droplets which is desirable but the need to large volume of pressurized gas makes it not a preferable choice [15, 61]. Figure (2-5) illustrates the effect of GLR on droplet Sauter mean diameter (SMD), defined as the ratio of volume-to-surface area, at different injection pressures.

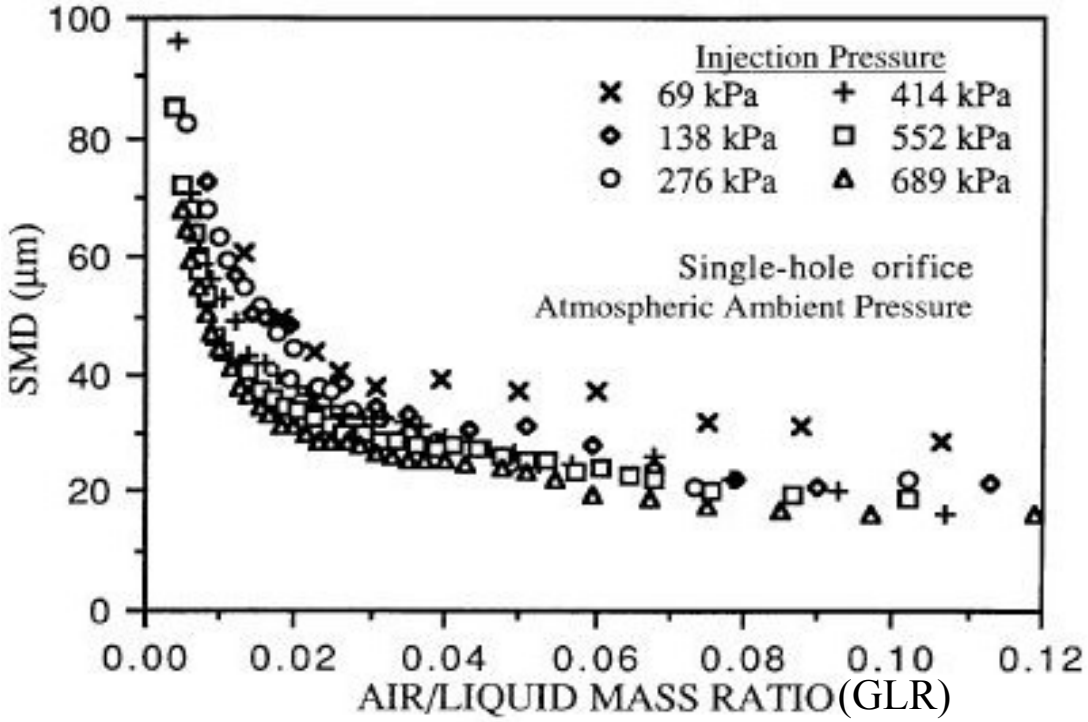

Figure 2-5: Effect of GLR on spray SMD at different injection pressures [52].

c- Liquid physical properties

Generally, the liquid properties, mainly viscosity and surface tension, have a strong influence on the atomization performance [13]. Many studies were conducted for analyzing the effect of both properties on the effervescent atomization mainly droplet size. Buckner and Sojka [52] concluded that the mean droplet diameter is not influenced by liquid viscosity. Lund et al. [62] and Sutherland et al. [52] reported that the viscosity has shown a small effect on the droplet size. They found that increasing viscosity by 400% resulted in increasing the SMD by only 15%. These results are in good agreement with the results of Qian et al. [63] which show the slight effect of the

viscosity on droplet size. This can be considered as a good indication of the effervescent atomizer to be used to atomize high viscosity liquids with a good efficiency.

The effect of surface tension on the atomization performance was investigated by many researchers. Sutherland et al. [52] found that changing surface tension did not affect SMD which remained almost constant. Qian et al. [63] showed that the surface tension has a clear effect on the droplet mean diameter. He found that decreasing surface tension from 72 to 22 g/s^2 reduced SMD by about 30%. Lund et al. [62] proposed a mathematical correlation relating the SMD to the liquid physical properties as shown in equation (2.8):

$$\mathrm{SMD} = \left[\frac{3}{2}\sqrt{2}\,\pi d_l^3\left(1+\frac{3\mu_l}{\sqrt{\rho_l\sigma_l d_l}}\right)^{1/2}\right]^{1/3} \qquad (2.14)$$

where d_l represents the ligament diameter and ρ_l, μ_l, and σ_l are the liquid density, viscosity, and surface tension, respectively.

Generally, many applications such as agricultural sprays and liquid rocket engines utilize the effervescent atomization where a well-atomized liquid injected into a cross flow of gas is required. Due to better atomization and mixing efficiencies, excessive use of toxic chemicals in agricultural sprays can be reduced [64]. Moreover, better combustion efficiency and reduced pollutant emissions in liquid fueled propulsion systems can be achieved. Lin et al. [64] carried out a comprehensive experimental investigation of the effervescent atomization for different liquids in a subsonic cross flow at different operating conditions. The results showed that the spray penetration height for the aerated liquid jet is larger than that of the pure (non-aerated) liquid jet under the same operating conditions. In addition, increasing the aerating gas amount results in

increasing the penetration height due to increasing the effective liquid-to-gas momentum flux ratio. The experimental results of Miller et al. [65] and Ghenai et al. [66] agreed with Lin's findings [64] in addition to that momentum flux ratio had a little effect on droplet size. Furthermore, higher atomization characteristics such as smaller droplet size and higher droplet velocity are obtained [64, 66]. A correlation for the spray penetration height has been reported by Lin [67] as follows,

$$(y - y_0)/d_0 = 0.9\,(GLR)^{0.46}\,M^{-0.64} q_0^{0.34}\,(x/d_0)^{0.39} \tag{2.15}$$

and

$$y_0/d_0 = 3.17\,q_0^{0.33}\,(x/d_0)^{0.40} \tag{2.16}$$

where y is the penetration height, y_0 is the non-aerated penetration height, q_0 is the momentum flux ratio of non-aerated jet, and M is the freestream Mach number.

2.3 Suspension Liquids

2.3.1 Properties

In spite of the importance of suspension atomization in many applications, the fundamental processes of suspension fragmentation within atomization are not quite well understood. The breakup process of suspension liquids in an atomization process is different from that of a single phase, pure liquid, by the effect of the suspended particles on the fragmentation kinetics [10]. The interactions among the three different phases (solid, liquid and gas) in a suspension spray in addition to the suspension properties which depend strongly on the solid particles content can play an effective role in the disintegration process. Consequently, it influences the quality of the final

product (mainly coating structure) [11, 68]. Generally, to control the suspension atomization process, the suspension properties mainly density, viscosity and surface tension should be known [3]. The suspension properties strongly depend on the solid particles concentration, particle material, size and shape, base fluid material, surfactants/additives composition and concentration and temperature [8, 69]. Moreover, it should be noted that most suspension properties are obtained from experiments and there is no comprehensive theory that covers all the dominant parameters such as particle concentration, particle material and particle size [8]. For predicting suspension properties, there are some empirical and theoretical correlations but most of them are applied under specific conditions and parameters [8, 69].

The density of suspension (ρ) is given by:

$$\rho = \left(1 - \alpha_p \right)\rho_l + \alpha_p \rho_p \tag{2.17}$$

and

$$\alpha_p = \frac{V_p}{V_p + V_l} \tag{2.18}$$

where ρ_l, ρ_p ,α_p, V_p and V_l are base liquid density, particle density, particle volume fraction, particles volume and base liquid volume, respectively [69].

Regarding the suspensions viscosity, it is greater than that of base fluid in general, and it depends mainly on particle volume fraction [8]. Einstein's equation is the first equation proposed for suspension viscosity (μ) in terms of the base fluid viscosity (μ_0) and (α_p) as shown in equation (2.19).

Einstein's equation:

$$\mu = \mu_0 \left(1 + 2.5\, \alpha_p \right) \tag{2.19}$$

Many correlations based on Einstein' formula are proposed such as Einstein-Batchelor's and Thomas's equations. The application of all of these equations is limited to Newtonian behavior and the particle size in micron and submicron scale in addition to applying for dilute suspensions ($\alpha_p \approx 1\%$) [8, 70].

A common correlation for suspension viscosity is the Krieger-Dougherty equation,

$$\mu = \mu_0 \left(\frac{1}{1 - \alpha_p / \alpha_{p_m}} \right)^2 \qquad (2.20)$$

where, α_{p_m} is the maximum packing volume fraction that should be selected appropriately [70]. For dilute and dense flows, the Krieger-Dougherty equation can give reasonable results [8, 70]. Regarding the viscosity of the nanofluids, all proposed equations are applied under limited conditions [8, 69].

Regarding the suspension surface tension calculation, there are a few experimental resources available in the literature. Generally, the equilibrium (static) surface tension is influenced by the particle size, particle material (wettability), volume fraction, base fluid material, surfactant and temperature [71]. By adding materials such surfactants, the static surface tension value of the resultant liquid is decreased from the value of its pure liquid as the surfactants adsorb at the interface [17, 19, 20]. The effect of adding very fine particles to a liquid is not clear yet to increase or decrease surface tension even in experimental results [17, 71]. For example, adding hydrophobic (non-wetting) particles to a fluid usually reduces the surface tension because hydrophobic particles are able to reach and adsorbed to the gas-liquid interface [8, 72]. Furthermore, when hydrophilic (wetting) particles are added to a fluid, the surface tension slightly

changes from its pure fluid value (the deviation is usually less than 5%) because the hydrophilic particles do not collect or adsorb at the gas-liquid interface [8, 17, 72]. Furthermore, adding surfactant to the suspension liquid can change the surface tension remarkably.

Although the dynamic surface tension is shown to be more appropriate than static surface tension for investigating the atomization of surfactant and suspensions solutions [23, 73], the literature relevant to suspensions is very poor. In addition, this limited literature focused mainly on studying the dynamic surface tension of coal water slurry (CWS) such as Kihm and Deignan [23] and Yuan et al. [73]. The dynamic surface tension of suspensions needs more effort to explore its effect on the characteristics of the atomization process.

2.3.2 Atomization

Generally, it is found that the solid particle size in the suspension has the main influence on the separation of the solid particles from liquid and controlling the resulting droplet size in the suspension spray. Son and Kihm [74] investigated the effect of coal particle size on coal water slurry (CWS) atomization by using different particle sizes. They found that atomization of slurry with smaller coal particle size produces larger droplets than that containing larger particles. They attributed this result to the increasing slurry viscosity and the increase of the capillary force between the particles with decreasing particle size. Dombrowski and Fraser [75] studied the stability of liquid sheets with suspended solid particles. They found that the particles had no influence on the breakup if they are wet by the liquid but using hydrophobic particles resulted in perforation of the sheet.

In contrast to pure liquid, there is lack of studies which investigate the effervescent atomization of suspensions. Jedelsky et al. [76] performed experiments on light heating oil loaded by suspended solid spherical particles with large size in the range of 1 to 1.5 mm and mass concentration of 10%. The results showed that the atomization of suspensions with large particles is similar to that of pure liquid and the effect of the suspended solid particles on the final spray is negligible. A similar result was obtained by Mostafa et al. [77]. They found that the results of the effervescent atomization of coal water slurry (CWS) having larger coal particles are closer to the results of the pure water than that having smaller coal particles. Mulhem et al. [68, 78] investigated the suspension atomization using a twin fluid atomizer. They concluded that when the suspended solid particle size exceeds a critical value, the solid particles are separated more from the liquid. The complete solid-liquid separation in the suspension spray may be achieved, where the pure liquid drops are significantly smaller than the separated solid particles. Ochowiak et al. [79] concluded that the droplet size is influenced by GLR while independent of suspended particles.

For suspensions liquids, many types of atomizers are used but the solid particles in the liquid may be agglomerated. As a consequence, this leads to the problem of atomizer clogging during the spraying process. Using effervescent atomizer was found to be a good option to solve the clogging problem [52, 76]. As shown in the literature review, studying of effervescent atomization of suspensions, whether in a quiescent or in a cross flow, is still a poor area of research. Only few relevant studies were found in the literature and more experimental and analytical investigation are needed. Next chapter presents an experimental investigation of effervescent atomization of suspensions in a cross flow of air.

Chapter 3

Effervescent Atomization in Cross flow

In this chapter, the effervescent atomization of water and suspensions injected into a crossflow of air are investigated experimentally. Hydrophilic and hydrophobic particles suspended in distilled water have been used in the tests. The experiments have been carried out at different liquid-to-gas momentum flux ratios (q) and gas to liquid mass ratios (GLR). Air, at atmospheric conditions with different velocities, is used as the gaseous cross flow in an open circuit wind tunnel. Flow visualization is carried out on the liquid sprays using shadowgraphy technique. Image processing has been performed to extract information regarding the spray features such as penetration height and jet trajectory. In this study, the penetration height is represented by the windward trajectory of the spray in the crossflow.

3.1 Experimental Methodology

3.1.1 Experimental Setup

The experiments were performed inside an open loop subsonic wind tunnel with a test section with a square cross-section of 0.1 × 0.1 m and length of 1.2 m. The test section is made of clear acrylic to allow optical access for flow visualization and imaging. The environmental air is blown into the wind tunnel by a 1.5 hp blower fan made by Brook Crompton (Canada). The velocity of the air can be changed by altering the rotational speed of the fan motor. The air velocity inside the test section can reach up to 42 m/s. The air velocities in the test section are measured by Pitot Tube Anemometer of type EXTECH-HD350 with an accuracy of 1%. In addition, the air velocities in the test section were characterized by Particle Image Velocimetry (PIV) measurements of a very fine spray in order to verify the measured values. The results showed a coincidence between the two methods of velocity measurements. Moreover, the PIV measurements showed that the air velocity is parallel and constant at each axial location in the test section except the narrow boundary layers on the wall, which are less than 5 mm thick on each side. Therefore, the air axial velocity can be considered uniform in the liquid jet's upstream. An effervescent injector of 1mm exit diameter is used in the experiments and mounted vertically on the top of the test section at an axial position of 0.2 m from its inlet plane. The center of the injector diameter lies on the symmetry plane of the test section. A schematic drawing for the wind tunnel and test section is illustrated in figure (3-1). The liquid and aerating gas injection circuit consists of air supply line from a central pressurizing compressed air which provides the atomizing gas. In addition, the air from this line is connected to a pressure tank made of stainless steel in which the tested liquid is filled in. The test liquid is pressurized by the compressed air from this feed line before each experiment. The liquid and aerating gas (air) volumetric flow rates are controlled by

pressure regulators and measured by two different flow meters. The measured liquid flow rate is used to calculate the liquid injection velocity based on the injector exit diameter. In order to have different GLRs in this study, the volume flow rate of the liquid has been kept constant while changing the air flow rates. A schematic drawing for the injection and aerating circuit is shown in figure (3-2).

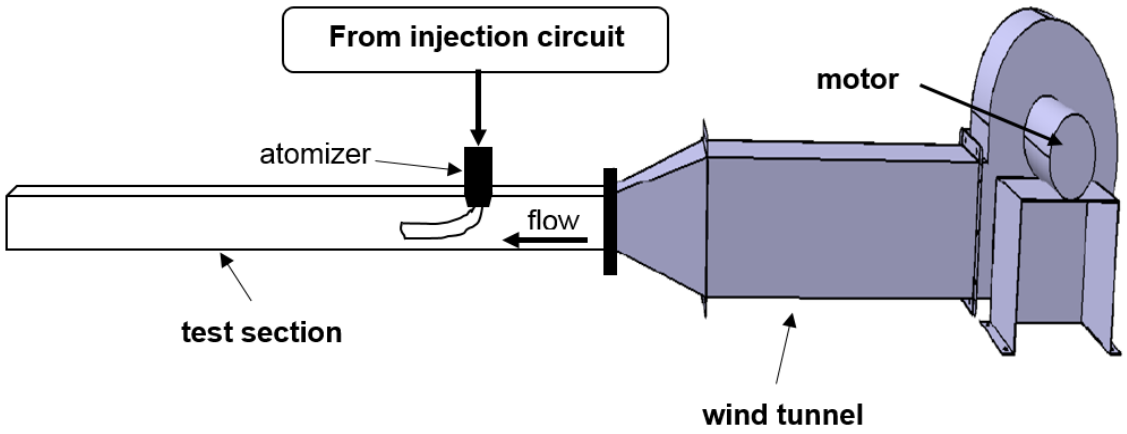

Figure 3-1: Schematic of the wind tunnel illustrating the test section.

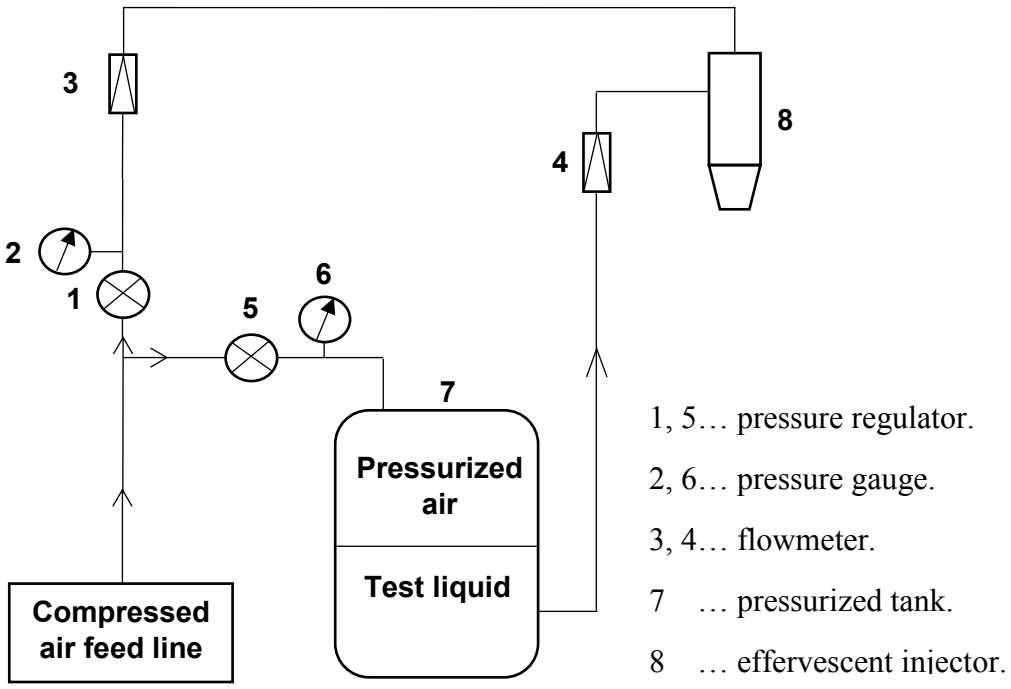

Figure 3-2: Schematic of the liquid injection and aerating circuit.

3.1.2 Liquid Preparation and Physical Properties Measurement

Before performing the experiments, the samples of liquids under test should be well prepared to get more appropriate results. The liquids used in this experimental investigation are distilled water, a solution of suspended glass particles in distilled water at concentrations 1.5, 5, and 10% (per weight) and a solution of suspended titania particles in distilled water at concentrations 1.5 and 5%. In case of titania particles, the experiments were carried out twice. First, the tests were done without adding a surfactant to the solution. Then, the experiments were repeated at the same concentrations of the suspended particles but with a surfactant added to the mixture. The glass particles are solid soda lime glass microspheres with an average size of 3-6 μm and density of 2.5 g/cc, purchased from Cospheric LLC (USA). The titania particles are methicone treated titanium dioxide with an average size of 0.7 μm and density of 3.95 g/cc, purchased from TKB Trading LLC (USA). It should be noted that the glass particles are hydrophilic while the titania particles are treated to be hydrophobic according to the suppliers. The surfactant used in the tests is Triton X-100, or TX-100 (octyylphenoxyethanol), purchased from Sigma-Aldrich Canada Co.

The suspension liquid sample had been prepared by adding the suspended particles gradually to the distilled water while homogenized by the magnetic stirrer which provides high rotation mixing. In order to ensure proper dispersion of the particles within the sample and avoid sedimentation and agglomeration, an ultrasonic liquid mixer (sonicator QSonica -Q700) was used inside the suspension liquid for about 40-60 min. In case of adding a surfactant, the same steps are followed except that the surfactant, TX-100, is added to the distilled water before the addition of the solid particles. It should be noted that the concentration of Triton X-100 used in the tests is 0.5%. This surfactant concentration is selected to be above 0.024% which is its critical micelle

concentration (CMC). The critical micelle concentration (CMC) is the concentration above which the equilibrium surface tension is approximately constant at its minimum value as the concentration is increased as illustrated in figure (3-3). Usually, the surfactant concentration used in such processes is selected to be at or above the CMC [17].

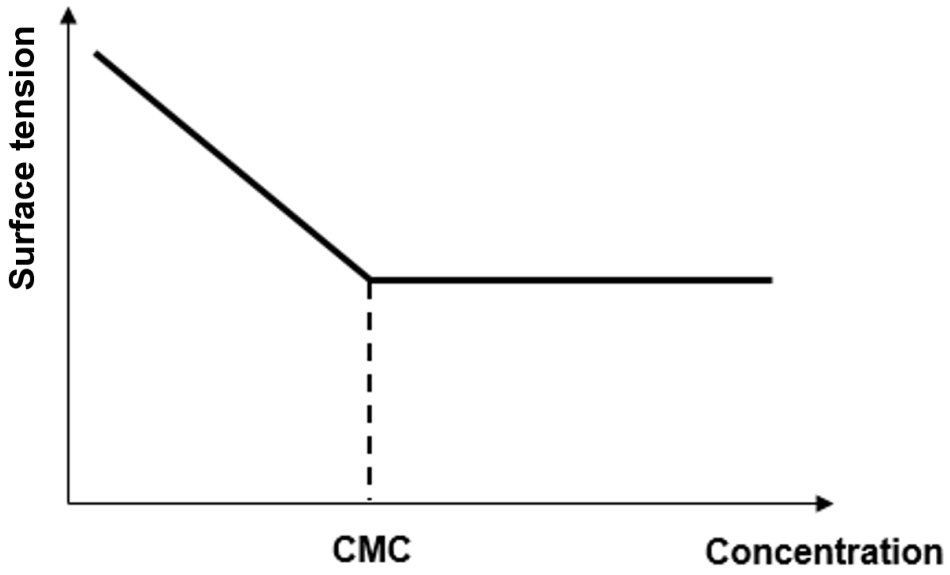

Figure 3-3: The variation of surface tension with concentration of a surfactant.

After obtaining a stable suspension liquid, its properties such as density, viscosity and surface tension are measured or calculated as follows.

a- <u>Density</u>

The density of suspension liquids (ρ) is calculated from equation (3.1) [69].

$$\rho = (1 - \alpha_p)\rho_l + \alpha_p \rho_p \qquad (3.1)$$

where ρ_l , ρ_p , α_p are the base liquid density, particle density and the particle volume fraction, respectively. Particle volume fraction is the ratio of particles volume to the total volume of solution or mixture as illustrated in equation (3.2) to (3.4).

$$\alpha_p = \frac{V_p}{V_p + V_l} \tag{3.2}$$

$$V_p = \frac{m_p}{\rho_p} \tag{3.3}$$

$$V_l = \frac{m_l}{\rho_l} \tag{3.4}$$

V_p, m_p, V_l and m_l are the particles volume, particles mass, base liquid volume and base liquid mass within the solution, respectively. It should be noted that in case of adding surfactant, the resultant solution density is fairly not affected because the used surfactant quantity is very small and can be neglected in mass calculation.

b- <u>Viscosity</u>

The viscosity (μ) is measured by Cannon-Fenske Opaque capillary viscometer (Model no. 9721F53-size 50) with an accuracy of 0.25% as shown in figure (3-4). For each sample, the measurements are performed two to three times to confirm repeatability.

Figure 3-4: Cannon-Fenske Opaque viscometer (Model no. 9721F53-size 50).

*c- **Static surface tension***

The static surface tension (σ_{st}) is measured by du Nouy ring method. In this method, a ring, usually made of iridium or platinum, is dipped into the studied liquid, and then removed slowly until detachment from the liquid occurs [80]. The maximum force measured in this case is the sum of the weight of the ring and the static tension force that acts on the perimeter of the ring. The used tensiometer is FISHER SCIENTIFIC - model 21 with accuracy of 0.5% as illustrated in figure (3-5). For each sample, the measurements were performed four times to confirm repeatability.

Figure 3-5: Du Nouy ring tensiometer (FISHER SCIENTIFIC - model 21).

3.1.3 Test Conditions

For each liquid, the tests are performed at four different momentum flux ratios (q) for four different gas to liquid ratios (GLR). Therefore, the test matrix for each liquid is composed of sixteen experiments. In all tests, the liquid flow rate is kept constant. For changing q, only the air velocity in the test section is changed. For obtaining different GLRs, only the air flow rate varied. The air flow rate is controlled by a flowmeter of type (Key Instrument-model no. Ki-1G08 R3) with an accuracy of 3%. The air flow rate varies from 0 to 7.4×10^{-5} m^3/sec. The liquid flowrate is kept at 1.28×10^{-6} m^3/sec. The liquid flow rate is controlled by a flowmeter of type (Aalborg-model no.PMR1-010972) with an accuracy of 2%. Additionally, the liquid flow rate is confirmed by manual volumetric measurement and the error is found to be within the accuracy range of the flowmeter. All experiments were carried out at room temperature, 24° C. Table (3-1) summarizes all the properties and the test conditions for all liquids under study.

Table 3-1: Experimental tests conditions

Liquid	ρ (kg/m3)	μ (Pa.s)	σ_{st} (N/m)	We_1	q_1	q_2	q_3	q_4	We_{g1}	We_{g2}	We_{g3}	We_{g4}	GLR_1 %	GLR_2 %	GLR_3 %	GLR_4 %
Water	997	0.0009	0.074	35.8	10.57	4.7	2.60	1.73	3.38	7.51	13.7	20.6	0	2.39	4.70	7.1
Water- 1.5% Glass	1006	0.001025	0.076	35.2	10.67	4.8	2.63	1.75	3.29	7.31	13.3	20	0	2.37	4.66	7.0
Water - 5% Glass	1028	0.001089	0.071	38.5	10.9	4.9	2.68	1.78	3.52	7.82	14.3	21.5	0	2.32	4.56	6.8
Water - 10% Glass	1060	0.00118	0.066	42.7	11.20	5.0	2.77	1.84	3.79	8.42	15.4	23.1	0	2.25	4.40	6.7
Water - 1.5% Titania	1008.3	0.00091	0.073	36.7	10.69	4.82	2.63	1.75	3.42	7.61	13.9	20.9	0	2.37	4.60	7.0
Water – 5% Titania	1035.4	0.000922	0.064	43	10.98	4.90	2.70	1.80	3.9	8.68	15.8	23.8	0	2.31	4.50	6.8
Water – 1.5% Titania - 0.5 % TX-100	1008.3	0.00093	0.039	68.7	10.69	4.82	2.63	1.75	6.42	14.2	26.	39.1	0	2.37	4.60	7.0
Water - 5% Titania - 0.5% TX-100	1035.4	0.00095	0.0355	77.5	10.98	4.90	2.70	1.80	7.05	15.6	28.6	43	0	2.31	4.52	6.8

3.2 Shadowgraphy and Image Processing

Shadowgraphy has been carried out by a high speed camera (Photron SA1.1, USA) and a diffused backlight source to illuminate the spray as shown in figure (3-6). The camera is mounted at 3D traverse and the backlighting was done by a halogen lighting. To make the background light more homogenous, a vellum paper is put in front of the light as a light diffuser. In order to have images with good contrast, even for the smallest droplets, the images were captured at 250 frames per second and the shutter speed was set at 12.2 µsec. In case of GLR = 0, the shutter speed was set at 29.3 µsec. A commercial software (Photron FASTCAM Viewer, from Photron, USA) is used to capture and store the raw images to a computer.

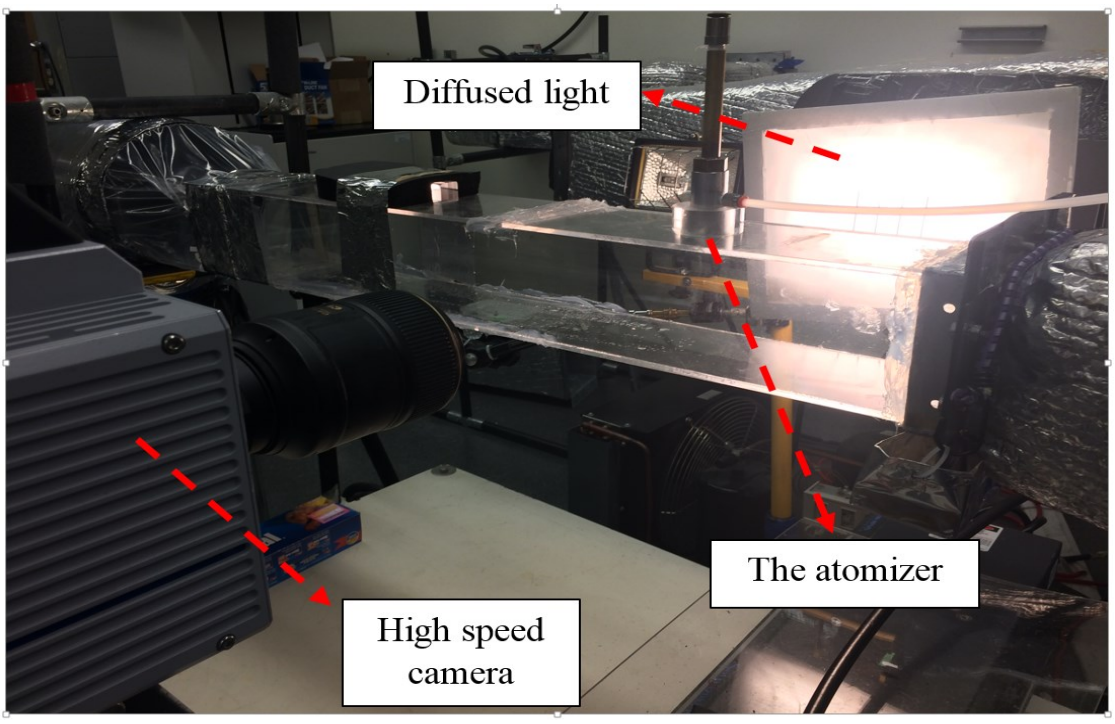

Figure 3-6: Shadowgraphy setup.

Before running the tests, an image was taken for a calibration grid which was placed vertically at the same plane of measurement (the atomizer axis) as illustrated in figure (3-7). Moreover, using this calibration grid helped in obtaining the best resolution of the resultant images as well as the scale value is calculated.

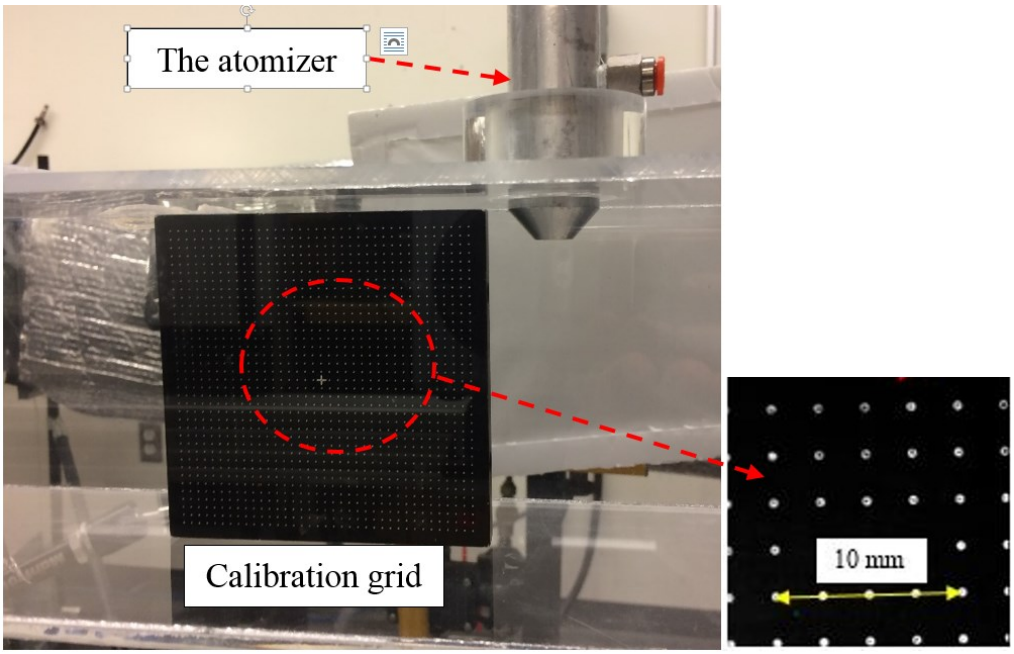

Figure 3-7: Image calibration.

For each test, a set of 500 images were captured. Then, these images were superimposed to get the average spray image. In addition, 500 images were captured for the background in absence of the spray and averaged too. In order to reduce the background noise from the spray image, the average background image was subtracted from the average spray image. After background subtraction, a threshold of 90% (i.e. 10% light cut-off threshold) was applied to the resultant image to determine the spray boundary. This threshold is used to reduce the noise without

significantly affecting the analysis of spray penetration height and selected based on similar studies reviewed in the literature [44, 67]. Image averaging, background subtraction and thresholding were done using ImageJ software.

Boundary tracing was applied to the windward trajectory of the thresholded image to determine the normalized penetration height of the spray (*y/d*). The tracing was done by manually selecting 30-40 points along the windward trajectory. PlotDigitizer software is used to digitalize the manually picked points. In this study, the measurements of penetration height were carried out up to the normalized downstream location (*x/d*) of the highest drop in the spray. In the present study, the liquids were sprayed in the gravity direction but for appropriate calculations, the coordinate system illustrated schematically in figure (3-8) is used.

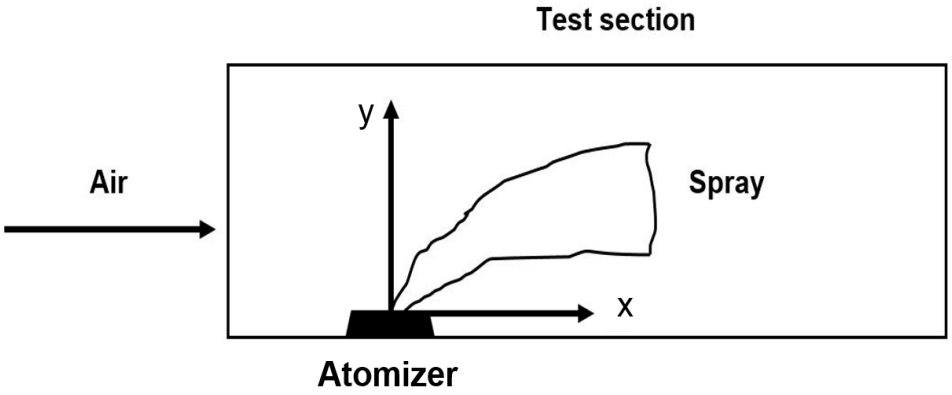

Figure 3-8: The measurement coordinate system.

The sequence of image processing and boundary tracing is illustrated by an example in figure (3-9). The case shown in the figure is associated to water at GLR=7.1% and q= 1.73.

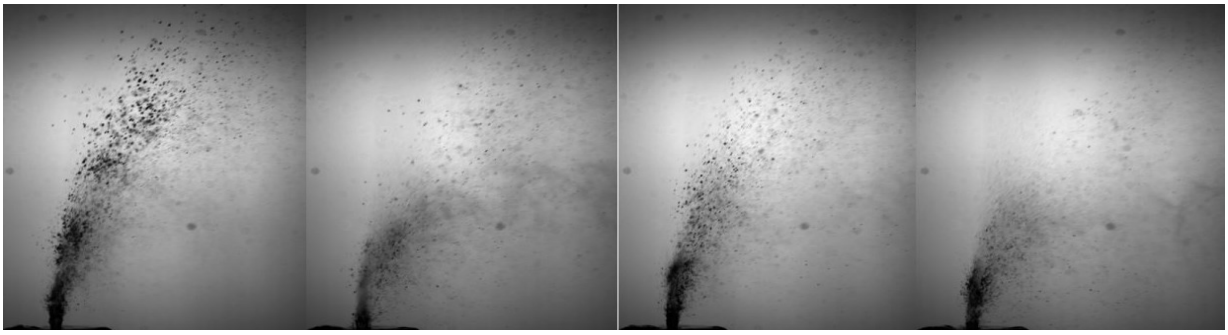

a) Samples of instantaneous images.

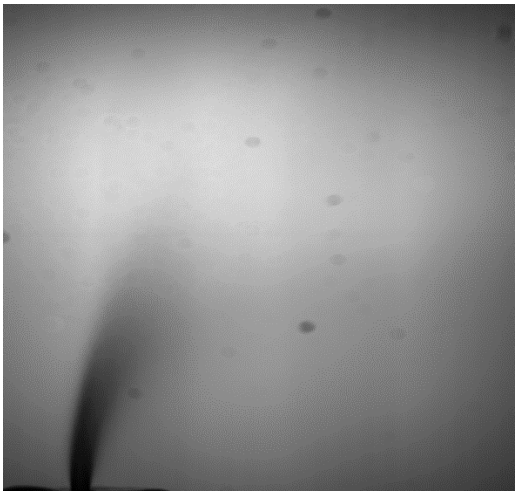

b) Average image.

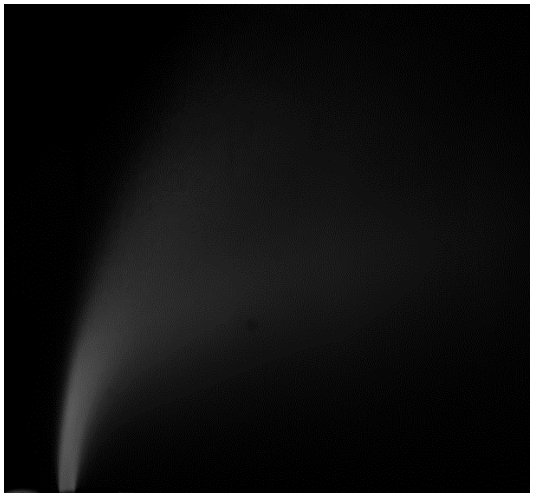

c) After background subtraction.

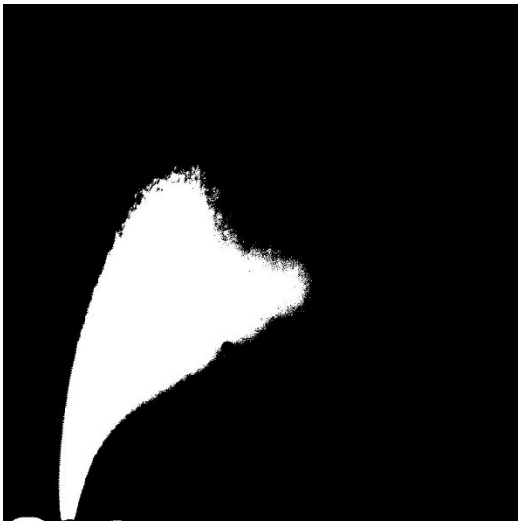

d) Thresholded image.

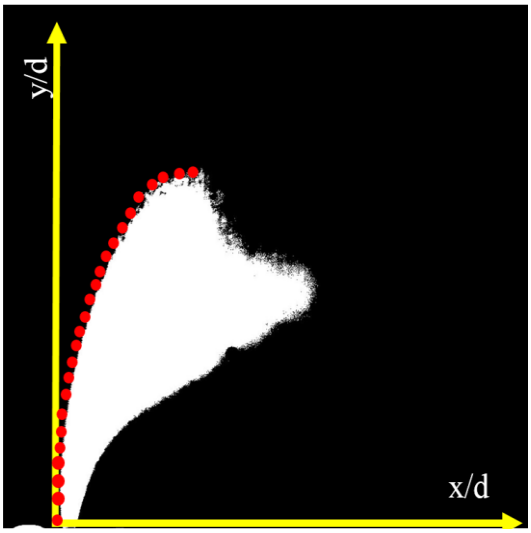

e) Boundary tracing.

Figure 3-9: Sequence of image processing and boundary tracing.

3.3 Results and Discussion

3.3.1 Spray Visualization

Flow visualization was carried out using shadowgraphy to investigate the behavior of the spray in the cases of non-aerated liquid jet (GLR=0) and aerated liquid jet (GLR≠0).

a- Non-aerated liquid jet (GLR = 0)

Figure (3-10) shows the breakup processes in the liquid jet of all studied liquids for GLR= 0 at different q and associated crossflow Weber number (We_g) as listed in table (3-1). In figure (3-10.a), it can be observed that breakup mode in cases (1) to (6) is the column breakup regime where $We_g < 4$. Although they have the same q, the breakup mode in cases (7) and (8) changes to the bag breakup regime. In these two cases, the surface tension is decreased significantly due to the effect of surfactant added to suspension liquid, resulted in increasing We_g to the range of bag breakup regime, $4 < We_g < 30$. Through figures (3-10.b) to (3-10.d), the bag breakup mode can be seen to be the dominant breakup regime because We_g of these cases lies between 4 and 30. Furthermore, it can be observed when We_g approaches or gets higher than 30, the multimode breakup regime appears at which some liquid ligaments are formed beside bags. These results show a good agreement to the jet breakup regimes in cross flow categorized by Sallam et al. [30], as mentioned in the literature review.

From the results, it can be noticed that the breakup regime can be changed by controlling We_g which is influenced by liquid surface tension. As shown in table (3-1), a significant change in the solution surface tension can be obtained by adding a surfactant and not suspended solid particles, at least at the studied test conditions range. As a conclusion, the effect of suspended

particles on the breakup regimes in a cross flow of gas at GLR=0, can be neglected in the range of the investigated operating condition and particle concentrations.

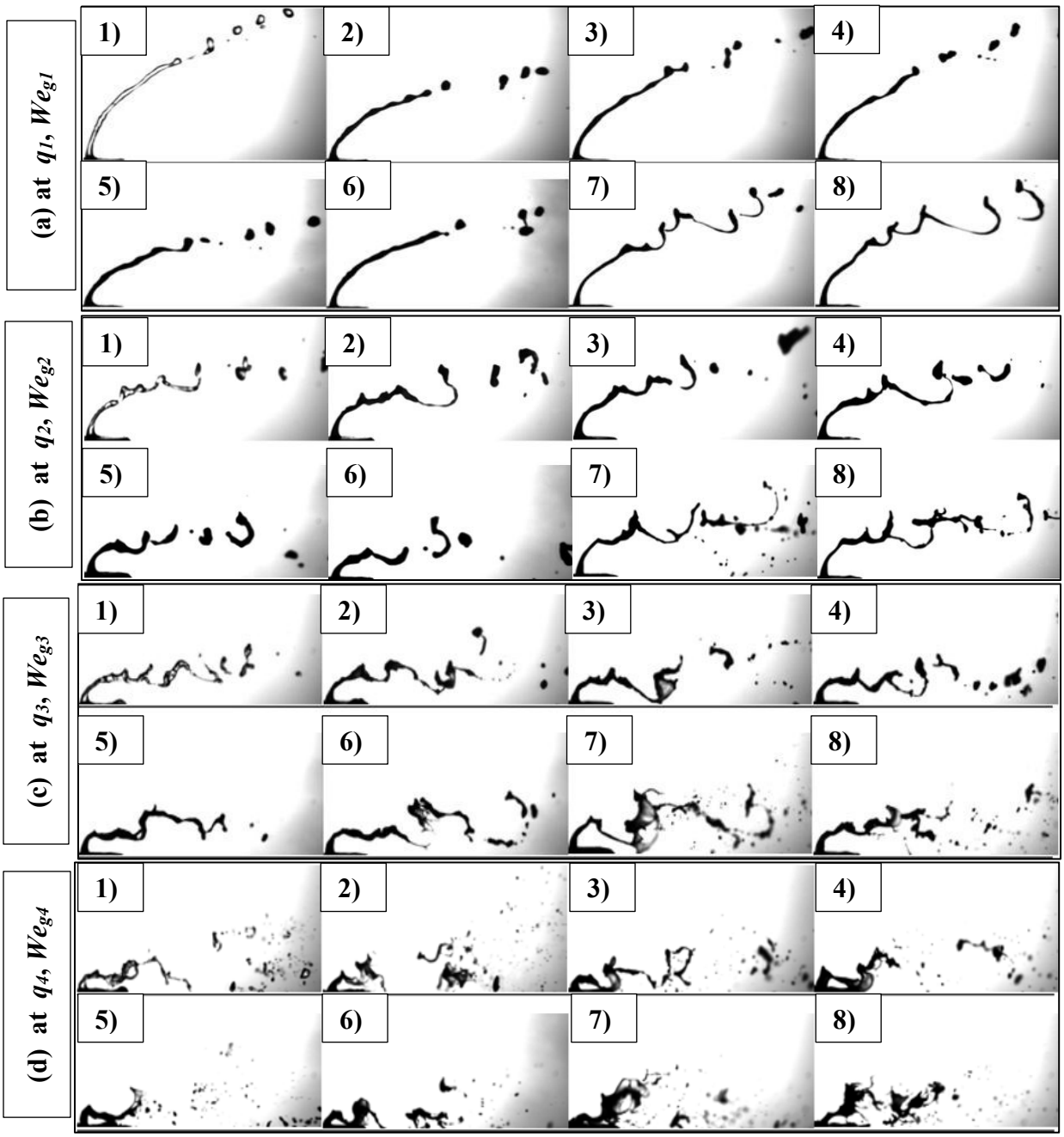

Figure 3-10: Shadowgraphy images of non-aerated (GLR=0) liquid jet at different liquid-to-gas momentum ratios (q);
(1) water, (2) water-1.5% glass, (3) water-5% glass, (4) water-10% glass,
(5) water-1.5% titania, (6) water-5% titania,
(7) water-1.5% titania-0.5% TX-100, and (8) water-5% titania-0.5% TX-100.

b- Aerated liquid jet (GLR ≠ 0)

Figure (3-11) shows the breakup of the liquid jet of some investigated liquids for different GLRs at $q = q_4$ (see table (3-1)). For all cases, the liquid flow rate is kept constant and only the air flow rate is changed. Generally, as can be seen in figure (3-11), the spray penetration height increases when the liquid jet is aerated for all liquids. Furthermore, spray penetration height is increasing by increasing the aeration level. It can be explained as follows; for atomizing a constant amount of liquid by an effervescent atomizer, the thickness of the liquid film decreases by increasing the amount of aerating gas, i.e., GLR. As a consequence, the liquid film velocity increases leading to increasing the effective jet to air momentum flux ratio of the aerated liquid jet with increasing GLR. Therefore, the spray can penetrate deeper into the air cross flow. At the same flow conditions, the effective momentum flux ratio for the aerated liquid jet is higher than that of the non-aerated liquid jet, while it is found to be difficult to quantify. Nevertheless, it has been shown that the momentum flux ratio of the non-aerated liquid jet can be used as the baseline momentum flux [67].

At GLR=2.4%, the liquid column is shown to have a rougher surface than that of the related non-aerated liquid jet. This change in appearance is resulted from the injected air that occupies spaces inside the liquid column and increases the perturbations. In addition, for all liquids, it can be observed that there are ligaments and large droplets within the spray plume. In cases of suspension liquids, it can be shown that the liquid trunk is almost intact for a certain streamwise distance before breakup begins. This may be attributed to the higher viscosity resulted from the suspended solid particles that delays the onset of breakup.

By further increase in GLR to 4.7% and 7.1%, the ligaments and droplets size is getting smaller. This is attributed to the structure of annular flow for the air-liquid mixture inside the

atomizer. Increasing the amount of injected air resulted in squeezing the liquid into a high speed thin annular film that attached to the atomizer wall. This high speed annular liquid film can be broken quickly and easily into smaller and finer ligaments and droplets once discharged into the air cross flow.

Generally, from the figures it can be concluded that the spray penetration height in the case of non-aerated liquid jet is very small compared to the aerated jets with the same liquid flow rate. The overall breakup process in the non-aerated jet is relatively slow and requires a considerable streamwise distance to generate a finite number of fine droplets. On the other hand, at the same flow conditions, the overall breakup process in the aerated jets is faster as well as a shorter streamwise distance is needed to produce a large number of fine droplets.

As shown in the experiments, suspension liquids with different solid particles at different properties are sprayed by the effervescent atomizer. The instantaneous shadowgraphy images show a similar behavior for atomization of pure liquid (water) and suspension liquids. In general, a higher penetration height and smaller droplets can be obtained by the effervescent atomizer. In addition, the clogging problem did not take place in spite of the presence of the suspended solid particles. It confirms the feasibility of the effervescent atomizer as a promising atomizer for atomization of variety of liquids regardless of their rheological properties.

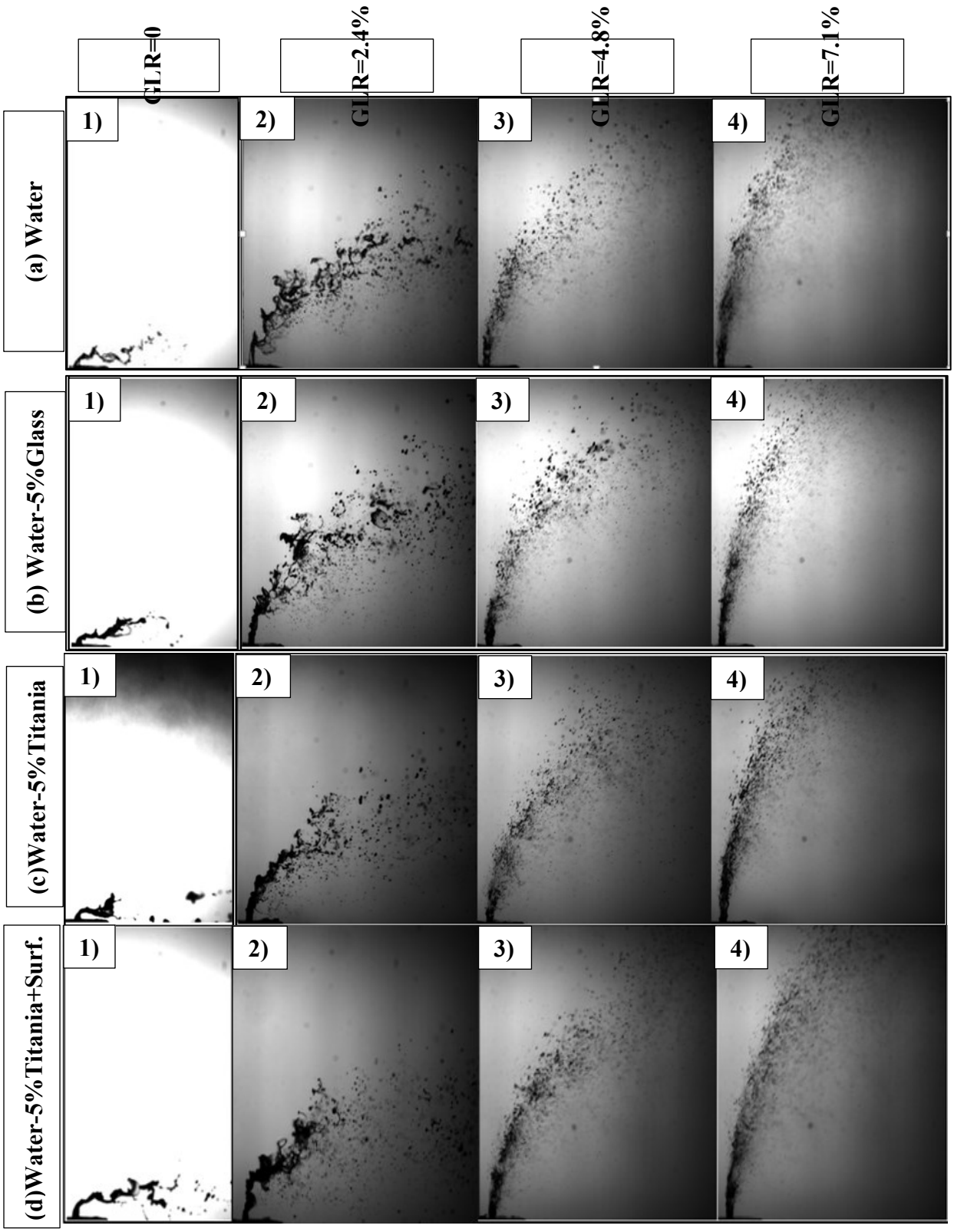

Figure 3-11: Shadowgraphy images of aerated liquid jets at $q = q_4$ and different GLR values.

3.3.2 Spray Penetration Height

For penetration height calculations, the thresholded image is used in both of the non-aerated and aerated liquid jets as described in figure (3-9).

a- <u>Non-aerated liquid jet (GLR = 0)</u>

The measurements of jet penetration height are performed up to the breaking up point at different q as illustrated in table (3-1). For all cases, this covers up to 40 diameters downstream from the atomizer, i.e., x/d ≤40. Samples of the penetration height measurements are presented in figure (3-12). As expected, the results show an increase of the penetration height of the non-aerated liquid jets with increasing momentum flux ratio (q) caused by decreasing the velocity of the air cross flow.

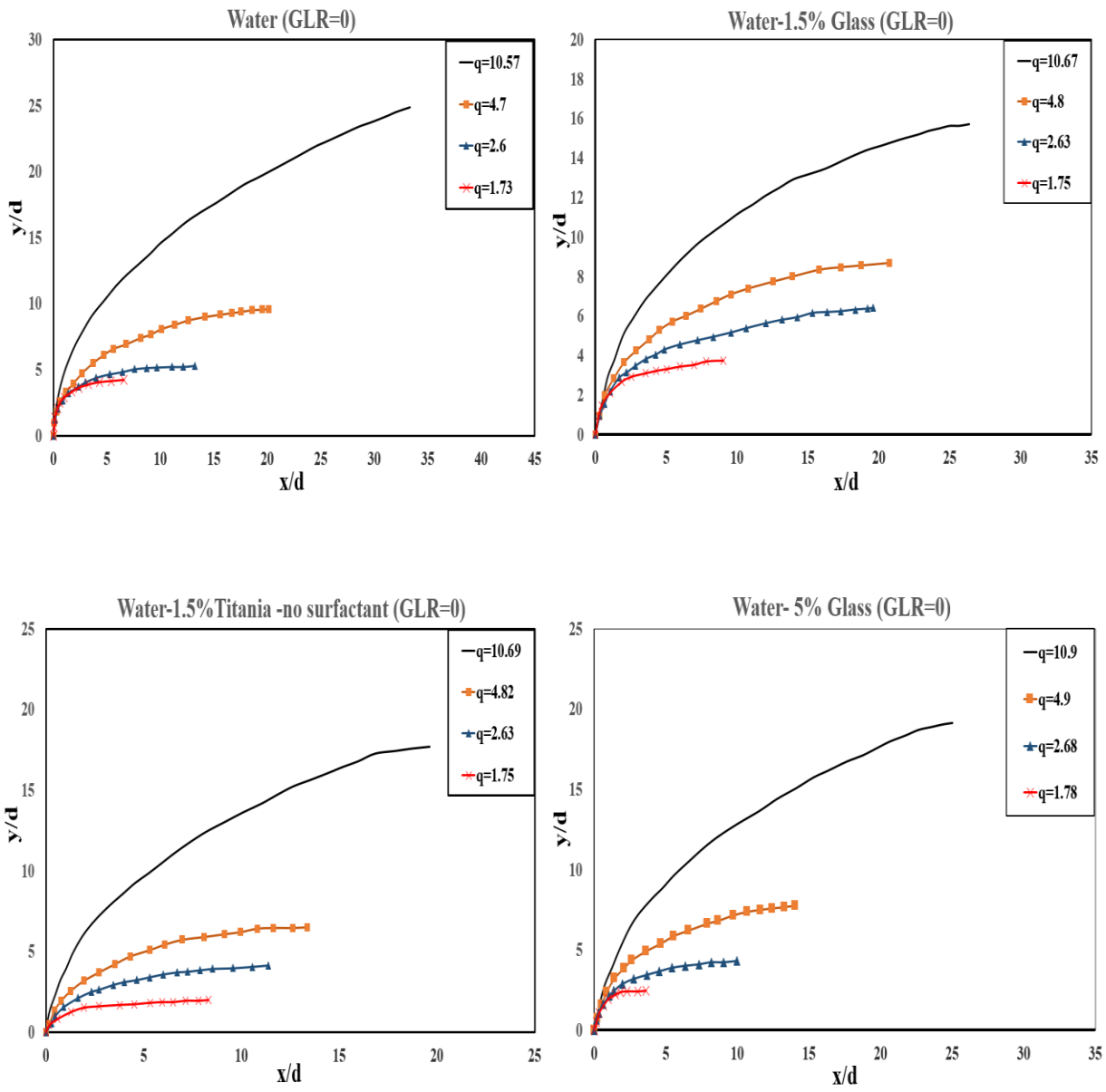

Figure 3-12: Samples of penetration height results of non-aerated liquid jets (GLR=0) at different liquid-to-gas momentum ratios (q).

As mentioned in the literature review in chapter (2), a detailed survey of the penetration height correlations can be found in work of No [39], Birouk et al.[40], Ashgriz [41] and Mashayek et al. [42]. Mainly, there are three different forms of correlations; power-law, exponential, and logarithmic. In the current study, many of these correlations were applied to find the best one that fits the present experimental results. The power model form illustrated by equation (3.5) has been found to have the best fit results.

$$\frac{y}{d} = A\, q^{b} \left(\frac{x}{d}\right)^{c} \tag{3.5}$$

Among the power-law based correlations, the correlation developed by Wotel et al. [28, 39] was found to give the closest results to the present ones as shown in figure (3-13). Wotel et al. proposed the correlation of,

$$\frac{y}{d} = 1.19\, q^{0.45} \left(\frac{x}{d}\right)^{0.45} \tag{3.6}$$

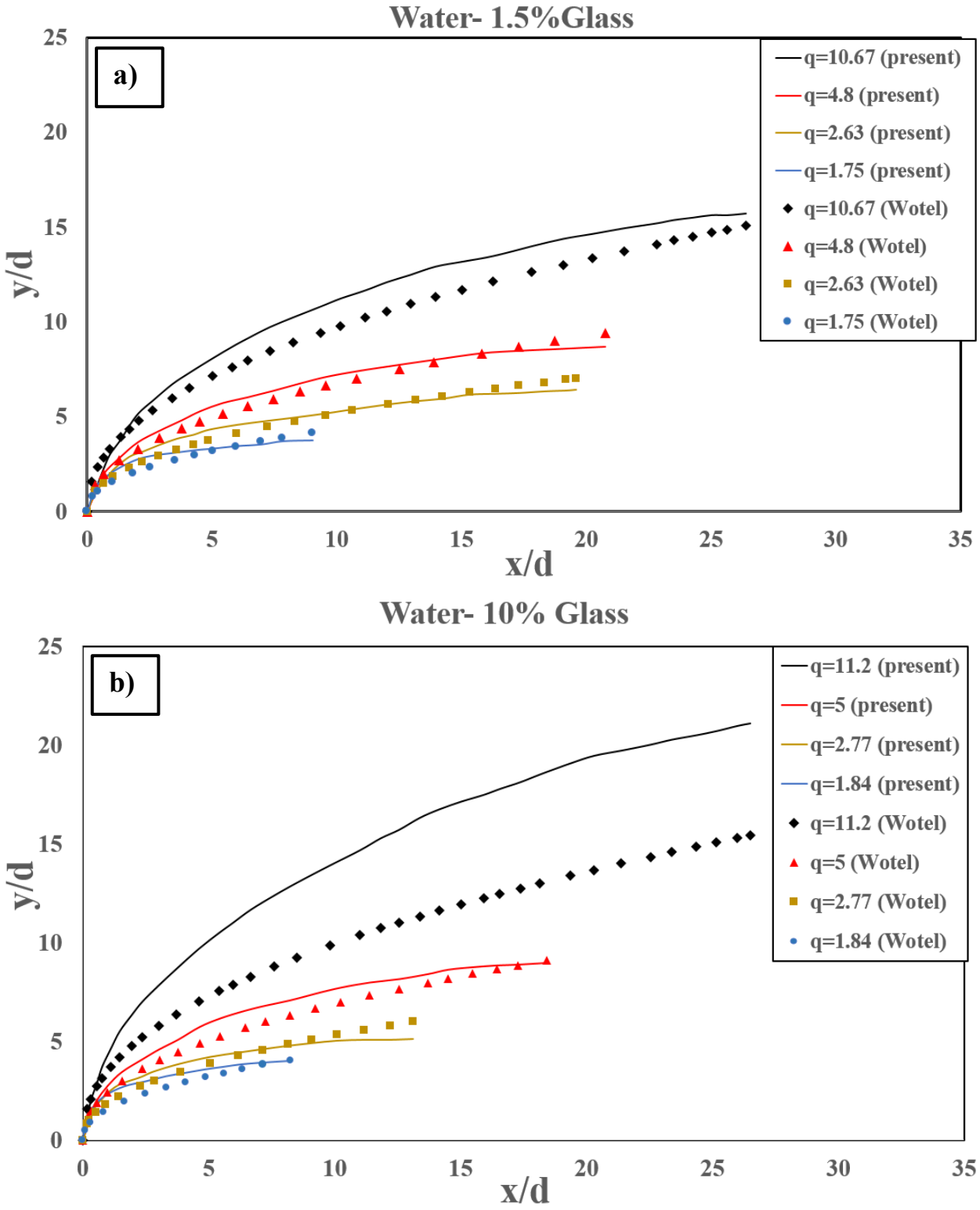

Figure 3-13: Comparison of the penetration height obtained in the present study with Wotel correlation; (a) water and (b) water-10% glass.

Therefore, in this study, new correlations are proposed based on equations (3.5) and (3.6) including the concentration of suspended solid particles (*C*). Based on the penetration heights of water and suspended glass particles only, a correlation in equation (3.7) is deduced,

$$\frac{y}{d} = (1.582\ C + 1.035)\ \ q^{0.52} \left(\frac{x}{d}\right)^{0.48} \tag{3.7}$$

where, the regression R^2 value is 0.93. The correlation results are shown in figure (3-14).

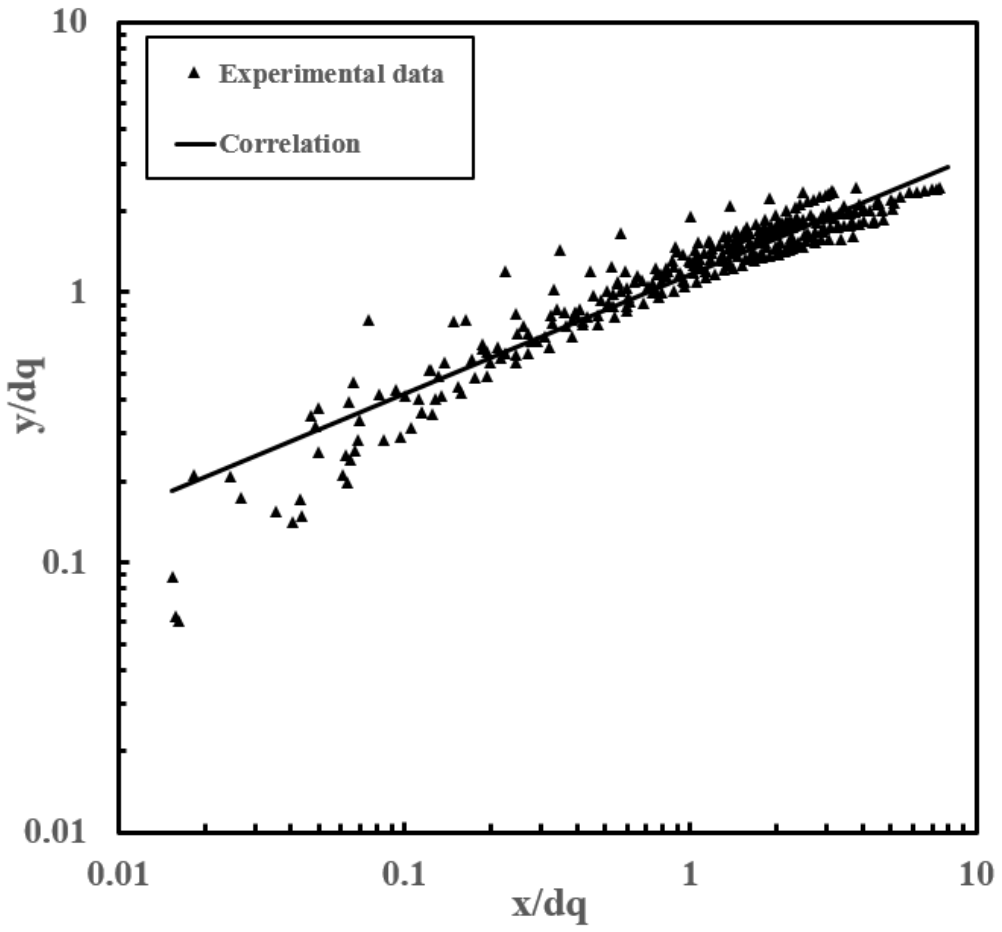

Figure 3-14: Measurements of spray penetration height of non-aerated liquid jets for water and glass particles.

By adding the penetration height results of suspended titania particles, a general correlation based on the results of water and all the suspended particles is deduced in equation (3.8):

$$\frac{y}{d} = (0.32\, e^{-(981.6\, C)} + 1.03\, e^{(1.38\, C)})\;\; q^{0.56} \left(\frac{x}{d}\right)^{0.44} \qquad (3.8)$$

where the regression R^2 value is 0.88. The correlation results are shown in figure (3-15). A comparison between the penetration height predicted by the correlation in equation (3.8) and the actual experimental values is illustrated in figure (3-16).

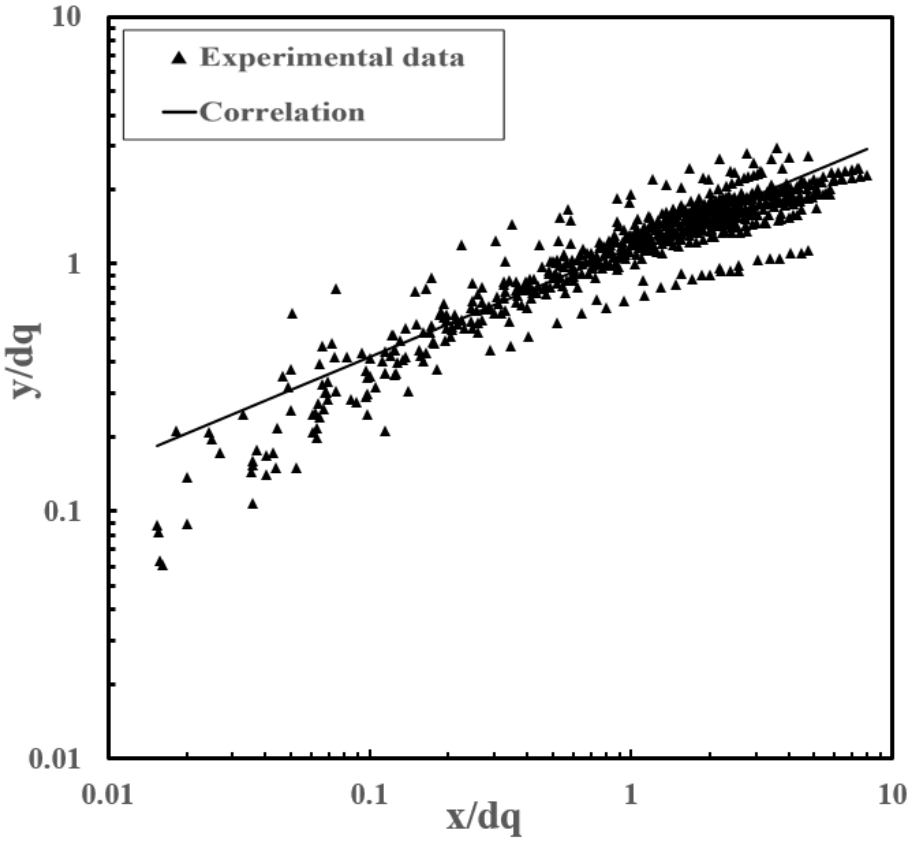

Figure 3-15: Measurements of spray penetration heights for non-aerated liquid jet (GLR=0).

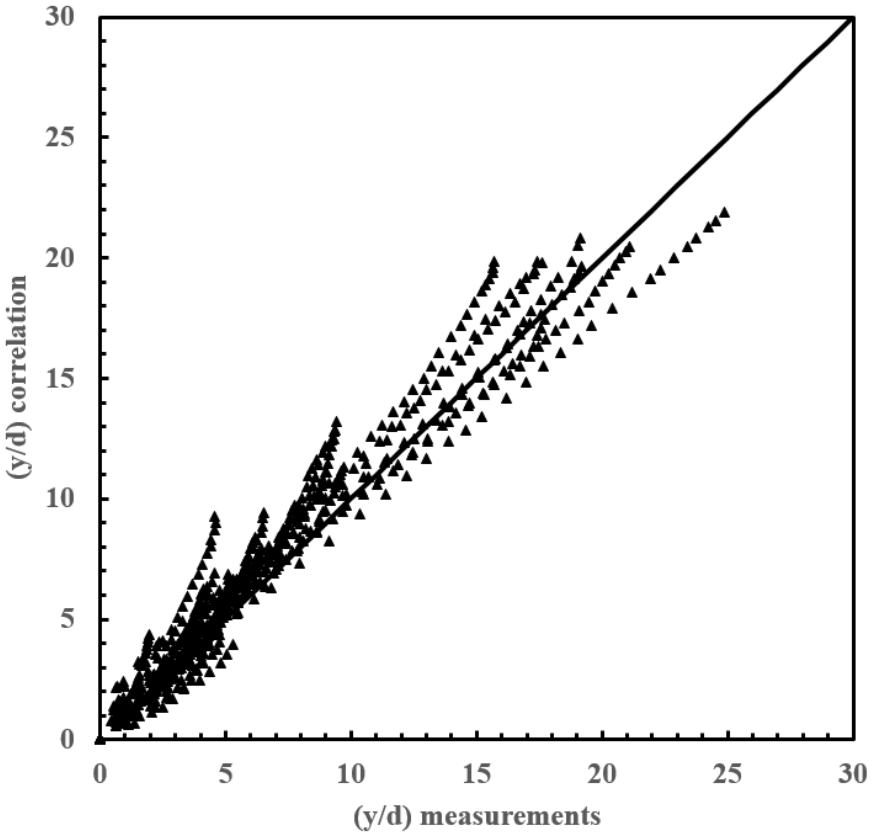

Figure 3-16: Comparison between experimental measurements and correlation predicted values of equation (3.8).

b- <u>Aerated liquid jet (GLR ≠ 0)</u>

The measurements of penetration height of aerated liquid jets are performed up to the downstream location (*x/d*) of the highest drop in the spray. For all cases, this covers up to 15 diameters distance downstream from the atomizer, i.e., $0 < x/d < 15$. Samples of the penetration height measurements for different cases are presented in figure (3-17).

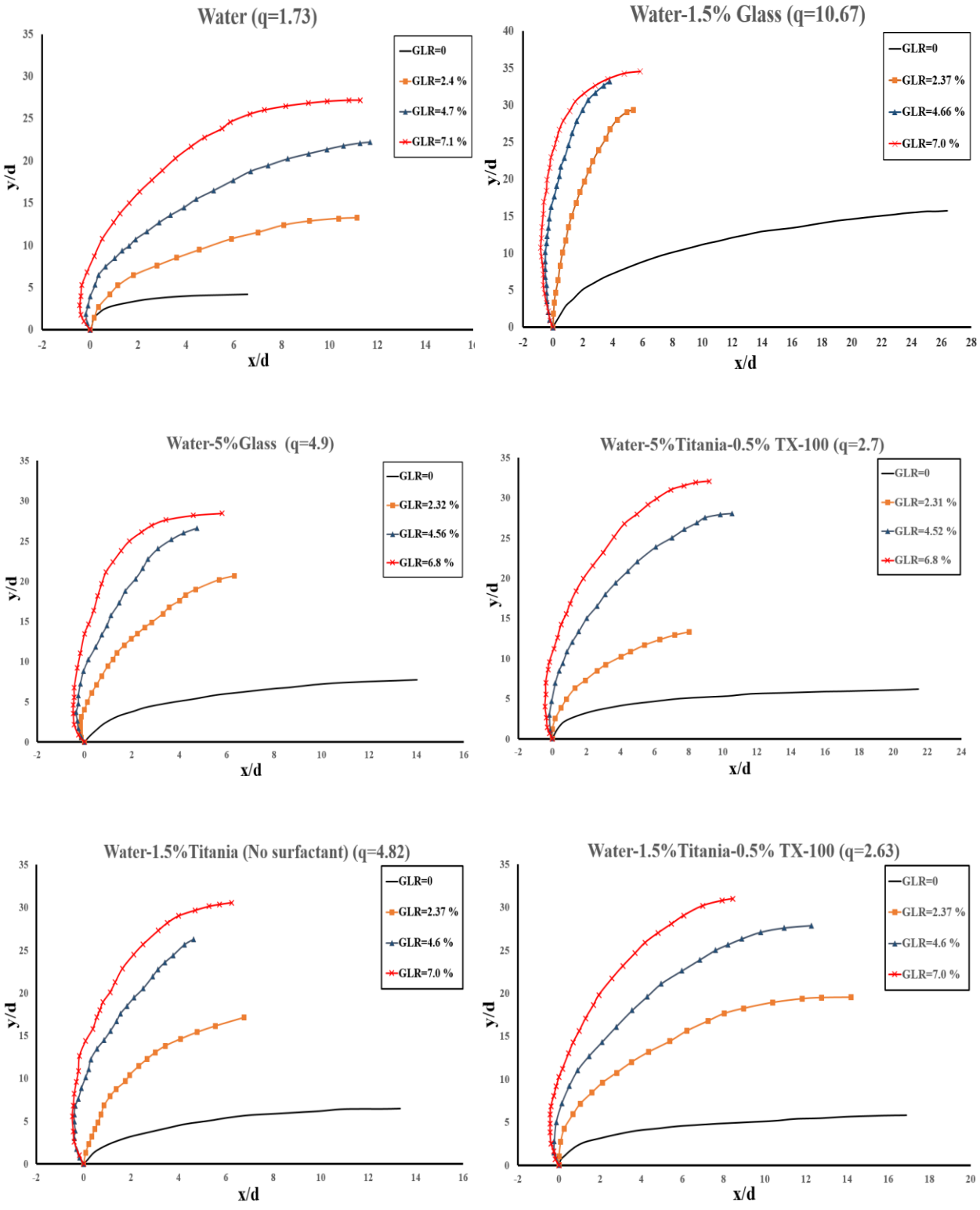

Figure 3-17: Samples of penetration height results of aerated liquid jets for different GLR and *q* values.

As can be seen in the figures, the spray penetration height in the aerated liquid jet is obviously higher than that of the non-aerated liquid jet under the same air flow conditions. Furthermore, the spray penetration height for the aerated liquid jets increases by increasing the amount of aerated gas. This increase in the spray penetration height is attributed to the increase in effective jet to air momentum flux ratio of the aerated liquid jet resulted from the accelerated thin annular liquid film inside the effervescent nozzle.

Compared to non-aerated liquid jets, the correlations of spray penetration height of the aerated liquid jets are very limited in the literature. In this work, a new correlation for deducing the spray penetration height in case of the aerated liquid jets (GLR ≠0) is developed. This correlation is a function of the non-aerated momentum flux ratio (q), the gas to liquid mass ratio (GLR), the normalized downstream distance (x/d) and the viscosity ratio (μ_l/μ_w) where μ_l and μ_w are the viscosities of the atomized liquid and the pure water, respectively. The correlation is given by equation (3.9).

$$\frac{y}{d} = 1.8\, q^{0.572} \left(\frac{x}{d}\right)^{0.428} \left(\frac{\mu_l}{\mu_w}\right)^{0.572} (GLR)^{\,0.756} \qquad (3.9)$$

for which the regression R^2 value is 0.95. The correlation results are shown in figure (3-18).

It should be noted that equation (3.8) is based on the results of suspension liquids only. If the pure water results are included, a similar correlation is deduced as shown in equation (3.10).

$$\frac{y}{d} = 1.8\, q^{0.555} \left(\frac{x}{d}\right)^{0.445} \left(\frac{\mu_l}{\mu_w}\right)^{0.555} (GLR)^{\,0.768} \qquad (3.10)$$

where the regression R^2 value is 0.94. The correlation results are shown in figure (3-19).

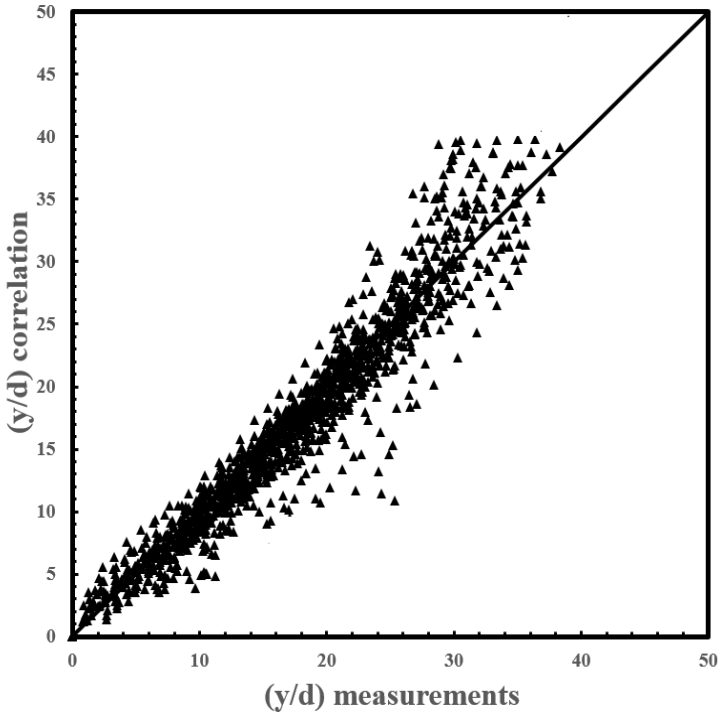

Figure 3-18: Comparison between experimental measurements and correlation predicted values for equation (3.9).

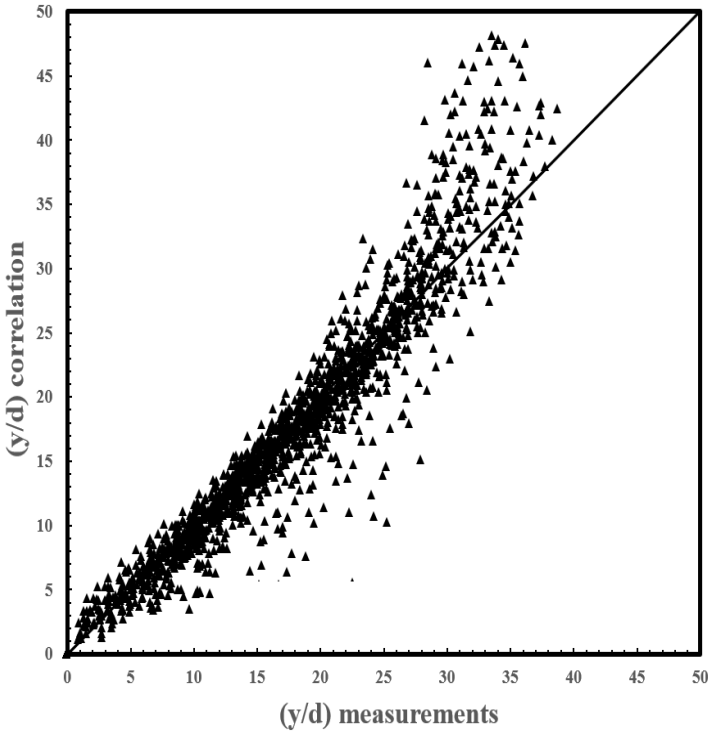

Figure 3-19: Comparison between experimental measurements and correlation predicted values for equation (3.10).

In this study, the penetration height of non-aerated and aerated liquid jets in a cross flow of air has been examined at different momentum flux ratios (q) and gas to liquid ratios (GLR). Suspension liquids with hydrophobic and hydrophilic particles at different concentrations were injected. Generally, the results show that the liquid jet aeration increases the jet penetration height due to an increase of the effective momentum flux ratio. Under the same flow conditions, the spray penetration height for an aerated liquid jet is obviously larger than that of related non-aerated liquid jet. Moreover, the spray penetration height when the liquid jets are aerated increases with increasing the GLR. No clear effect of the suspended solid particles has been noticed to influence the penetration height and breakup process of both non-aerated and aerated liquid jets except their effect on the liquid viscosity. New correlations for the penetration height of non-aerated liquid jets and aerated liquid jets in cross flow were developed. Next chapter presents an experimental investigation of the dynamic surface tension of suspension liquids.

.

Chapter 4

Measurement of Dynamic Surface Tension of Suspensions

Dynamic surface tension is an important property as it plays a crucial role in many industrial applications and processes such as fiber spinning, paper production, printing, emulsifiers, dispersants and agricultural sprays [81]. In all of these applications, dynamic surface tension should be analyzed since many changes in the surface occur before the surface tension reaches its static value [19, 81]. In the atomization process, it is important to monitor the dynamic surface tension value at the timescale of droplets formation (milliseconds) because this is the value that affects the droplets size, not necessarily the static value which attained after equilibrium [19]. Therefore, the surface tension of new interfaces on the millisecond time scale needs to be determined accurately.

There are several techniques that used for determining dynamic surface tension relevant to spray formation, including the growing drop, the maximum bubble pressure and the oscillating jet techniques [80, 82-84]. The growing drop technique is based on growing a drop at the end of a fine capillary. This method is based on simultaneous measuring of the instantaneous pressure inside the drop and its radius of curvature. The drop is assumed to be a section of a sphere. With an ultra-high-speed video camera combined with image analysis system, radius of curvature and drop pressure are determined down to 1/6 ms [85]. Then, the surface tension can be deduced by using the static Young-Laplace formula $\Delta p = 2\sigma/R$. However, Young-Laplace formula is not applicable below 20 ms because of oscillations in the drop at earlier times [83, 84].

In the maximum bubble pressure technique, a flow of gas is injected into a reservoir of the test liquid producing a stream of bubbles. The surface tension of the gas/liquid interface is deduced from measurement of the pressure value at the moment of detaching each bubble into the liquid reservoir. There are drawbacks of this technique associated to the millisecond timescale measurements related to spraying processes. First, the rate of stream of bubbles per second is limited which yields measurements for a surface age of several hundreds of second. Moreover, the bubble pressure technique is calibrated against two known systems, typically pure water/nitrogen and alcohol/nitrogen, from which the technique interpolates all other interfaces. Applying this technique to different materials may have less accuracy [82]. Among these techniques, oscillating jet technique is more appropriated for calculating dynamic surface tension on the very short timescales related to spraying process [82], as will be explained in the next section.

4.1 The Oscillating Jet Technique

The oscillating jet can be defined as a liquid/gas system in which a new free surface is created constantly. The key of utilizing this technique is the axis switching phenomena described as follows; when a fluid exits from an elliptical orifice, the initial cross section is elliptical and surface tension tries to minimize the surface area to a circular shape by decreasing the major axis and increasing the minor axis. Due to the inertia effect, the cross section overshoots the circular shape and continues to deform to become elliptical, but this time perpendicular to the initial elliptic cross section (i.e. with major axis perpendicular to that of the orifice). Further down the jet, this process continues and the cross section again approximates an ellipse, this time with major axis parallel to that of the orifice as shown in figure (4-1) [25, 86]. This oscillation between two perpendicular directions continues until either the oscillations are damped or the jet breaks up due to capillary instability.

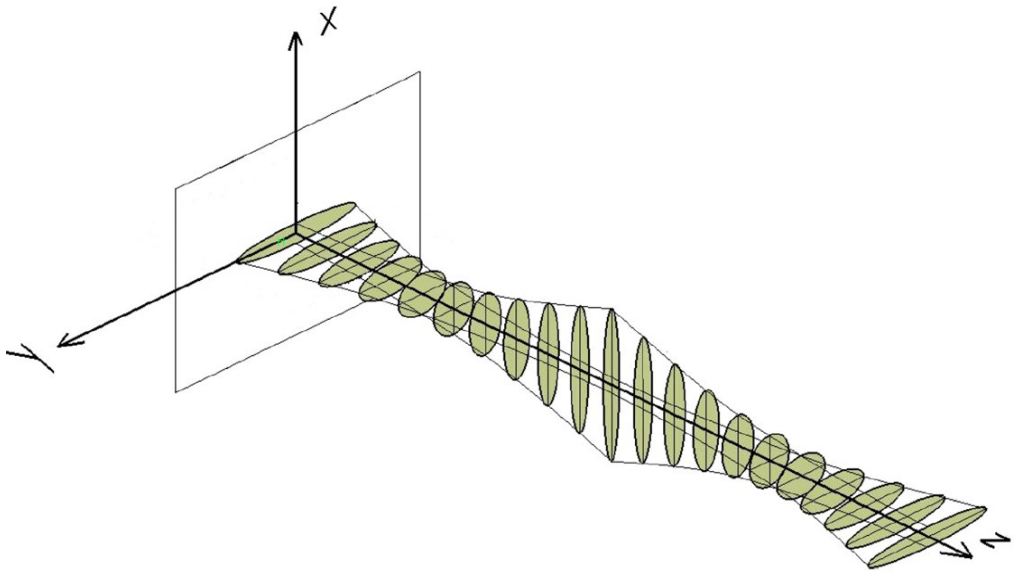

Figure 4-1: Schematic illustration of the axis-switching phenomena related to the elliptical jet [87].

By using a suitable orifice at right flow conditions, almost any fluid can exhibit a stationary oscillating jet profile for the length of the jet before breakup occurs. This stationary shape is the key to the use of the oscillating jet as an experimental technique that allows high quality measurement of jet features such as amplitude and wavelength. These features and their variation down the jet depend strongly on the evolution of surface tension. The age of the surface at a particular axial location on the jet, beginning at zero age at the orifice, can be deduced from the flow rate of the test fluid and the orifice size. As an important advantage over the other techniques, the measurements in the oscillating jet technique are made on a flow which closely approximates the stage of spraying process formation. In the oscillating jet experiment, the fluid is first forced through a capillary, in which shear rates are very high, and then creation of a free surface in air or other gas as the same as in industrial spraying processes [82, 83].

For calculating dynamic surface tension from the oscillating jet phenomenon, measurements of the oscillating jet free surface have to be combined with an analytical model at which these measurements are related to the surface tension. The first development of a simplified analytical model was performed by Lord Rayleigh (1879) [25, 88]. In his model, Rayleigh assumed the flow is inviscid, the gravity is negligible and the departure of the free surface cross section from a circle, i.e., ellipticity, is small. Also, he assumed that the surface tension and density are constant over the axial length at which the measurements are taken [82, 83, 89]. The main drawback of Rayleigh's model is the inviscid assumption which is unrealistic for many liquids. In addition, small departures from a circular cross section cannot be measured with a sufficient degree of accuracy. An improved model was proposed by Bohr in the early twentieth century [90] in which the effect of viscosity on the period of oscillation of the jet is taken into account for a weakly Newtonian viscous fluid. Similar to Rayleigh's assumptions, Bohr neglected the effect of gravity.

Due to these assumptions, the axial velocity of the jet and the amplitude and wavelength of the free surface oscillation are constant along the jet axis. Although there are practical limitations due to these assumptions, Bohr's model is still considered one of the state of the art for calculating dynamic surface tension in combination with measurements of oscillating jets [90]. There are various modifications of Bohr's model which have been applied in combination with oscillating jet measurements to determine dynamic surface tension such as Defay & Hommelen [91] as well as Kouchurova & Rusanov [92]. For calculating surface tension from all of these models, density (ρ) and viscosity (μ) have to be measured independently. In addition, flow rate (Q) of the jet is either controlled or measured. The free surface features such as wavelength (λ), which is defined as the distance measured between two consecutive crests or troughs, and maximum and minimum radii of one oscillation (R_{max}, R_{min}) are measured from a single transverse profile of the oscillating jet as shown in figure (4-2).

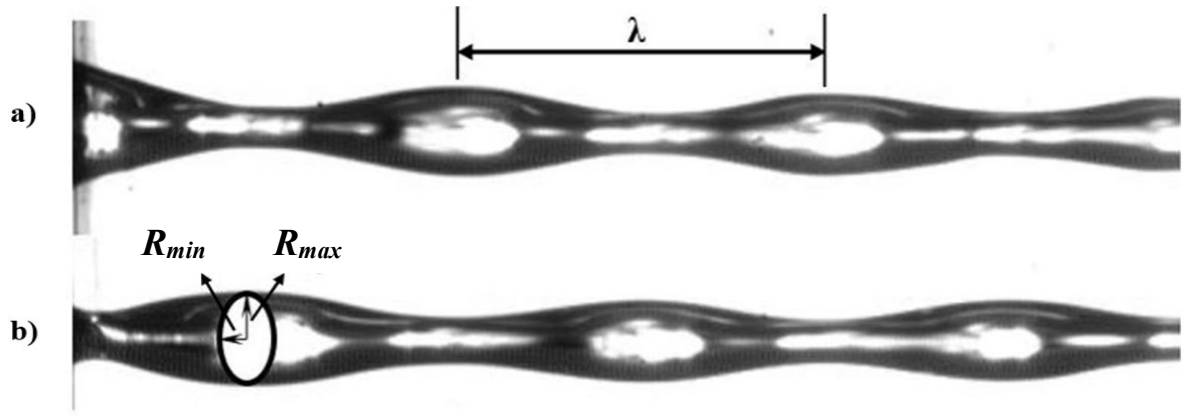

Figure 4-2: Measurements taken of the oscillating jet;
(a) major axis view and (b) minor axis view.

By inserting all of these measured parameters into Bohr's or its modified models, surface tension (σ) can be deduced. It should be noted that all of these models can calculate the average value of surface tension over this wavelength, and cannot resolve the changing value of surface tension within the wavelength. In the spraying process, it is important to deduce the surface tension value at the time when the jet breaks up into droplets because this value affects the droplets size. Additionally, for solutions not resulted from pure liquids such as surfactant solutions, the surface tension can change rapidly in very short time until reaching its equilibrium value.

Bechtel et al. [82, 83, 93] significantly improved calculation of the surface tension combined with the oscillating jet technique in two ways; they deduced an analytical model that removes many of the restrictive assumptions of Bohr's analysis such as taking the gravity and viscosity effects into consideration. In addition, producing surface tension as an essentially continuous function of axial position and consequently surface age is allowed by utilizing pointwise measurements of the jet's free surface shape in two perpendicular views within the successive wavelengths. Moreover, Bechtel's group model has been developed to take non-Newtonian viscosity into account.

4.2 Analytical Model

Bechtel's analytical model is one of the most recent and accurate models in calculating dynamic surface tension [83]. Compared to the other models such as Bohr's and Rayleigh's, this model is less restrictive, more suitable to be used with the oscillating jet experiments and its assumptions are more practical and realistic in applications. Importantly, the cross section is not limited to be near to a circle for the model to be valid. This model allows for the departure of the cross section from a circle to be large enough to allow for accurate measurement of features of the

free surface oscillation such as amplitude decay and axis-switching wavelength. The effects of gravity and viscosity are included as well. Moreover, this model relates the evolution of the free surface profile to the value of surface tension at each axial location. Consequently, it relates the surface tension to the surface age [82, 83]. The following assumptions are employed to derive the Bechtel's group model:

a- The oscillating jet flows in the direction of gravity.

b- The jet is slender (the ratio of the mean radius of the jet to the jet length over the domain of measurements is very small).

c- The flow is steady.

d- The fluid density is constant along the wavelength over which measurements are performed.

e- The jet exits an elliptical orifice while its cross section remains elliptical for the distance over which measurements are taken.

From the last assumption, the jet free surface can be represented by:

$$\frac{x^2}{\phi_1^2(z)} + \frac{y^2}{\phi_2^2(z)} = 1 \qquad (4.1)$$

where x and y are coordinates in the cross-sectional plane. $\phi_1(z)$, $\phi_2(z)$ are the major and minor semi axes of the elliptical cross section at any axial location z as shown in figure (4-3).

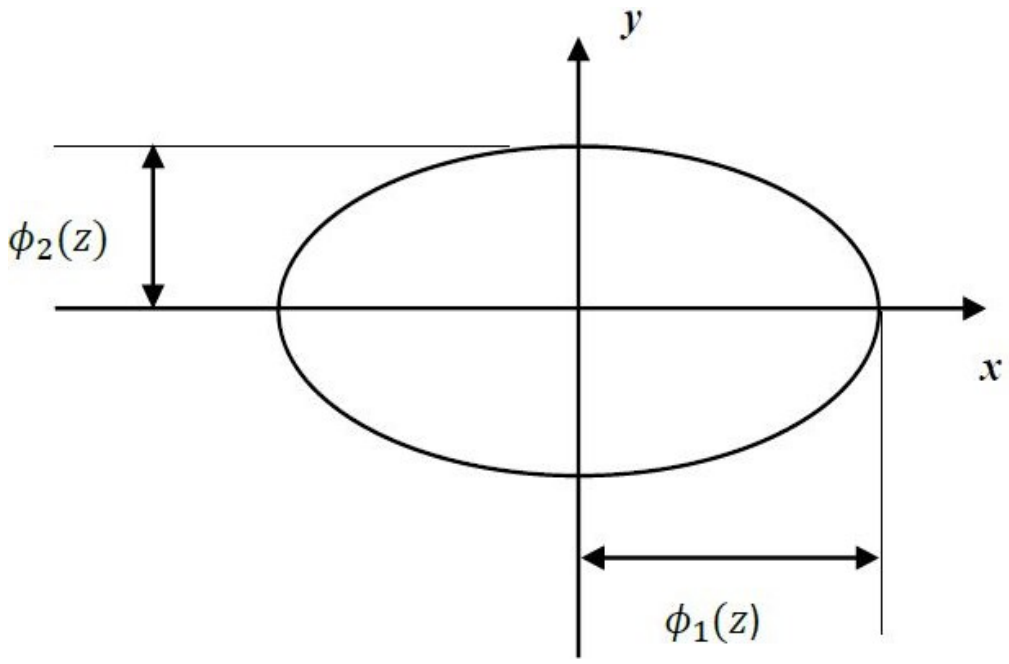

Figure 4-3: Major and minor semi axes of the elliptical jet cross section.

By integrating momentum equation over the jet cross section in the transverse directions and using the free surface boundary condition, the steady oscillating jet profile $\phi_1(z)$ is deduced and represented in equation (4.2) as follows,

$$\left(1+\frac{\pi^2}{Q^2}\ {\phi_1}^4\, v^2\right)\phi_{1,zz}-\frac{2}{\phi_1}\,\phi_{1,z}^2 + \left(\frac{4\sigma(z)}{\rho Q v}\,{\phi_1}^3\times\int_0^{2\pi}\frac{\cos^2\theta\ -\ \sin^2\theta}{\left[{\phi_1}^2\sin^2\theta\ +\ \left(\frac{Q}{\pi v\phi_1}\right)^2\cos^2\theta\ \right]^{3/2}}\,d\theta\right) + \frac{g\,\pi^2}{Q^2}\,\phi_{1,z}\left[{\phi_1}^4-\left(\frac{Q}{\pi v}\right)^2\right]-\frac{2\,g^2}{v^4}\,\phi_1+\frac{16\,\pi^2\,\mu}{\rho Q^2 v}{\phi_1}^2\left(v^2\phi_{1,z}+\frac{g}{2}\,\phi_1\right) = 0 \qquad (4.2)$$

where $\phi_z(z)$ and $\phi_{zz}(z)$ are the first and second derivatives of the free surface profile function at any axial location that represent slope and curvature, respectively.

Based on incompressible continuity equation and the assumption of steady flow, the free surface semi-axes of the oscillating jet can be related by the following equation:

$$\phi_2(z) = \frac{Q}{\pi \phi_1(z) v(z)} \tag{4.3}$$

Due to the effect of gravity, the rate of increase of velocity can be derived from conservation of momentum in the axial direction (z) as follows.

$$v v_z = g \tag{4.4}$$

To obtain an expression for $v\,(z)$ to be used in equations (4.2) and (4.3), the value of axial velocity at one particular location along the jet is needed to integrate equation (4.4) over z. This particular axial location is referred to as $(\bar{z})$ at which the jet profile major and minor semi axes are measured and referred to as $\phi_1(\bar{z})$ and $\phi_2(\bar{z})$. From the assumption of elliptical cross section, the axial velocity at $(\bar{z})$ is:

$$v(\bar{z}) = \frac{Q}{\pi\, \phi_1(\bar{z}) \phi_2(\bar{z})} \tag{4.5}$$

Then integration of equation (4.4) gives equation (4.6).

$$v(z) = \sqrt{2g(z - \bar{z}) + \left(\frac{Q}{\pi\, \phi_1(\bar{z}) \phi_2(\bar{z})}\right)^2} \tag{4.6}$$

By substitution of $\upsilon\ (z)$ in equations (4.2) and using the major free surface profile $\phi_1(z)$, one can calculate the evolution of surface tension at each axial location $\sigma_1(z)$. By replacing the minor free surface profile $\phi_2(z)$ from equation (4.3) instead of $\phi_1(z)$ in equation (4.2), the evolution of surface tension $\sigma_2(z)$ is also calculated. Equation (4.3) is used to calculate surface tension as a function of axial distance z down the jet. To relate surface tension to surface age *(T)*, the axial distance is related to surface age *(T)* through equation (4.7) as,

$$T(z) = \int_0^z \frac{dz}{\upsilon(z)} = \frac{1}{g}\left(\sqrt{2g(z-\bar{z}) + \left(\frac{Q}{\pi\,\phi_1(\bar{z})\phi_2(\bar{z})}\right)^2} - \sqrt{\left(\frac{Q}{\pi\,\phi_1(\bar{z})\phi_2(\bar{z})}\right)^2 - 2g\bar{z}}\ \right) \quad (4.7)$$

It should be noted that the surface age is zero when the jet exits the orifice at $z = 0$.

From equation (4.3), the surface tension $\sigma_1(z)$ reads as,

$$\sigma_1(z) = \frac{m_1(z)}{n_1(z)} \quad (4.8)$$

where,

$$m_1(z) = -\left(1 + \frac{\pi^2}{Q^2}\ {\phi_1}^4\,\upsilon^2\right)\phi_{1,zz} + \frac{2}{\phi_1}\,\phi_{1,z}^2 - \frac{g\,\pi^2}{Q^2}\,\phi_{1,z}\left[{\phi_1}^4 - \left(\frac{Q}{\pi\upsilon}\right)^2\right] + \frac{2\,g^2}{\upsilon^4}\,\phi_1 - \frac{16\,\pi^2\,\mu}{\rho Q^2\upsilon}{\phi_1}^2\left(\upsilon^2\phi_{1,z} + \frac{g}{2}\,\phi_1\right)$$

$$n_1(z) = \left(\frac{4{\phi_1}^3}{\rho Q\upsilon} \times \int_0^{2\pi} \frac{cos^2\theta - sin^2\theta}{\left[{\phi_1}^2 sin^2\theta + \left(\frac{Q}{\pi\upsilon\phi_1}\right)^2 cos^2\theta\right]^{3/2}}\ d\theta\right)$$

By using equations (4.7) and (4.8), surface tension can be converted from a function of axial location to a function of surface age as follows.

$$\sigma_1(z) = \sigma_1\big(T(z)\big) = \sigma_1'(T)\,, \qquad \sigma_2(z) = \sigma_2\big(T(z)\big) = \sigma_2'(T) \tag{4.9}$$

In order to use Bechtel's analytical model to calculate the evolution of surface tension, several parameters are needed to be measured and calculated as illustrated in the following section.

4.3 Experimental Measurements

To validate the oscillating jet technique combined with Bechtel's analytical model, the methodology is applied to different types of liquids before applying to suspension liquids. First, pure liquids of distilled water and ethanol, with well-known and constant surface tension, are tested. Then, aqueous solutions of a surfactant, Triton X-100, at three concentrations 0.015, 0.1 and 0.5% of weight with time changing surface tension are investigated. This type of surfactant is the same of that used in the suspension liquids under study. Finally, the measurements are carried out on the same suspension liquids used in the effervescent atomization tests. To the best of our knowledge, measuring surface tension of suspended solid particles using oscillating jet technique combined with an analytical modal is not carried out before.

4.3.1 Liquids Preparation

Before performing the experiments, the samples of under test liquids should be well prepared to get more appropriate results. The same steps used for samples preparation in effervescent atomization tests are followed (see section 3.1.2).

4.3.2 Free Surface Measurement of the Oscillating Jet

The main parameters to be measured are the free surface profiles of the oscillating elliptical jet in order to obtain the values of the semi axes ϕ_1 and ϕ_2 at each axial location of the jet. To do so, an experimental setup is developed for measuring the free surface profile as shown in figures (4-4) and (4-5). A pressurized tank is used to supply the liquid to the nozzle. The liquid is ejected through an elliptical nozzle into the air in the direction of gravity. The major and minor axes of the orifice used in measurement are 0.93 mm and 0.28 mm, respectively. The orifice was fabricated from Aluminum by a wire-cut electro discharge machining process as shown in figure (4-6) [12]. The liquid flow rate through the nozzle, Q, is controlled and determined by a flowmeter, in addition to confirmation by manual volume/time measurement.

To visualize and record the jet images, shadowgraph technique is utilized. Shadowgraphy was found to be an effective method to distinguish the jet borders from the surroundings i.e., free surface [6, 94]. Shadowgraphy was performed by a high speed camera (Photron SA1.1, USA) mounted on 3D traverse and a diffused backlight source with adjustable intensity to uniformly illuminate the jet. The backlighting was done by LED lighting (SCHOTT-KL 2500). In order to have images with good contrast, with trial and error it was noticed that the images should be captured at 125 frames per second and the shutter speed be set at 110 μsec. A commercial software (Photron FASTCAM Viewer, from Photron, USA) is used to capture and store the images. For each test, a set of 100 images were captured. In addition, 100 images were captured for the background before running any experiment without any liquid jet. In order to obtain images of the major and minor axes simultaneously, a mirror is used and placed inclined by 45 degrees close to the jet. The image of the major axis view is a direct view but that of the minor axis reflected off

the mirror as shown in figure (4-7). Because the flow is steady, the semi axes $\phi_1(z)$ and $\phi_2(z)$ are independent of time and are function of axial distance (z) only.

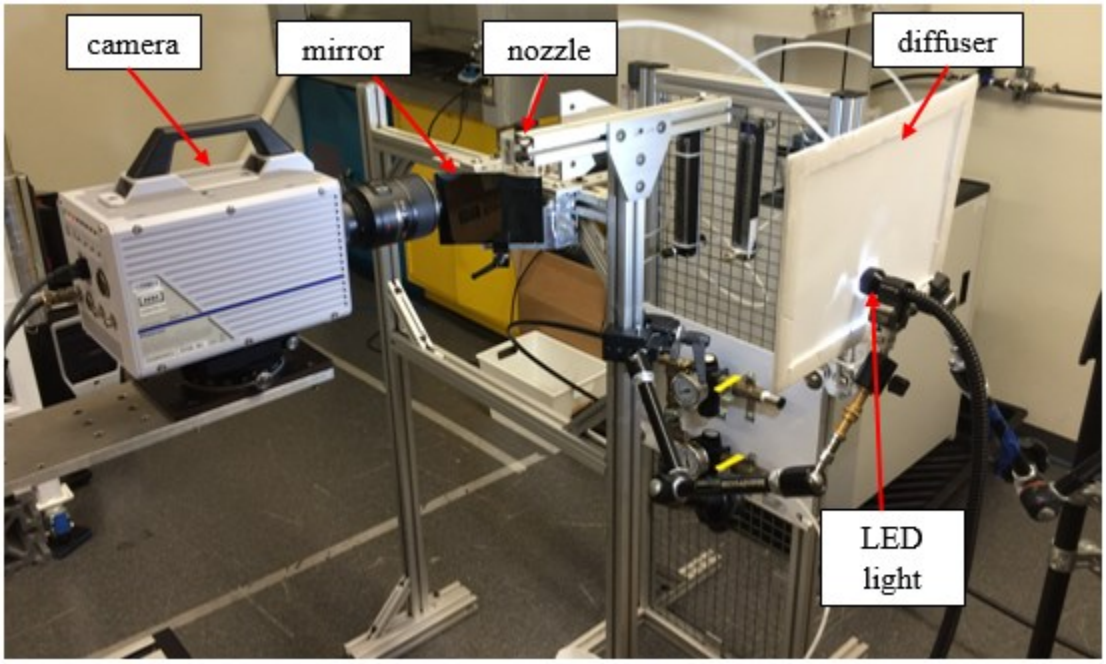

Figure 4-4: The experimental setup.

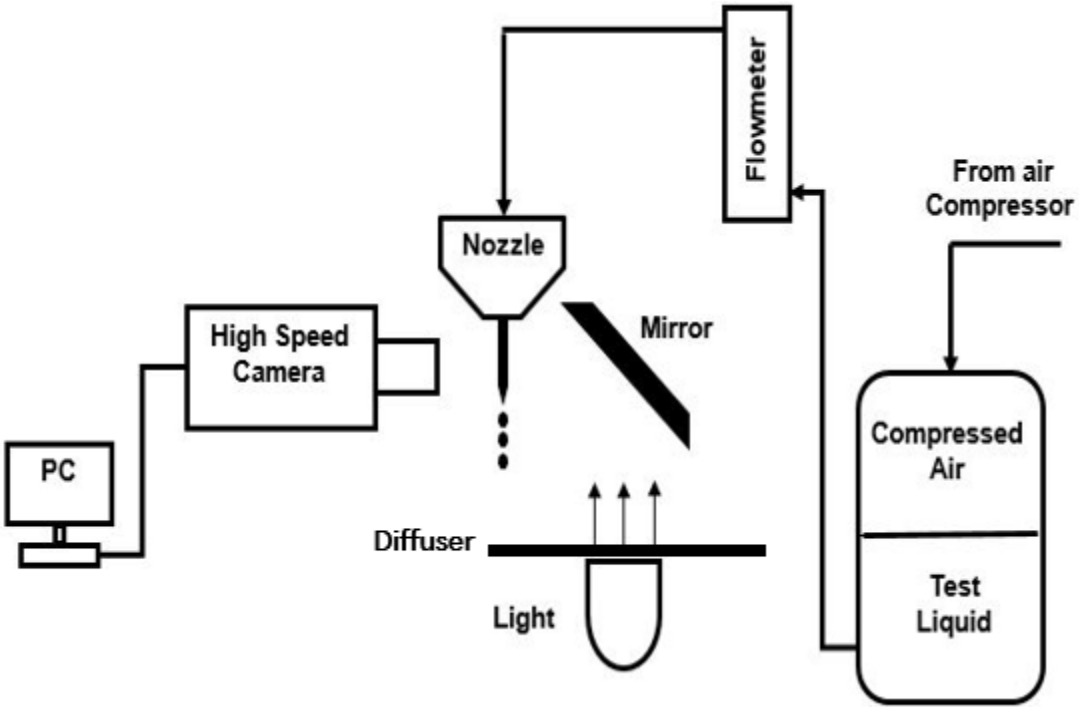

Figure 4-5: A schematic illustration of the experimental setup for oscillating elliptical jets.

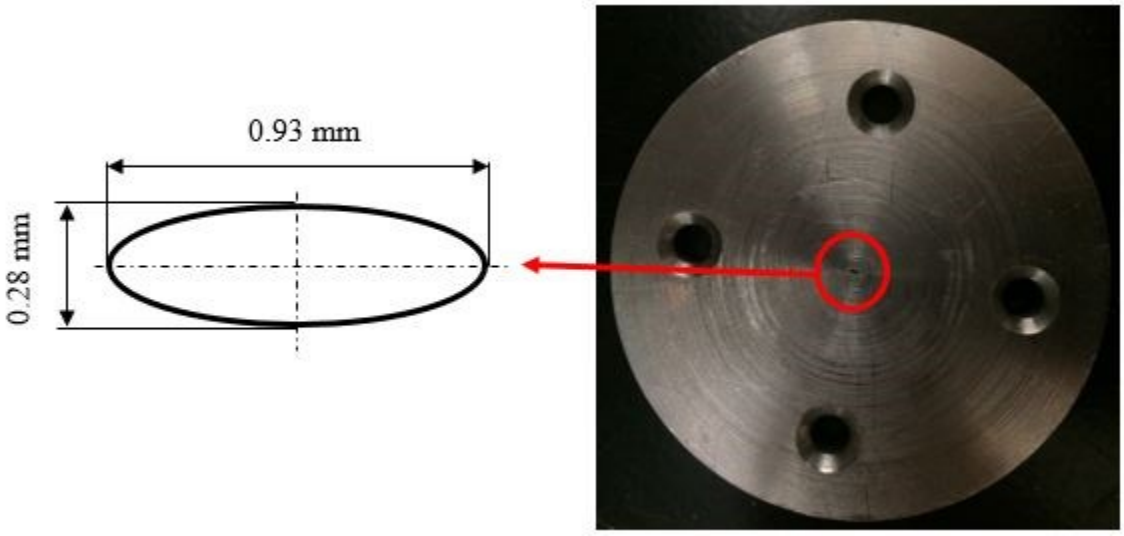

Figure 4-6: The elliptical orifice used in the measurements.

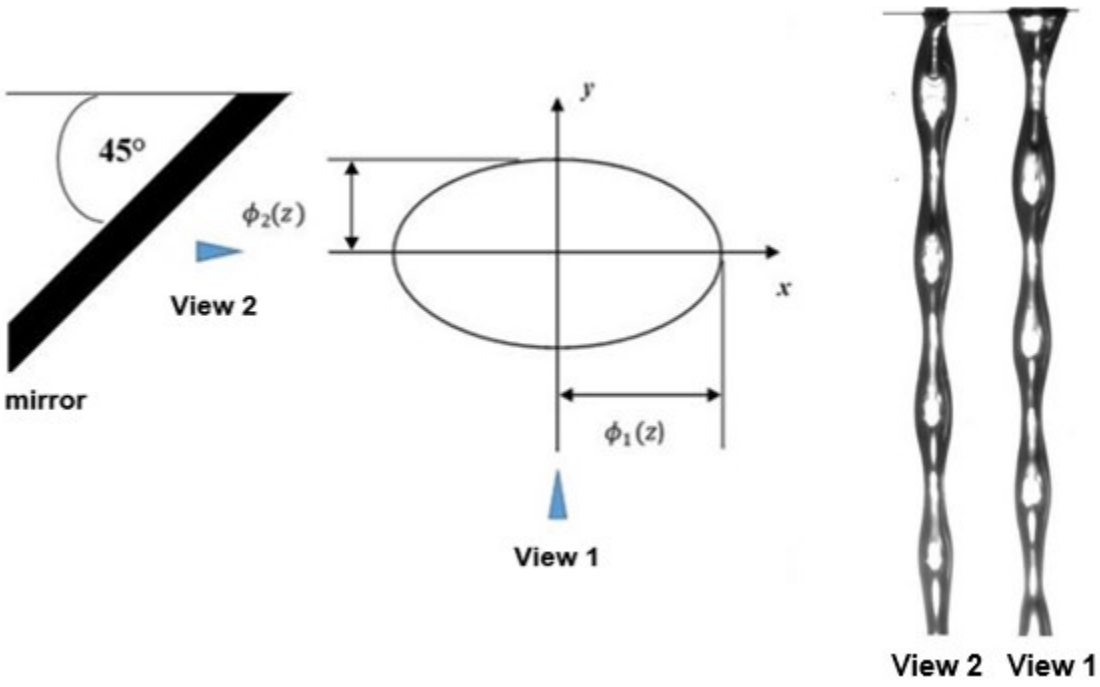

Figure 4-7: The simultaneous perpendicular views of the jet profile.

4.3.3 Image Processing

In image processing, the unit of measurement is in pixel. To convert pixel measurements to physical length (millimeters), image calibration was carried out first before running any experiments. A calibration image is taken for a calibration grid which is put vertically at the plane of measurement of the oscillating jet (at the major axis of the elliptical orifice) as illustrated in figure (4-8). Moreover, using this calibration grid helps in obtaining the best resolution of the resultant images. After calibration is done, the physical length of one pixel is calculated and referred to as the mapping value. To confirm the accuracy of the calibration, an image of a circular object with a well-known diameter size is captured. The diameter is measured from the captured image based on the calibration mapping value and compared to its actual diameter which is measured by a Vernier caliper. In all experiments, the error in the captured image was kept within ±1 pixel.

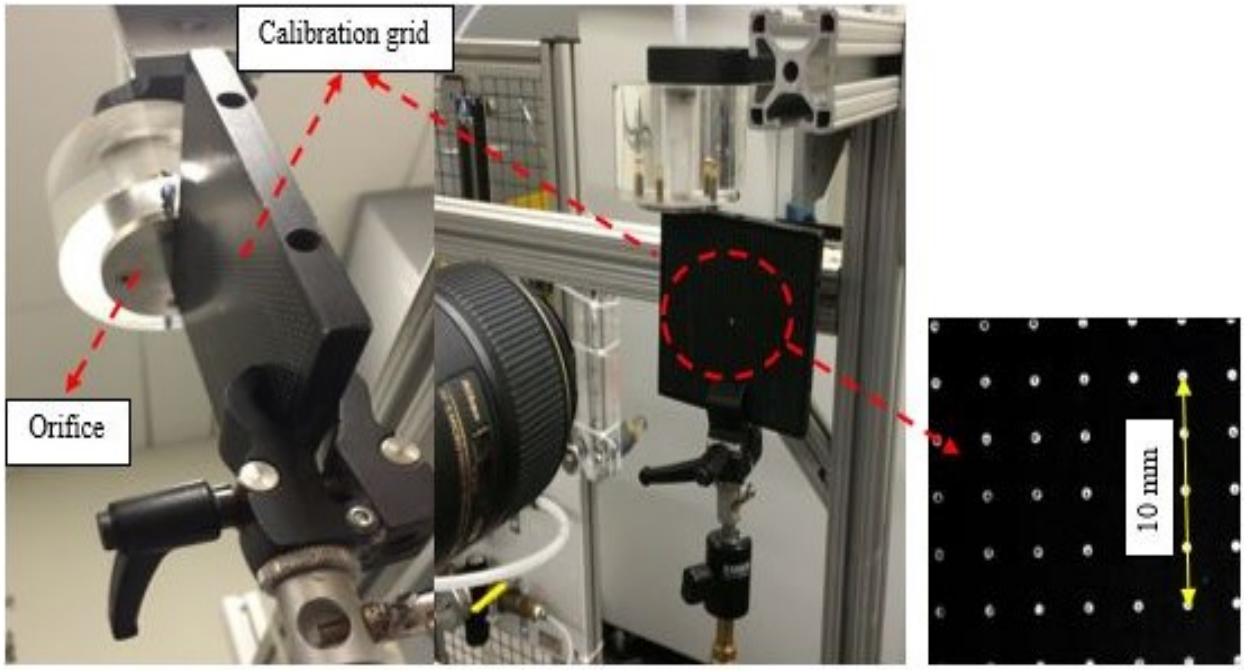

Figure 4-8: Image calibration.

In order to obtain quantitative values for the semi axes surface profiles $\phi_1(z)$ and $\phi_2(z)$, an algorithm has been created by utilizing MATLAB image processing toolbox. The main use of this image processing algorithm is edge detection for the jet free surface and measuring the jet width at the two perpendicular views ϕ_1 and ϕ_2 at each axial location of the jet. First, the developed algorithm removes the background which reduces noise and leads to identify the jet more accurately. Background removal was done by subtracting the average of background images (recorded before starting the flow) from the captured images of the test. Based on the image subtraction process, a new image which only shows the jet is created. In terms of actual image processing, the functions used in this algorithm to achieve this goal include image filtration, conversion of the resultant image to binary, and edge detection as shown in figure (4-9). After the edge detection is finished, running down line by line between the jet edges is done to find the number of starting and ending column for each axial location. Once the starting and ending column values are obtained, the distance between the left and right edge of the jet can be estimated at this axial particular location along the jet length in pixels and stored in arrays. By identifying the mapping value obtained from calibration, the distance in pixels is converted to length in mm. Then this data corresponding to the jet width ϕ_1 and ϕ_2 at each axial location is obtained and used directly for analysis. Moreover, this algorithm allows carrying out the measurements for any number of images recorded by the high speed camera and collect these data in an organized fashion for the subsequent analyses.

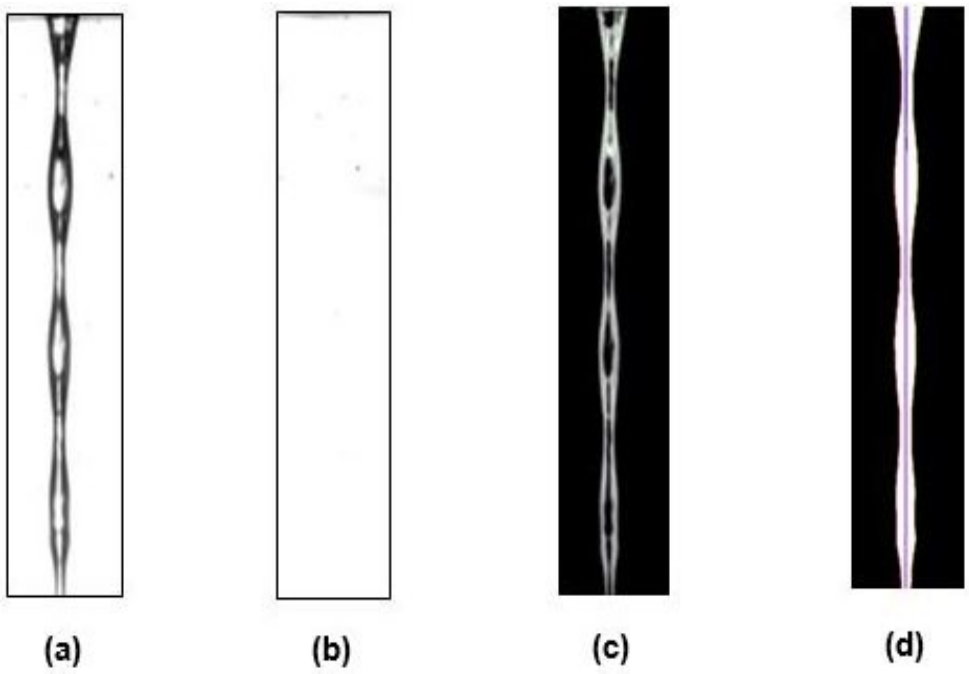

Figure 4-9: Jet edge detection steps using image processing;
(a) raw image, (b) background image, (c) background removal and conversion to binary, and d) Edge detection.

In each measurement for all liquids types, the images are overlaid to produce the jet free surface profile along the studied wavelength. As a result of the discrete nature of the raw experimental data related to the jet free surface profile, smooth first and second derivatives $\phi_{i,z}$ and $\phi_{i,zz}$,(i=1,2), cannot be obtained directly which leads to wrong calculations of the surface tension. In order to solve this problem, the average free surface profile is deduced after obtaining the raw experimental data of the free surface profiles and overlaying the images. Then curve fitting is performed for this average profile and the free surface profile function $\phi_i(z)$ is deduced. Based on a spatial stability analysis, Amini and Dolatabadi [95] showed that elliptic jet profile can be approximated by a finite Fourier series. This series, including superposition of four waves with different amplitudes and frequencies, represents both axis-switching and breakup of the elliptic jet

[95]. Following this idea, the free surface profile function is deduced in the formulation of Fourier series equation by using curve fitting toolbox in MATLAB which is able to use up to eight terms. Figure (4-10) illustrates an example of the raw experimental data of the free surface profiles for the overlaid images in case of water as operating flow. An example of the average surface profile and its fitting curve as well as its profile equation are shown in figure (4-11). By using the new fitted data as the free surface profile functions $\phi_1(z)$ and $\phi_2(z)$, the smooth first and the second derivatives $\phi_{1,z}(z)$, $\phi_{1,zz}(z)$, $\phi_{2,z}(z)$ and $\phi_{2,zz}(z)$ are obtained then used in the analytical model. Figure (4-13) shows an example of the first and second derivatives of the fitted surface profile including the raw surface profile for $\phi_1(z)$ in case of distilled water. As shown in figure (4-12), there is a great difference between the values of the derivatives of fitted profile in compare with the raw experimental surface profile, due to the discrete values of the raw data, which prevents the calculation of surface tension properly. In order to solve equation (4.8), the integration in the function $n_1(z)$ is computed numerically using the trapezoidal rule.

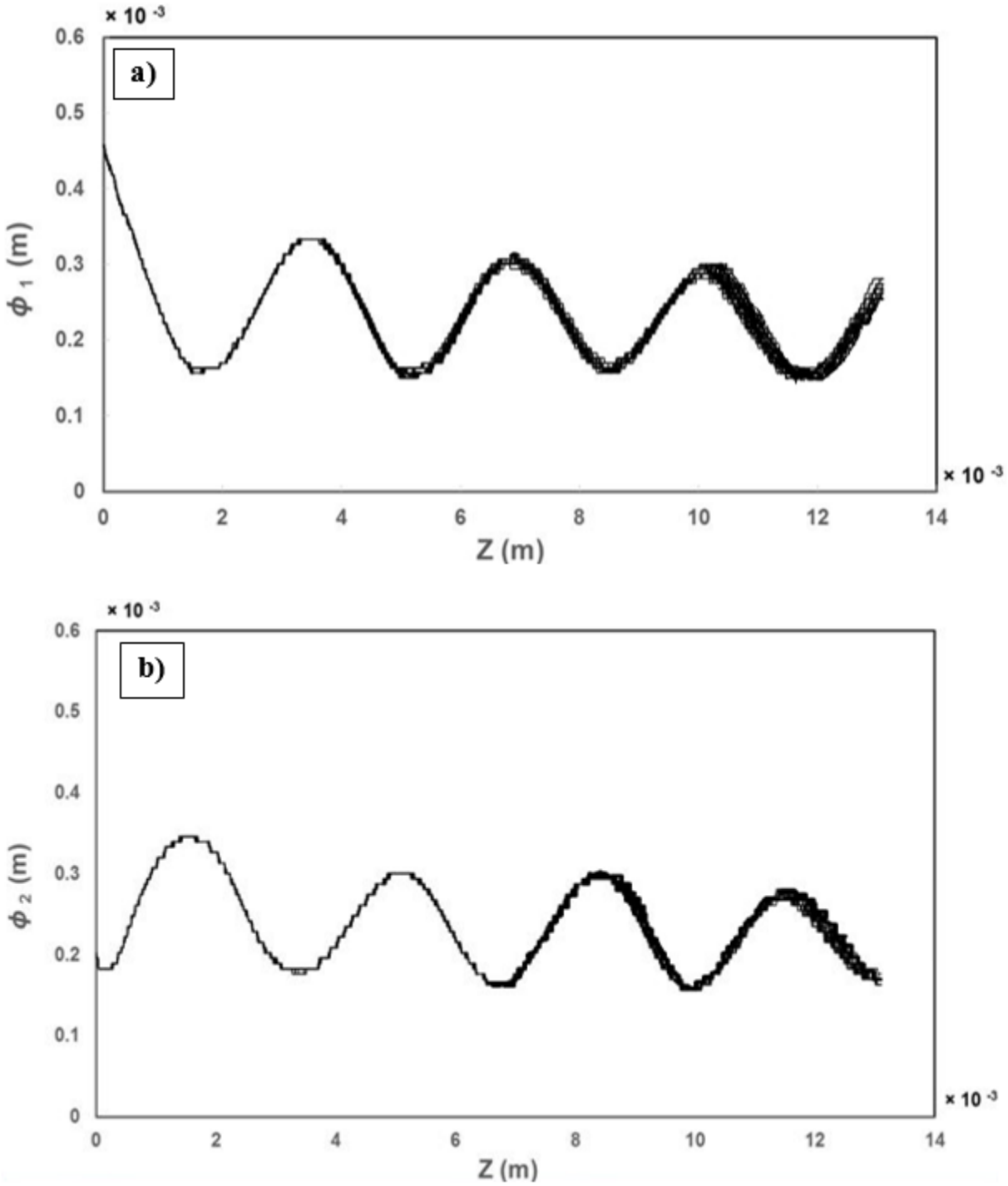

Figure 4-10: Raw data of the overlaid free surface profiles for water;

(a) $\phi_1(z)$ and (b) $\phi_2(z)$.

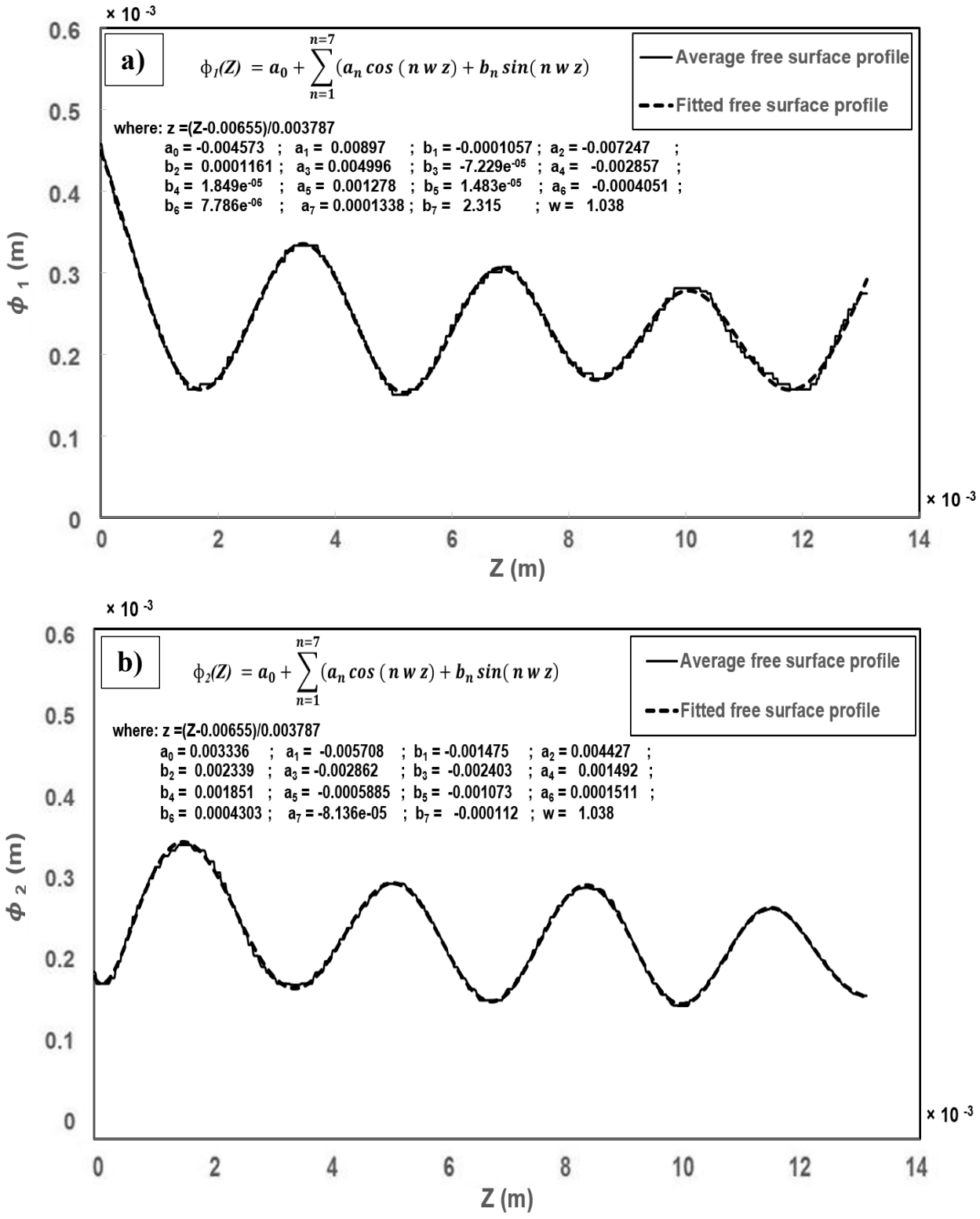

Figure 4-11: Average and fitted surface profiles for water;

(a) $\phi_1(z)$ and (b) $\phi_2(z)$.

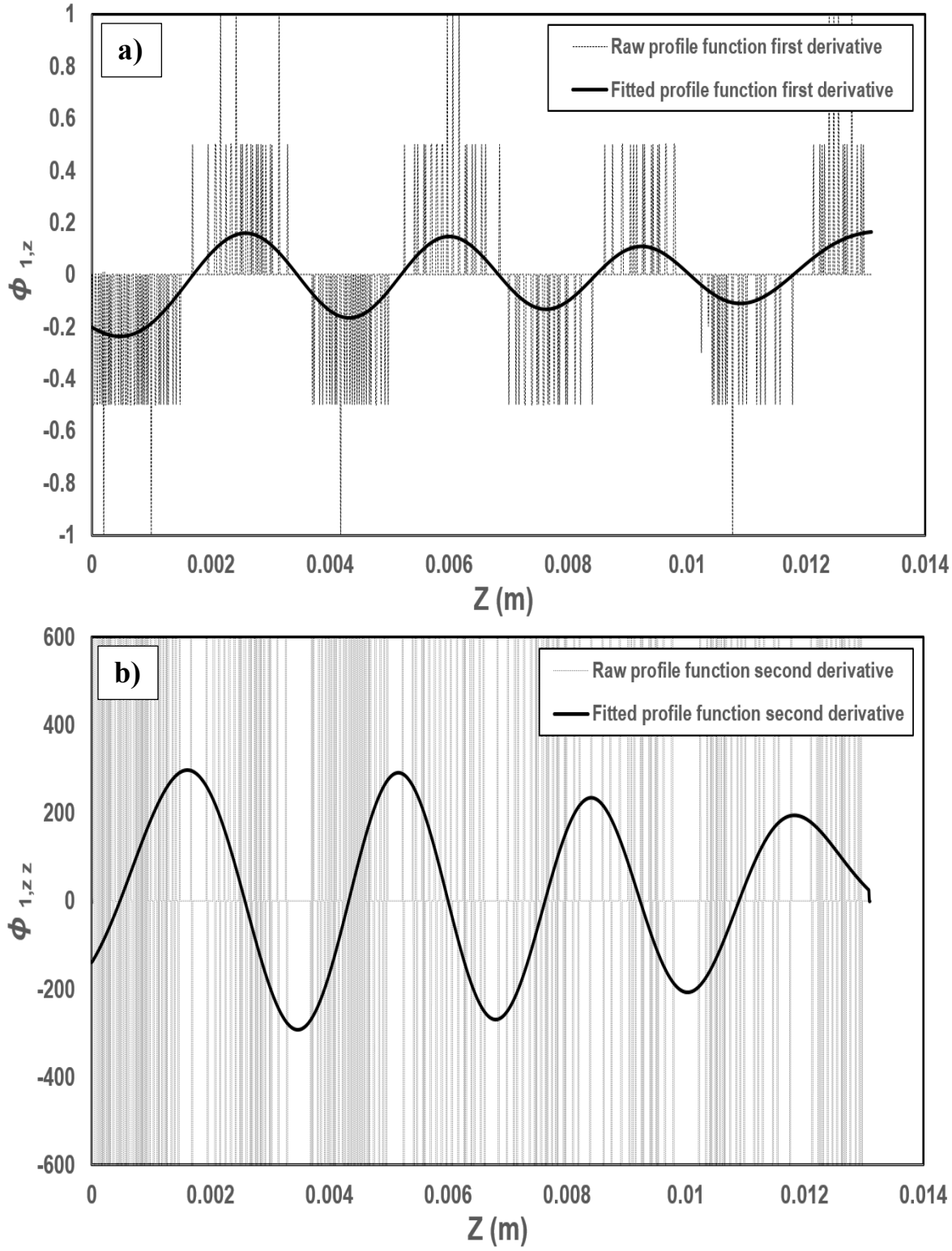

Figure 4-12: The derivatives of the fitted and raw surface profile $\phi_1(z)$ for water; (a)the first derivative (slope), and (b) the second derivative (curvature).

4.3.4 Other Flow Parameters

In addition to the measurement of free surface profile, the analytical model needs some input parameters to be measured or calculated. These parameters are liquid properties including density (ρ) and viscosity (μ). Moreover, the flow rate (Q) is another required parameter to be measured. Furthermore, the reference axial location ($\bar{z}$) has to be determined. In addition, static surface tension (σ_{st}) is measured to be compared with the dynamic surface tension. All experiments were carried out at room temperature, 24° C.

a- Liquid properties

Measurement of the density (ρ), viscosity (μ) and static surface tension (σ_{st}) of the studied liquids were performed by the same methods used in effervescent atomization tests. (see section 3.1.2).

b- Flowrate (Q)

The liquid flow rate (Q) is determined by volumetric measurement. The liquid is collected during a time period of 60 seconds followed by measuring its mass. The flow rate is calculated by dividing the mass by the time multiplied by the liquid density. The measurements were carried out for three times and taking the average.

c- The reference axial location ($\bar{z}$)

For calculation of the flow velocity and relating surface age at each axial location in equations (4.5) to (4.7), a specific reference axial location ($\bar{z}$) is selected at which reference semi-major and semi-minor axes $\phi_1(\bar{z})$ and $\phi_2(\bar{z})$ are measured. The analytical model is proven to be insensitive to the selection of location of the reference axial point ($\bar{z}$) [83]. In all experiments, ($\bar{z}$) is selected

to be the axial location of the first maximum of $\phi_1(z)$. All the reference axial locations, the tested liquid properties and the flow rates for all experiments are listed in table (4-1). Concentrations included are per weight

Table 4-1: Tested liquids parameters.

Liquid	Q **(m^3/s)**	ρ **(kg/m^3)**	μ **(Pa.s)**	σ_{st} **(N/m)**	$\bar{z}$ **(m)**	$\phi_1(\bar{z})\phi_2(\bar{z})$ **(m^2)**
Water	5.5×10^{-7}	997	0.0009	0.074	3.85×10^{-3}	5.07×10^{-8}
Ethanol	3.2×10^{-7}	785	0.0012	0.022	0.94×10^{-3}	6.53×10^{-8}
Water-0.015%TX-100	3.9×10^{-7}	997	0.000936	0.0375	2.98×10^{-3}	5.82×10^{-8}
Water-0.1%TX-100	3.5×10^{-7}	997.3	0.001	0.034	2.6×10^{-3}	4.58×10^{-8}
Water-0.5%TX-100	4.1×10^{-7}	997.5	0.001024	0.033	2.79×10^{-3}	4×10^{-8}
Water-1.5% Glass	4.9×10^{-7}	1006	0.001025	0.076	3.51×10^{-3}	5.68×10^{-8}
Water -5% Glass	4.9×10^{-7}	1028	0.001089	0.071	3.23×10^{-3}	6.49×10^{-8}
Water - 10% Glass	4.7×10^{-7}	1060	0.00118	0.066	3.065×10^{-3}	6.34×10^{-8}
Water - 1.5% Titania	4.2×10^{-7}	1008.3	0.00091	0.073	3.19×10^{-3}	5.47×10^{-8}
Water -5% Titania	4.6×10^{-7}	1035.4	0.000922	0.064	3.13×10^{-3}	5.96×10^{-8}
Water - 1.5% Titania - (0.5% TX-100)	4.3×10^{-7}	1008.3	0.00093	0.039	3.02×10^{-3}	6.63×10^{-8}
Water - 5% Titania - (0.5% TX-100)	3.9×10^{-7}	1035.4	0.00095	0.0355	2.74×10^{-3}	6.75×10^{-8}

4.4 Results and Discussion

In all experiments, surface tensions $\sigma_1(T)$ and $\sigma_2(T)$ in addition to the average surface tension ($\sigma_{av} = 0.5\ (\sigma_1(T) + \sigma_2(T))$) are calculated and plotted together with the static (equilibrium) surface tension (σ_{st}) measured by the static technique. The experiments were performed on the liquids mentioned in the same order as in table (4-1) and all concentrations included are per weight. The results obtained from surface tension calculation of the tested liquid are shown in figures (4-13) to (4-24).

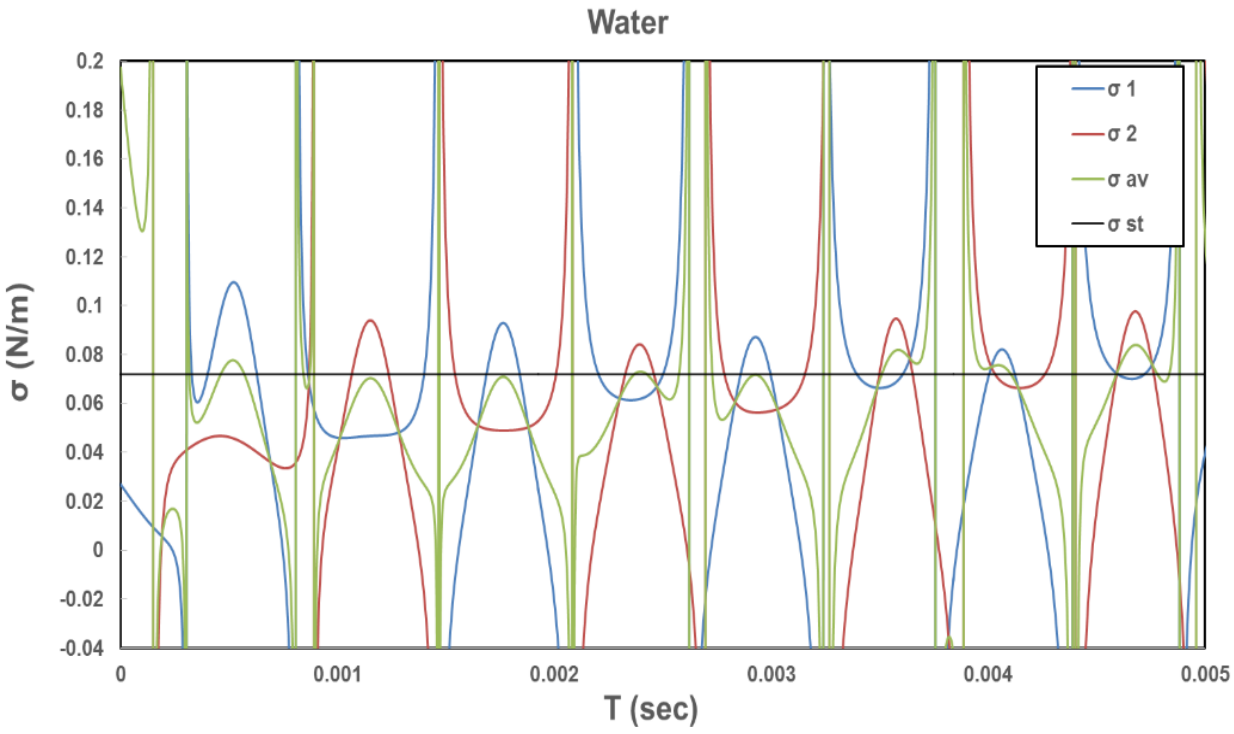

Figure 4-13: Surface tensions $\sigma_1(T)$, $\sigma_2(T)$, $\sigma_{av}(T)$ and σ_{st} for water.

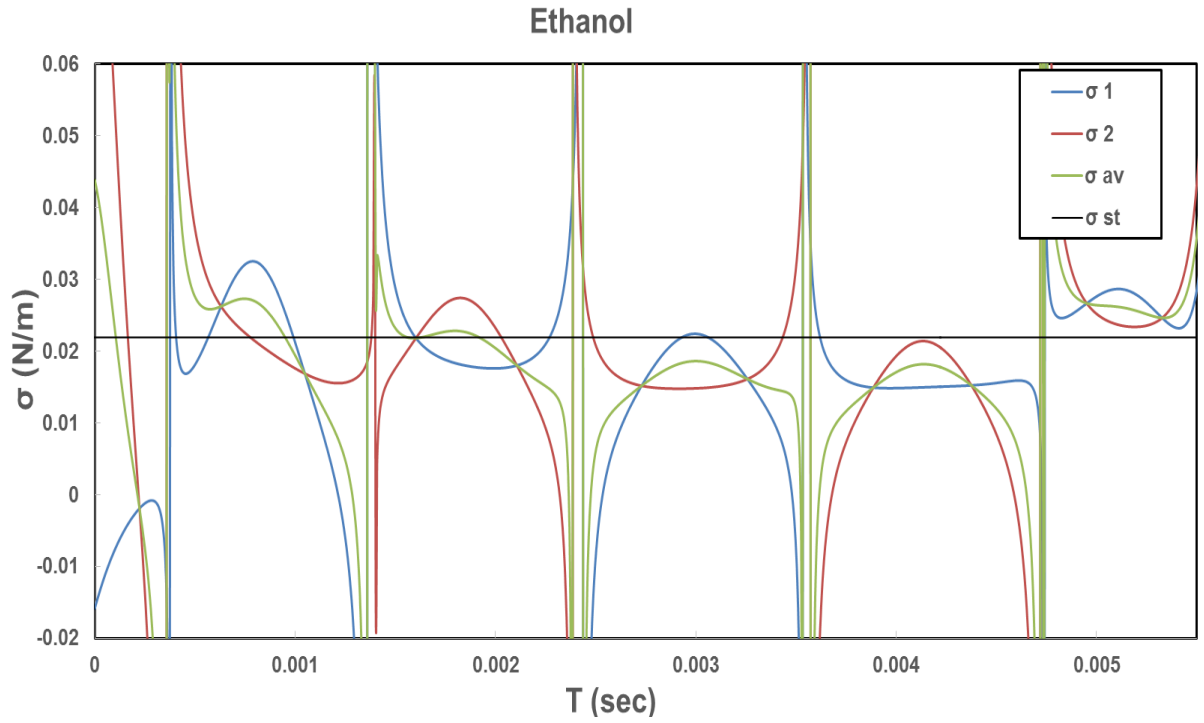

Figure 4-14: Surface tensions $\sigma_1(T)$, $\sigma_2(T)$, $\sigma_{av}(T)$ and σ_{st} for ethanol.

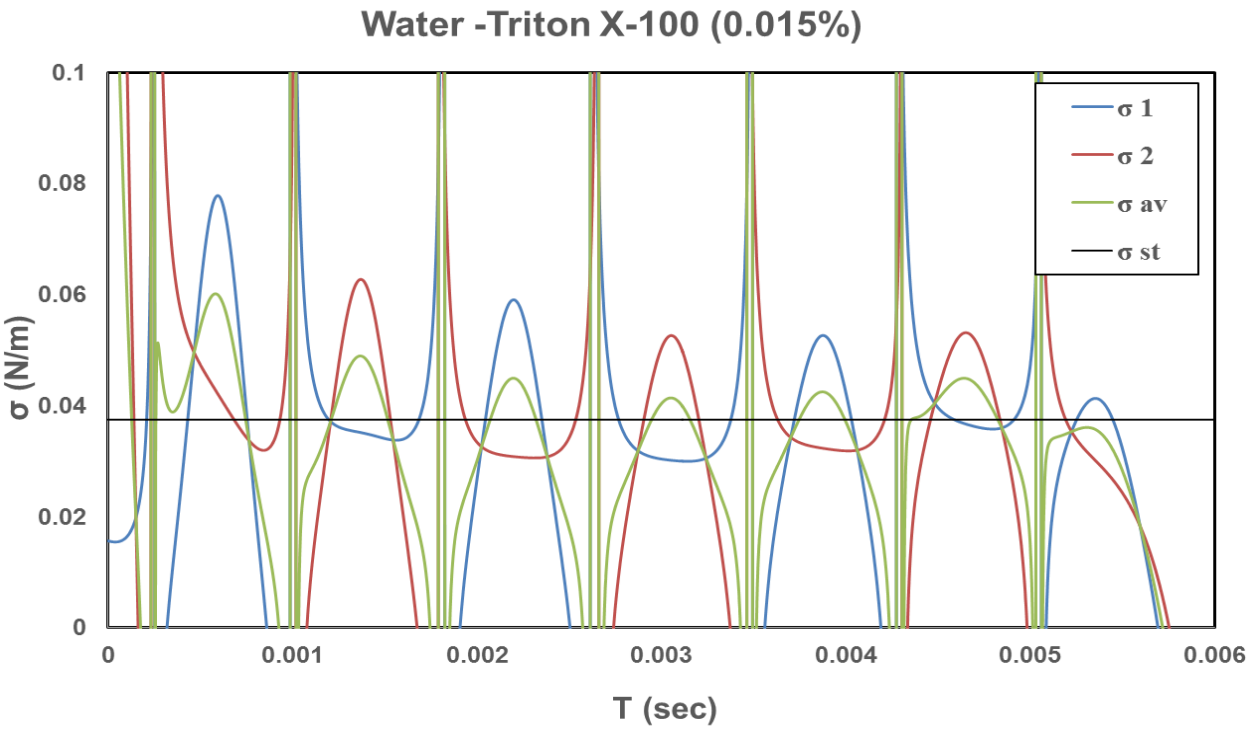

Figure 4-15: Surface tensions $\sigma_1(T)$, $\sigma_2(T)$, $\sigma_{av}(T)$ and σ_{st} for water-0.015% TX-100.

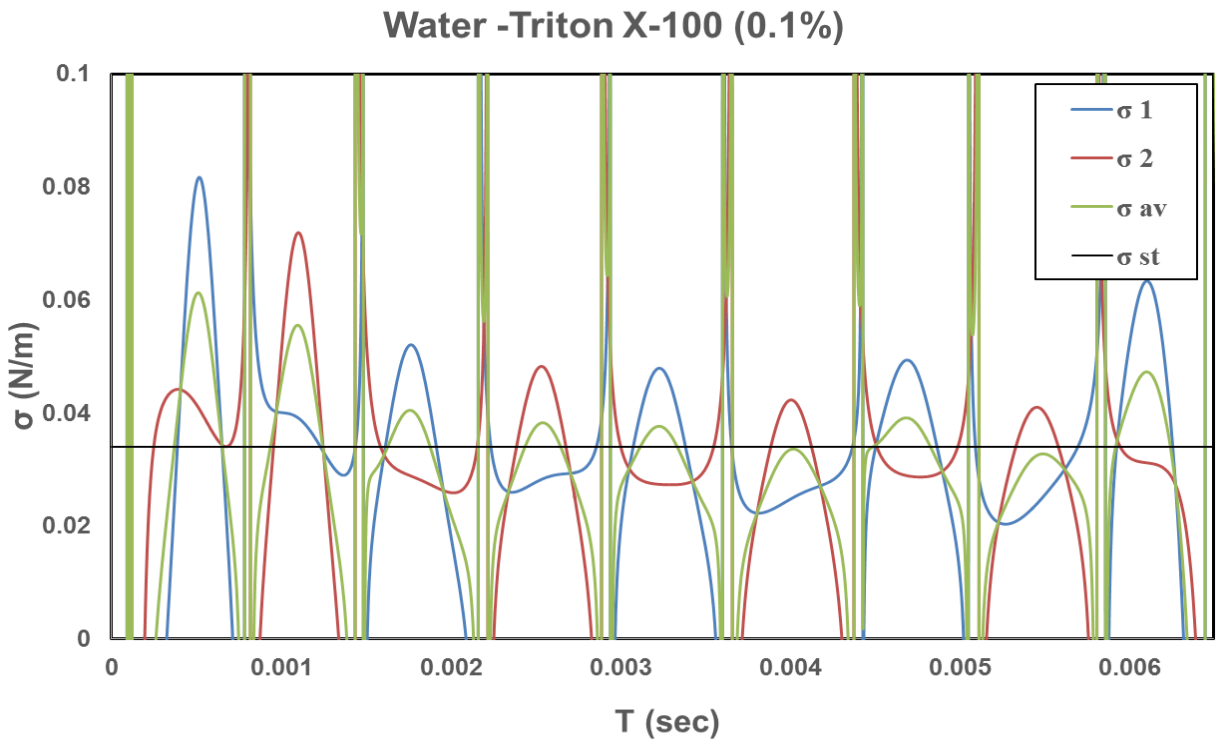

Figure 4-16: Surface tensions $\sigma_1(T)$, $\sigma_2(T)$, $\sigma_{av}(T)$ and σ_{st} for water-0.1% TX-100.

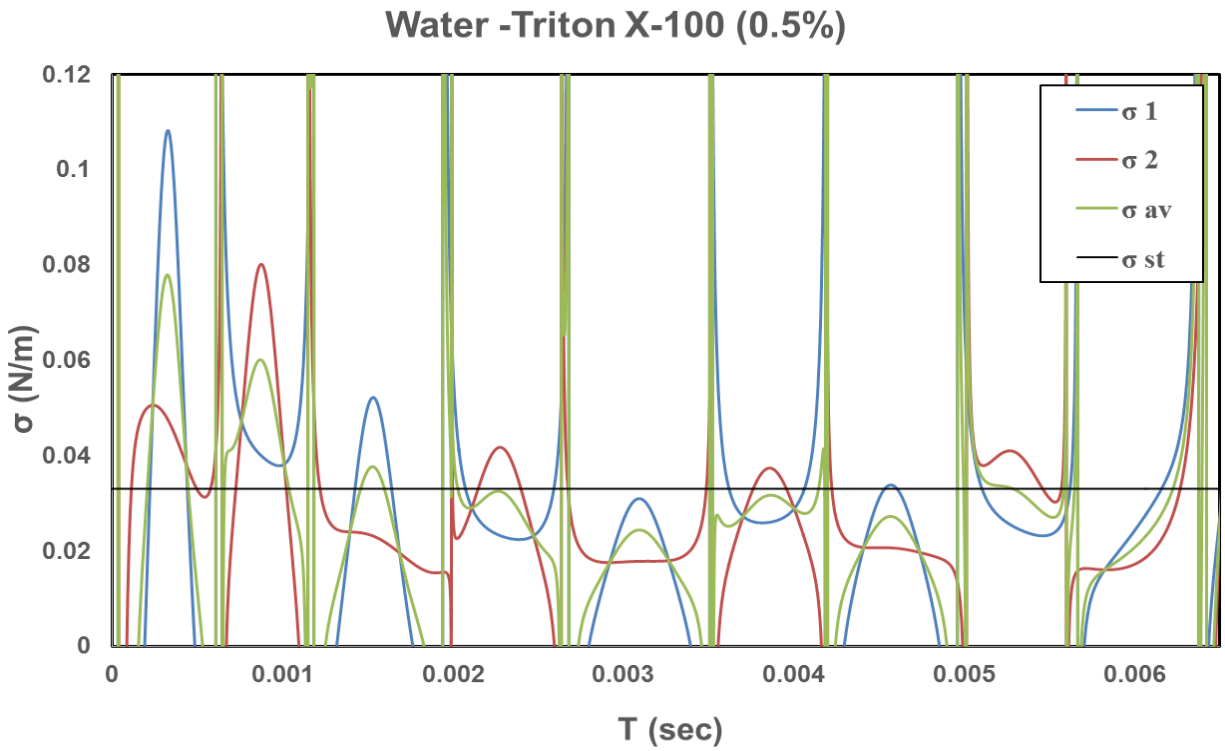

Figure 4-17: Surface tensions $\sigma_1(T)$, $\sigma_2(T)$, $\sigma_{av}(T)$ and σ_{st} for water-0.5% TX-100.

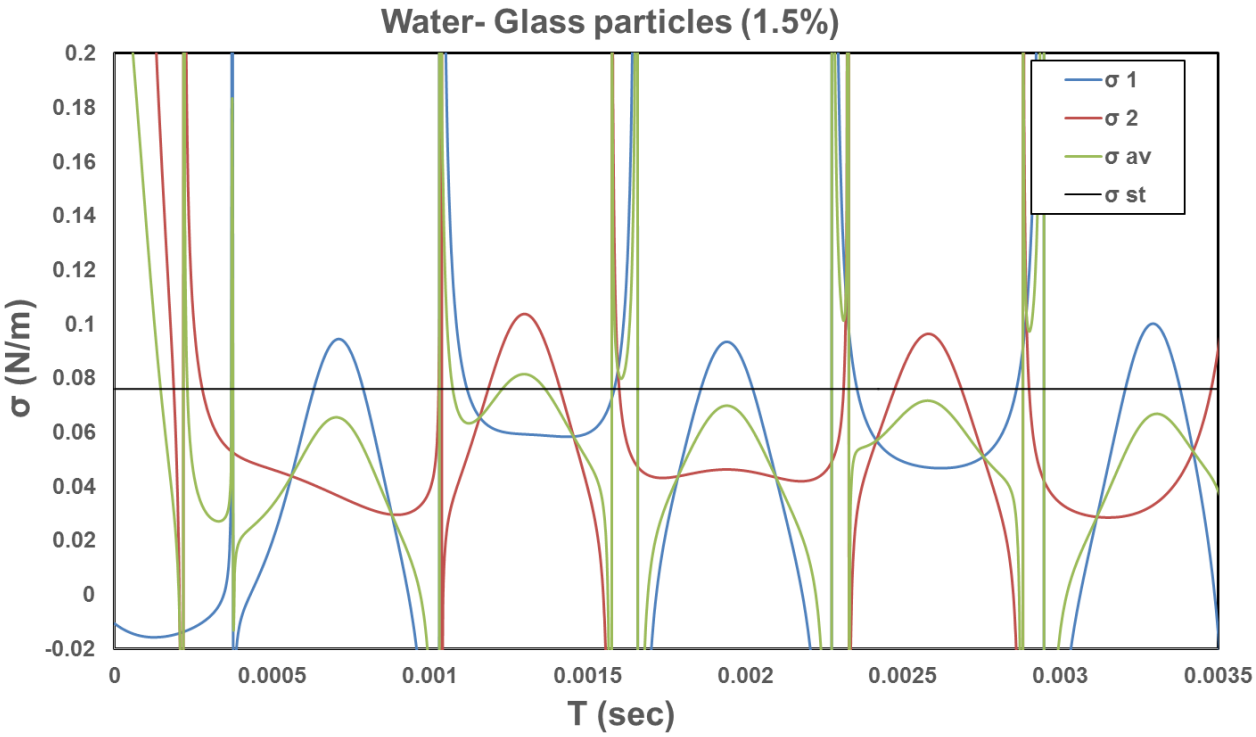

Figure 4-18: Surface tensions $\sigma_1(T)$, $\sigma_2(T)$, $\sigma_{av}(T)$ and σ_{st} for water-1.5% glass particles.

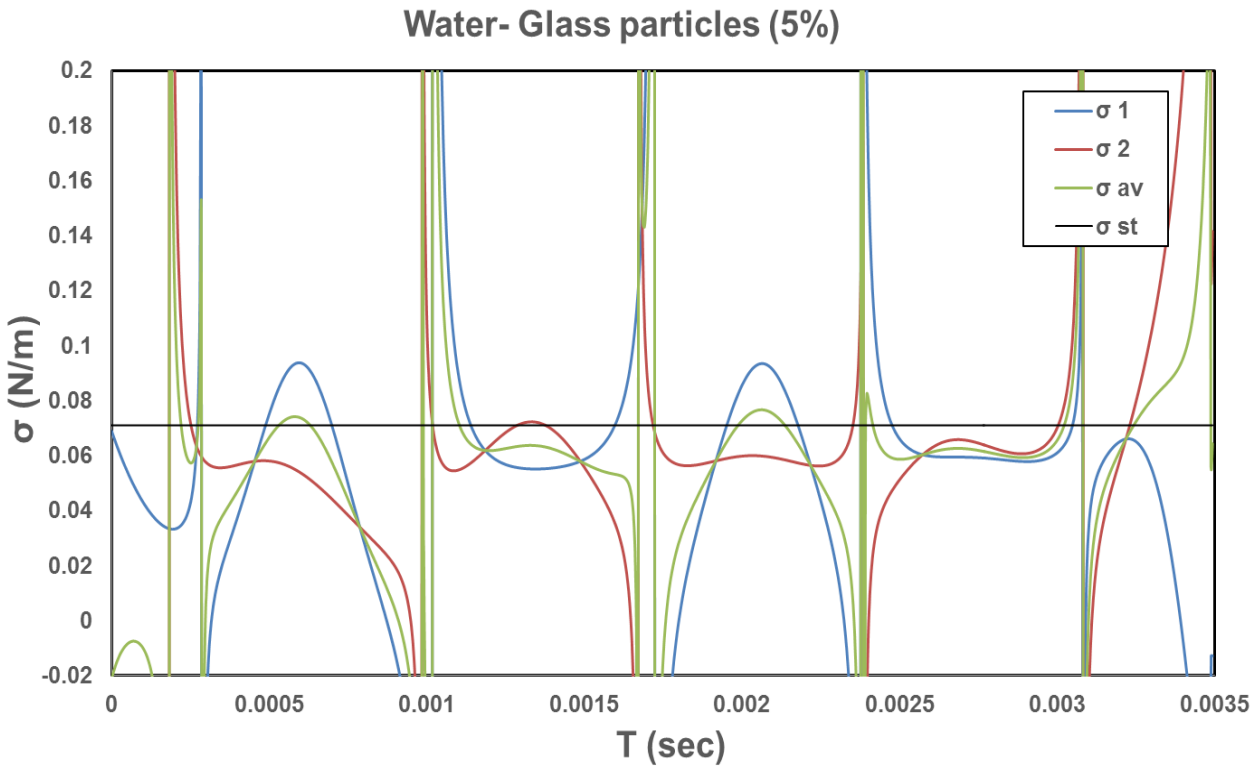

Figure 4-19: Surface tensions $\sigma_1(T)$, $\sigma_2(T)$, $\sigma_{av}(T)$ and σ_{st} for water-5% glass particles.

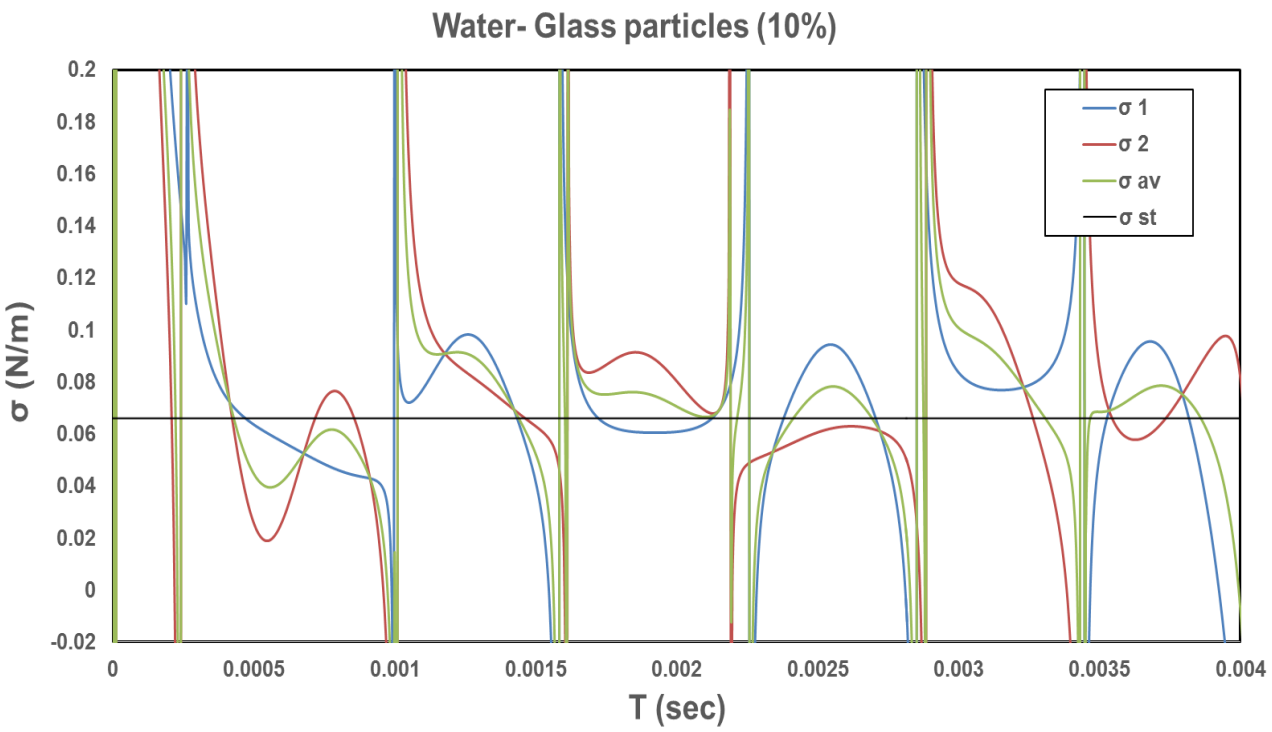

Figure 4-20: Surface tensions $\sigma_1(T)$, $\sigma_2(T)$, $\sigma_{av}(T)$ and σ_{st} for water-10% glass particles.

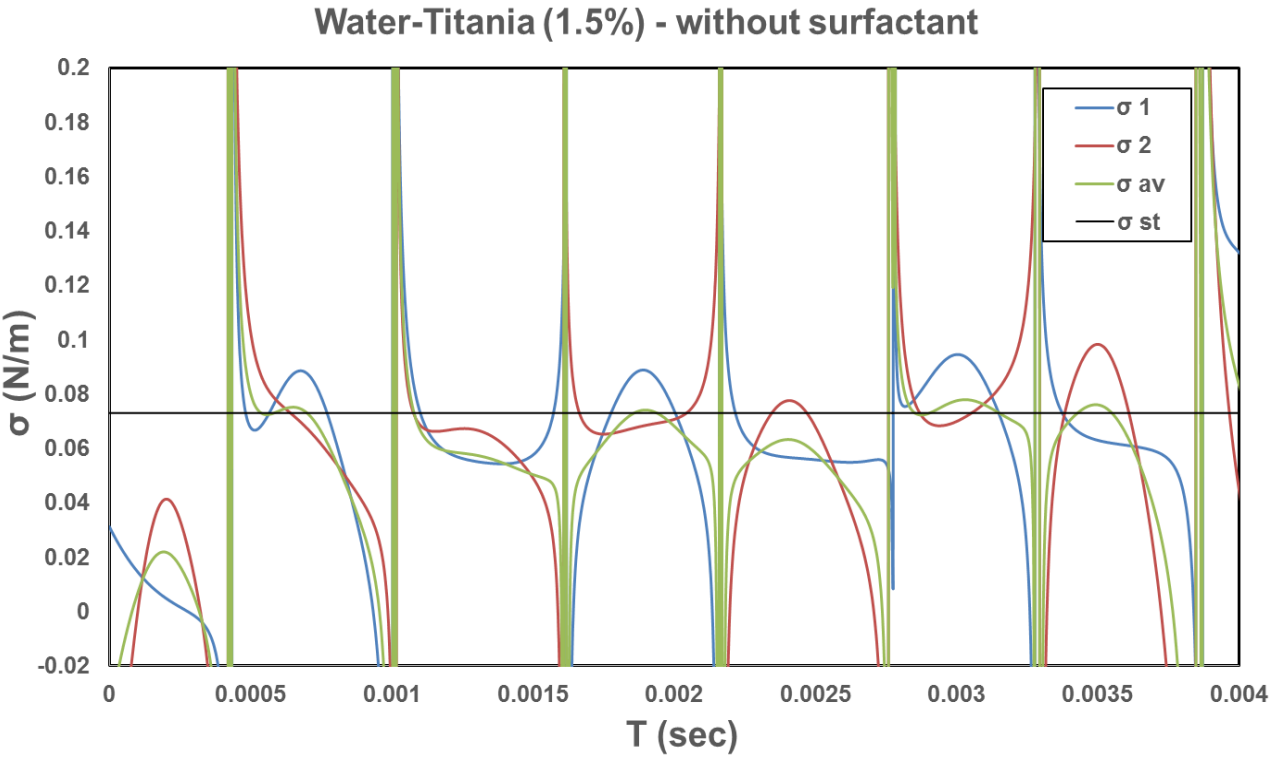

Figure 4-21: Surface tensions $\sigma_1(T)$, $\sigma_2(T)$, $\sigma_{av}(T)$ and σ_{st} for water-1.5% titania particles without a surfactant.

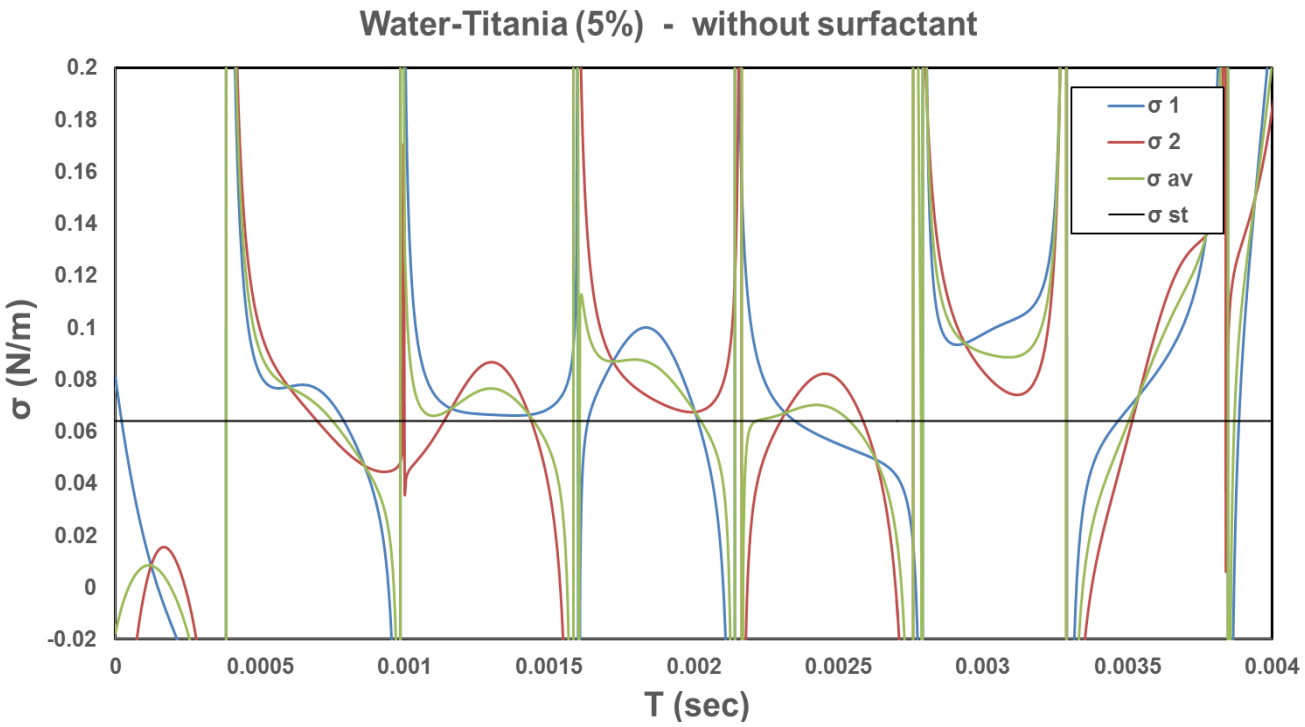

Figure 4-22: Surface tensions $\sigma_1(T)$, $\sigma_2(T)$, $\sigma_{av}(T)$ and σ_{st} for water-5% titania particles without a surfactant.

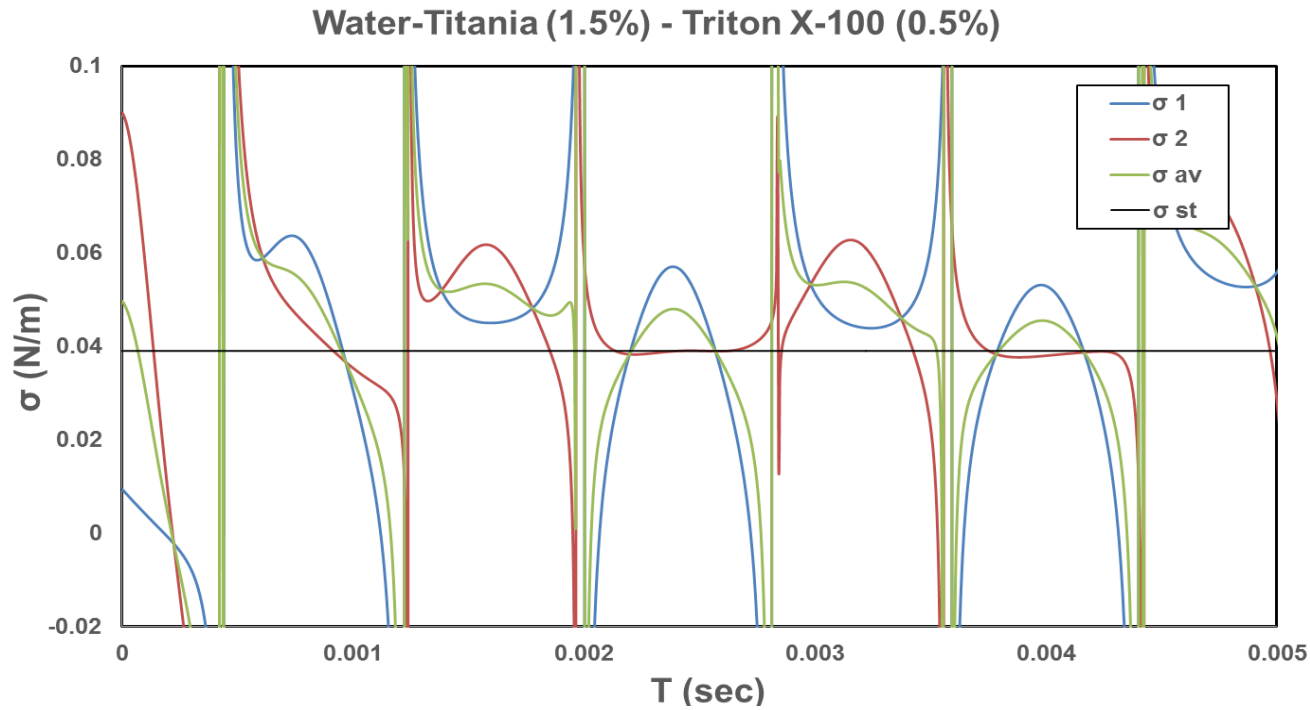

Figure 4-23: Surface tensions $\sigma_1(T)$, $\sigma_2(T)$, $\sigma_{av}(T)$ and σ_{st} for water-1.5% titania particles with a surfactant.

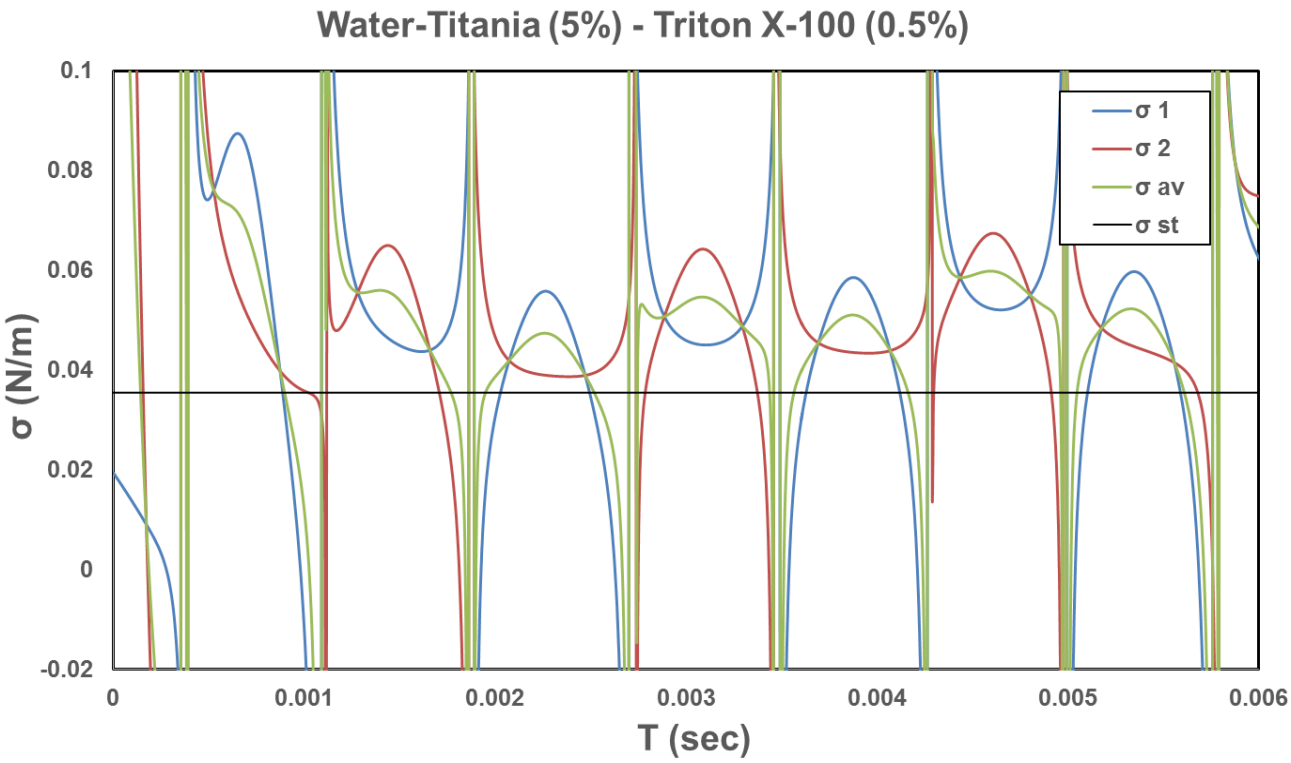

Figure 4-24: Surface tensions $\sigma_1(T)$, $\sigma_2(T)$, $\sigma_{av}(T)$ and σ_{st} for water-5% titania particles with a surfactant.

As these figures show, there are some spikes on the calculated surface tension. These spikes appear at the axial locations where the jet cross section is nearly circular ($\phi_1 = \phi_2$) due to surface tension calculation by equation (4.8) [83]. These spikes cannot be eliminated and this issue is considered a drawback in calculated surface tension using Bechtel's model. Detailed explanation for the reason of these spikes is introduced in reference [83]. In our experiments, the calculated average dynamic surface tension is selected to be an indication for our results. By plotting the average surface tension at the intermediate features between the successive spikes, figures (4-25) to (4-36) are obtained. It should be noted that the fluid flow exiting the nozzle needs a short time to be settled into the oscillating jet form on which the analytical model is valid. Therefore, the values of surface tension obtained at very early ages (around 0.2 ms) can be neglected [83].

4.4.1 Results Validation

Before applying the analysis to the suspension case, the results of liquids with well characterized properties are validated. Distilled water and ethanol are tested as they have a constant surface tension value with no dependence on time (surface age). As shown in figures (4-25) and (4-26), the behavior of the calculated dynamic surface tension is constant and has values close to the static surface tension as expected for both liquids based on the average dynamic surface tension.

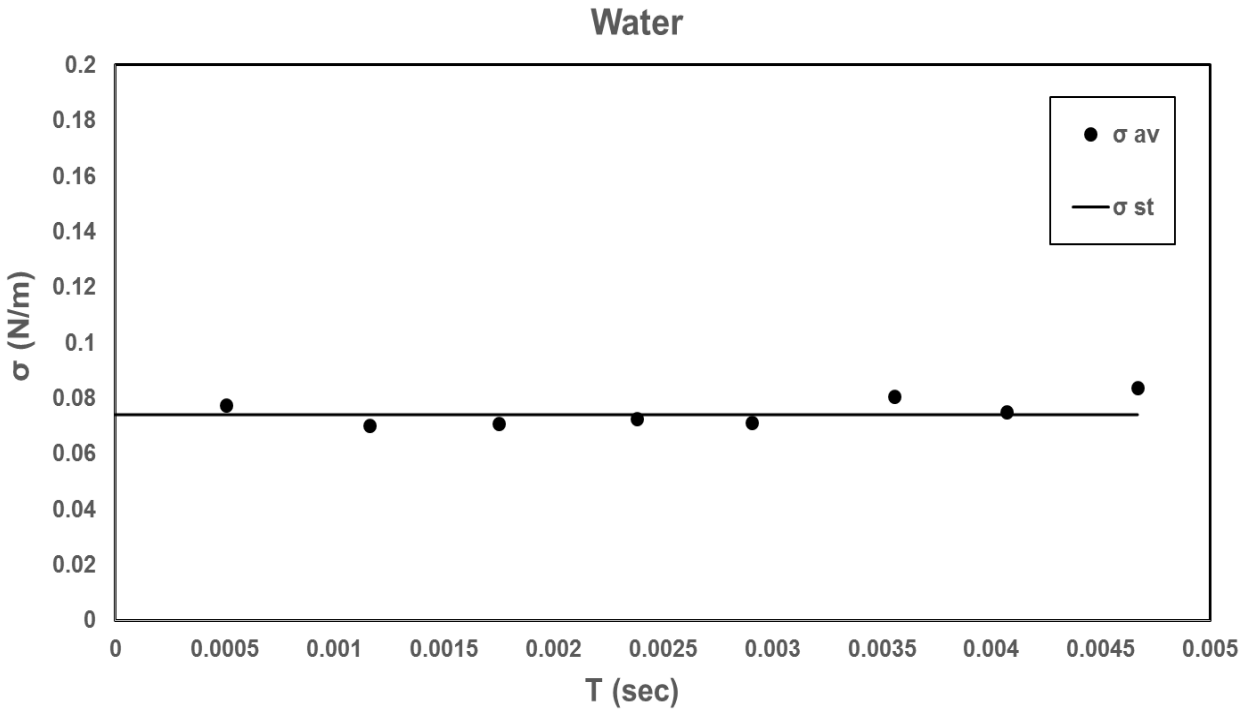

Figure 4-25: Static and average dynamic surface tension σ_{st} and $\sigma_{av}(T)$ for water.

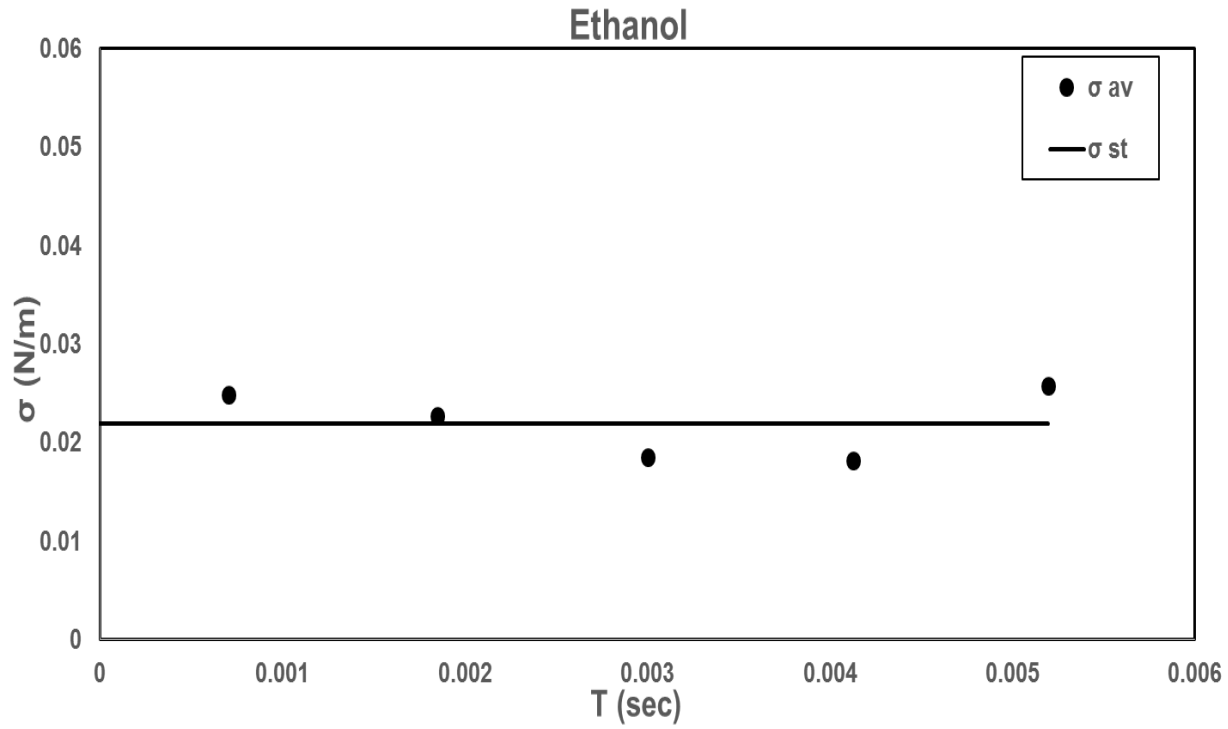

Figure 4-26: Static and average dynamic surface tension σ_{st} and $\sigma_{av}(T)$ for ethanol.

Secondly, the methodology was applied on liquids with changing surface tensions. Aqueous solutions of a surfactant, Triton X-100, at concentrations of 0.015, 0.1, and 0.5% by weight were tested. The critical micelle concentration, CMC (explained in Chapter 3), for TX-100 is 0.02 %; the first concentration is below the CMC while the other two concentrations are above the CMC. Therefore, the static surface tensions of the two solutions above the CMC are nearly the same as appears in table (4-1). Due to the surfactant effect, it can be shown that there is a decay in surface tension values with surface age through figures (4-27) to (4-29). In figure (4-27), for surfactant concentration 0.015%, the surface tension decays to a value almost equals to the static (equilibrium) surface tension in nearly 3-4 ms. In figure (4-28), for surfactant concentration 0.1%, the decay of surface tension to the static value occurs in nearly 2-3 ms. By increasing the concentration of the surfactant to 0.5%, the decay of surface tension to the static value occurs in

about 2 ms as shown in figure (4-29). It can be summarized that the surface tension decaying occurs more rapidly, until reaching the static (equilibrium) value, with increasing the surfactant concentration. The results of the experiments of concentration 0.1% and 0.5% of Triton X-100 are in a good agreement with the results of Bechtel et al. for the same cases [83].

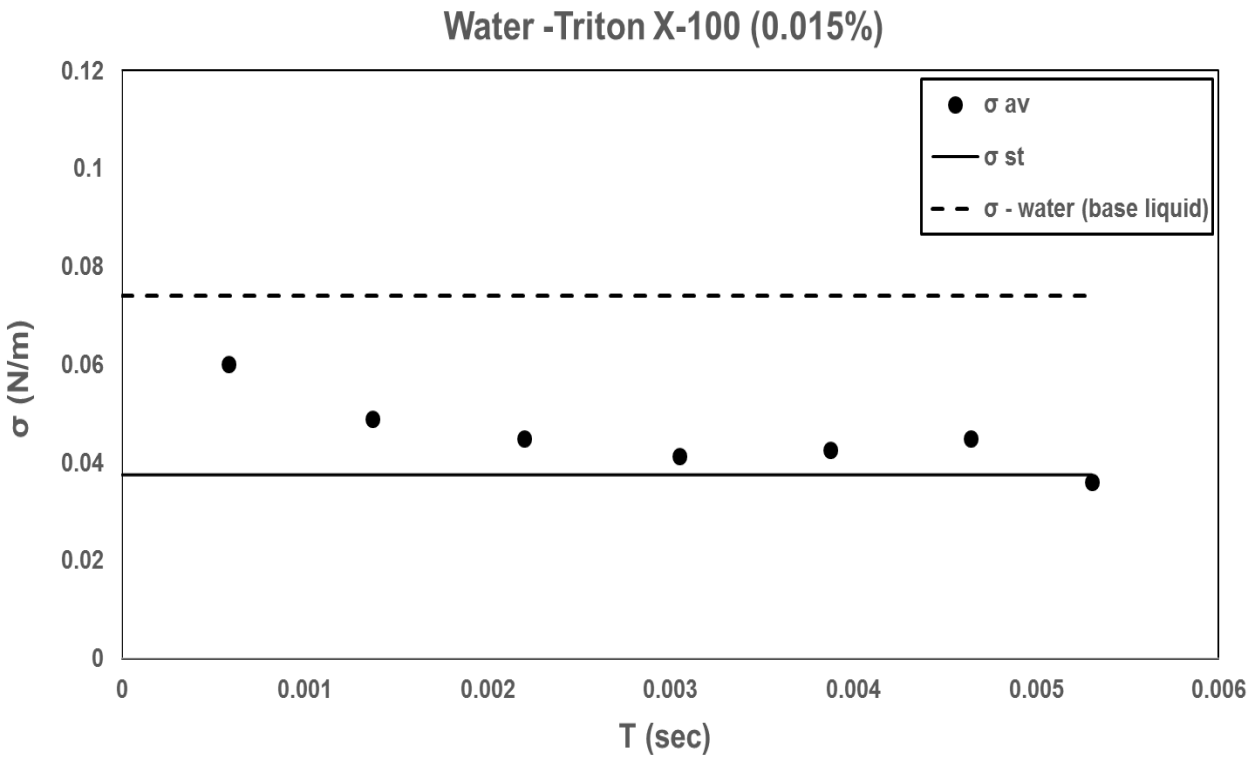

Figure 4-27: Static and average dynamic surface tension σ_{st} and $\sigma_{av}(T)$ for water-0.015% TX-100.

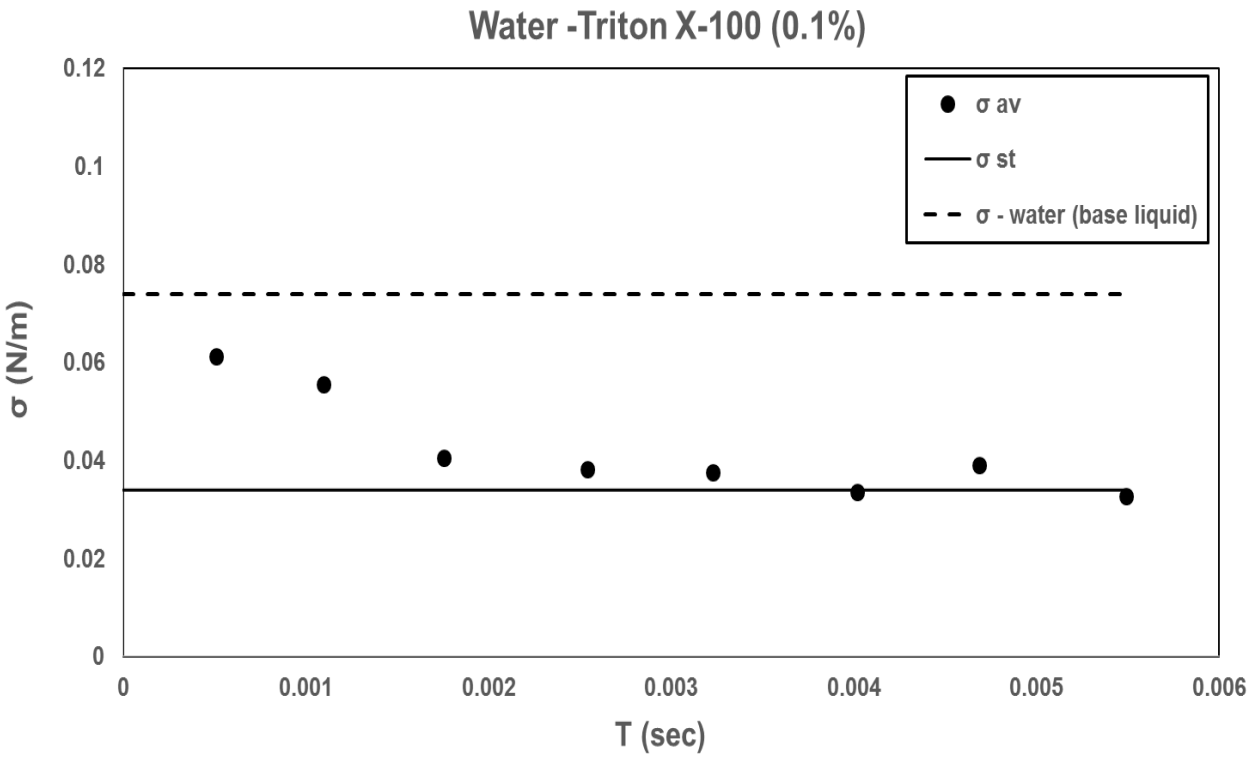

Figure 4-28: Static and average dynamic surface tension σ_{st} and $\sigma_{av}(T)$ for water-0.1% TX-100.

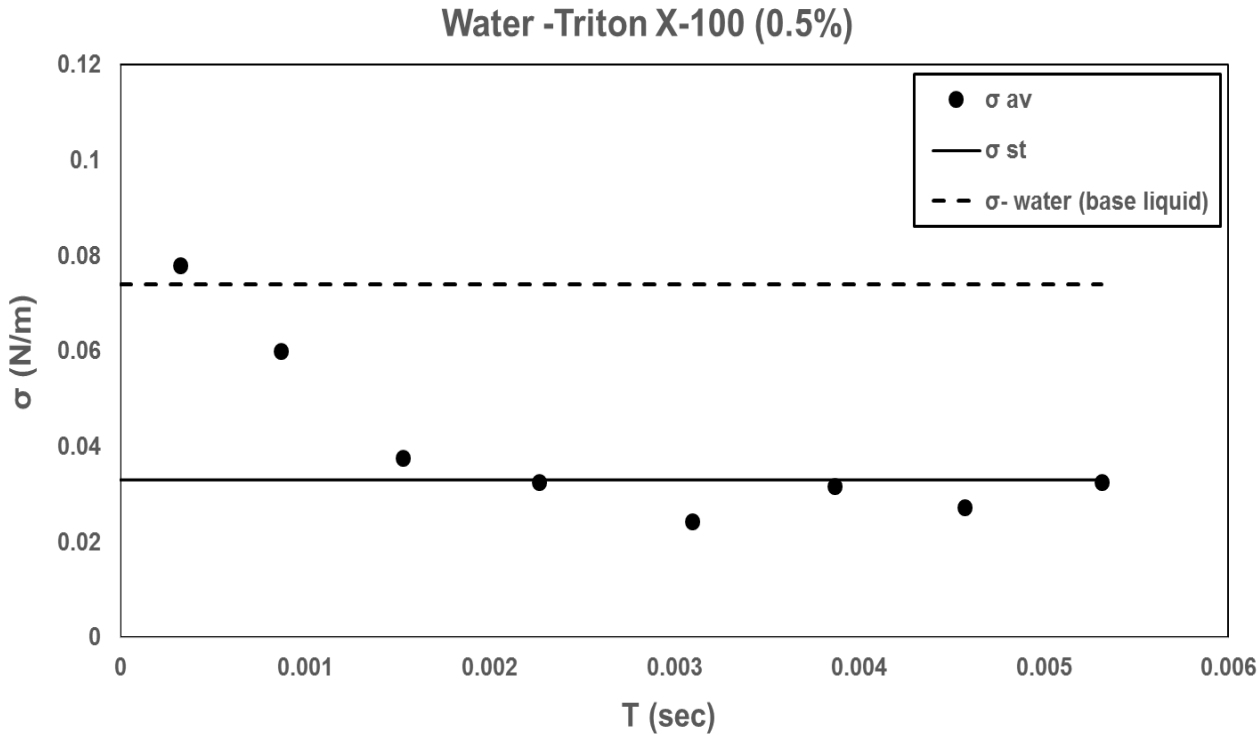

Figure 4-29: Static and average dynamic surface tension σ_{st} and $\sigma_{av}(T)$ for water-0.5% TX-100.

From these results, it can be concluded that the oscillating jet technique combined with Bechtel's analytical model [83]can give reasonable results for dynamic surface tension measurement.

4.4.2 Suspensions Results Analysis

The validated methodology is applied to the same suspension liquids that used in the effervescent atomization tests in chapter (3). For suspended hydrophilic glass particles at concentrations of 1.5% and 5 % in distilled water at figures (4-30) and (4-31), the measured static surface tensions are 0.076 and 0.071 N/m respectively. These results show slight increase or decrease than the measured static surface tension of pure water (0.074 N/m). These results may be attributed to the tendency of the hydrophilic glass particles to not attach to the air-water interface. These results are in a good agreement with other works in the literature [17, 96].

By increasing glass particles concentration to 10% as shown in figure (4-32), the static surface tension decreased to 0.066 N/m. This trend agrees with the results obtained by other researchers who considered that increasing concentration may lead to more particles to accumulate on the interface after enough time [97]. They attributed the decrease in surface tension to the Brownian motion of the particles which has an influence in redistribution of the particles to the lowest total free energy at the surface [97]. The Brownian motion of the particles can lead to its interaction with the liquid molecules resulting in reducing the cohesion energy at the interface [21].

Regarding dynamic surface tension for all glass particles concentrations, the behavior of dynamic surface tension is not obvious enough to be analyzed at this range of millisecond time

scale. Its general behavior tends to be close to the surface tension of the distilled water (base fluid). This behavior can be attributed to the fact that the glass particles are hydrophilic. As a consequence, the particles migration from the liquid bulk to the surface is slow to diffuse. More time than the studied time scale range is needed to settle and adsorb at the new created interface to reach the equilibrium value of surface tension. This behavior agrees with the results obtained by other researchers [17].

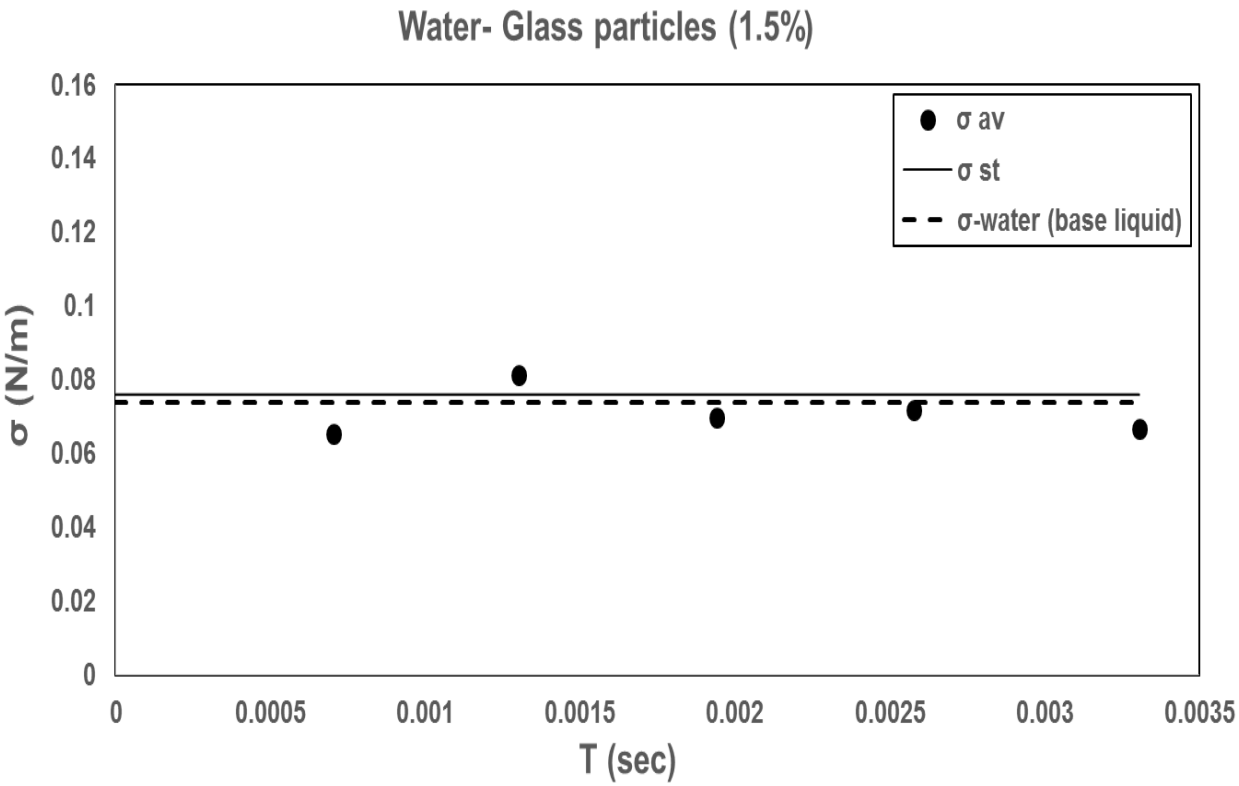

Figure 4-30: Static and average dynamic surface tension σ_{st} and $\sigma_{av(T)}$ for water-1.5% glass particles.

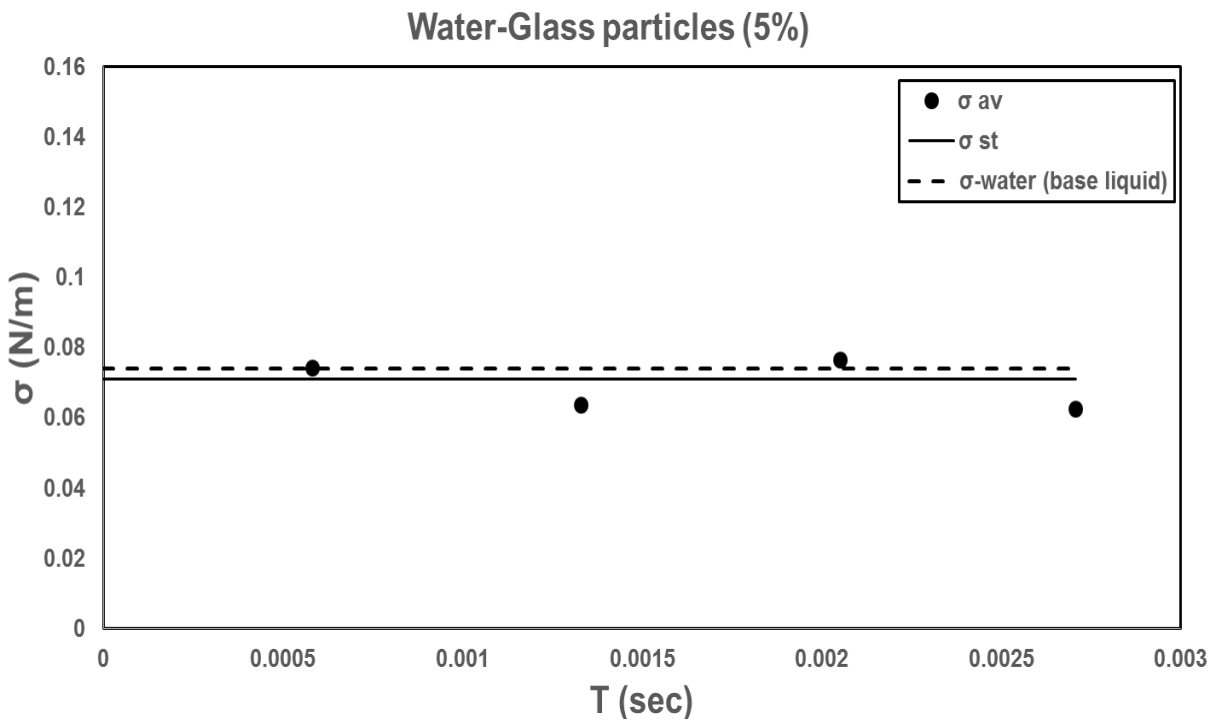

Figure 4-31: Static and average dynamic surface tension σ_{st} and $\sigma_{av}(T)$ for water-5% glass particles.

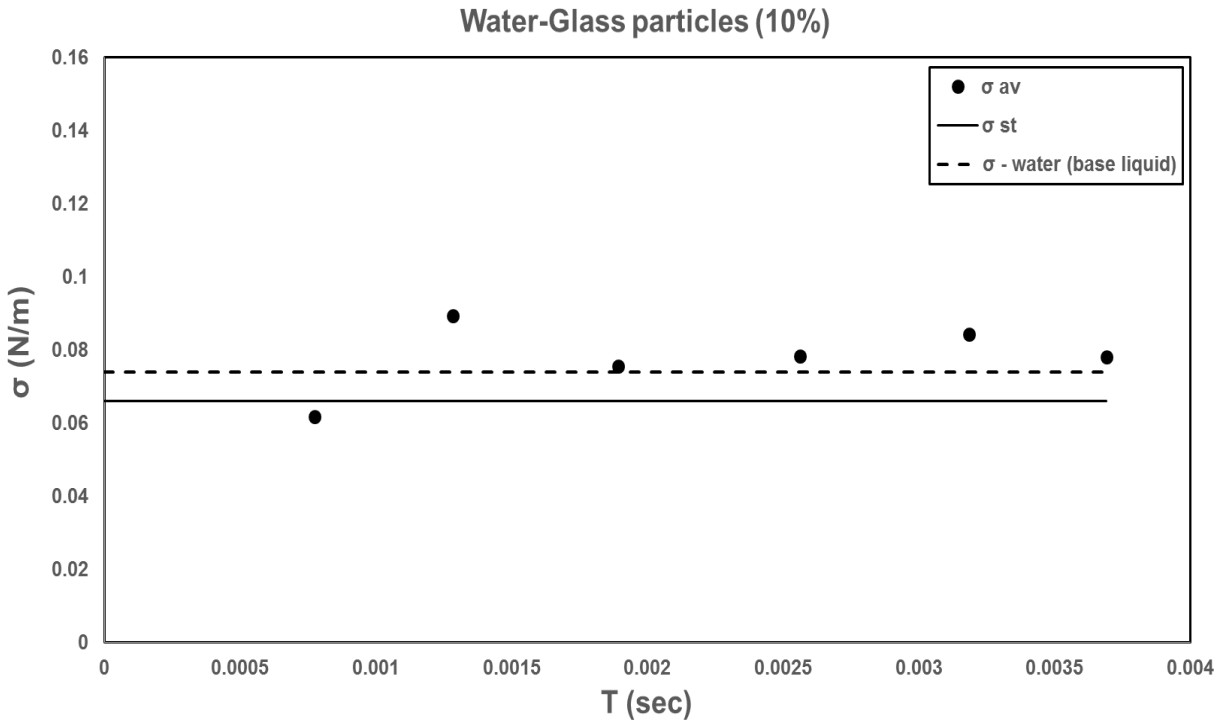

Figure 4-32: Static and average dynamic surface tension σ_{st} and $\sigma_{av}(T)$ for water-10% glass particles.

In case of suspended hydrophobic titania particles at a concentration of 1.5% without a surfactant added, the static surface tension is 0.073 N/m as illustrated in figure (4-33). This value is almost equal to the surface tension of the distilled water (base liquid). This can be interpreted as the number of particles attached to the surface at low concentrations is very small and not enough to significantly change the surface tension of the base fluid. This means that the effect of suspended particles on equilibrium surface tension can be neglected at low concentrations, even if these particles are hydrophobic. However, by increasing the concentration to 5% as in figure (4-34), the equilibrium surface tension reduces to 0.064 N/m. This reduction is attributed to increasing the number of particles adsorbed at the interface by increasing concentration. Similar results were reported in the work of Okubo [96]. It is noted that the equilibrium surface tension is decreasing in the case of hydrophobic particles more than hydrophilic particles for the same concentration due to the low surface activity of the hydrophilic ones.

The dynamic surface tension of the hydrophobic titania particles at both concentrations has the same behavior as that of the hydrophilic glass particles. In both cases, it tends to be close to the surface tension of the distilled water (base fluid). It can be concluded that the migration of hydrophobic titania particles to the surface is slow in the studied time scale of milliseconds.

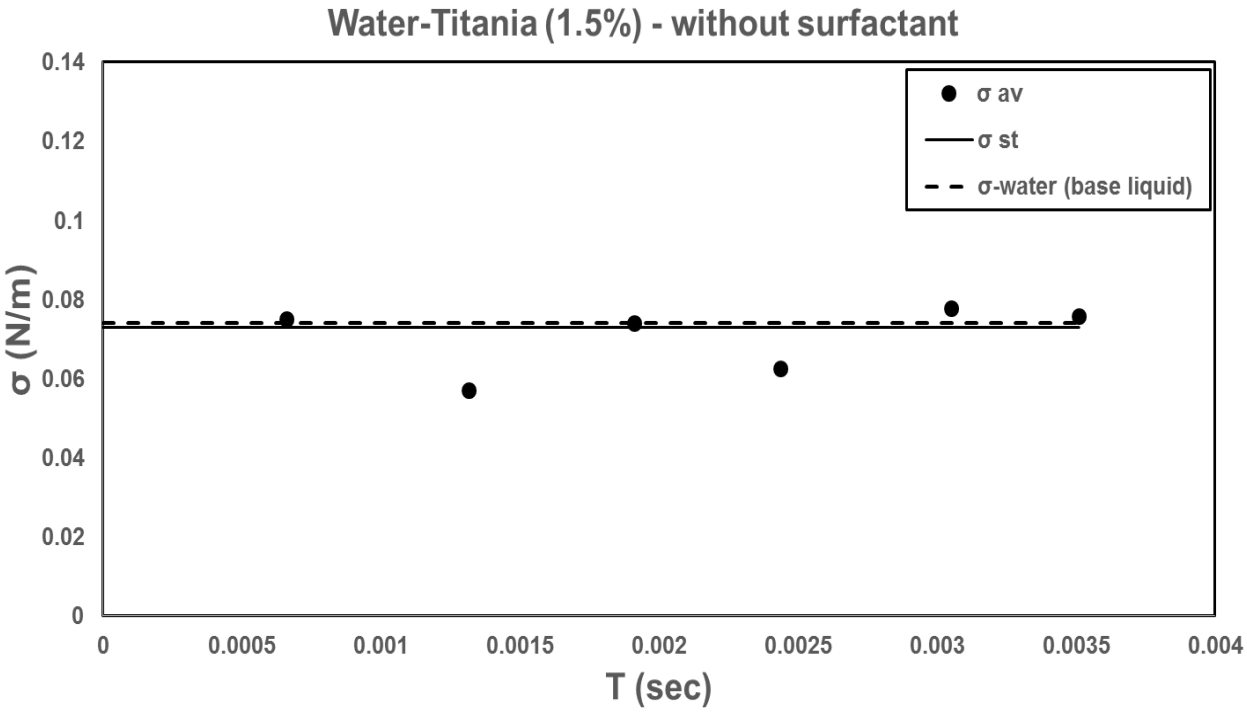

Figure 4-33: Static and average dynamic surface tension σ_{st} and $\sigma_{av}(T)$ for water-1.5% titania particles without a surfactant.

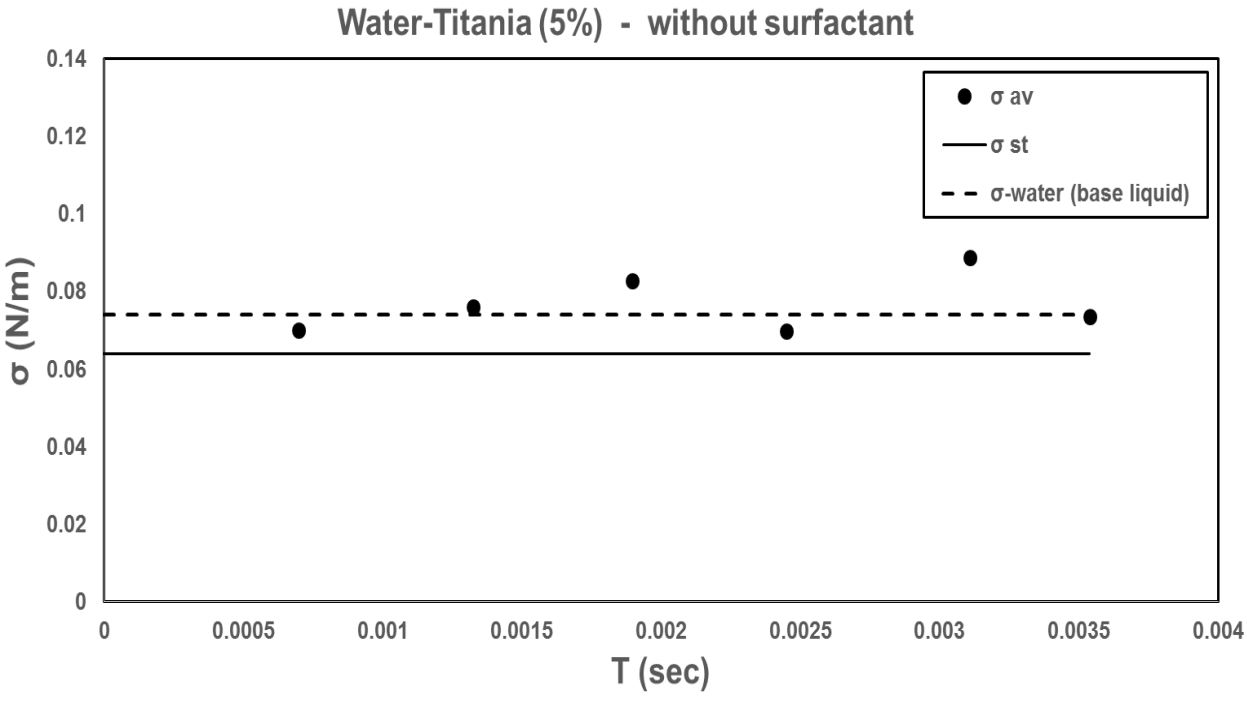

Figure 4-34: Static and average dynamic surface tension σ_{st} and $\sigma_{av}(T)$ for water-5% titania particles without a surfactant.

Figures (4-35) and (4-36) show the results of the same experiments of hydrophobic titania particles at the same concentrations, but in case of an added surfactant. The surfactant used is Triton X-100 at a concentration of 0.5% which is above the CMC. In both concentrations of 1.5% and 5%, for suspended titania particles, the static surface tension is obviously reduced than that of the base liquid. It decreased from 0.074 N/m to 0.039 and 0.0355 N/m, respectively. Compared to the same cases without a surfactant, it is clear that reduction is due to the effect of the added surfactant. In case of 5% concentration, the surface tension reduction is more than that of 1.5% concentration due to the further effect of increasing particles concentration.

The dynamic surface tension in both cases is less than the equilibrium surface tension of the base liquid but is higher than that of the solution. However, the dynamic surface tension of the suspension liquids has a lower reduction rate in comparison to the dynamic surface tension of the surfactant solutions as shown in figure (4-29). It can be concluded that the migration of the hydrophobic particles with surfactant is slower than that of the surfactant alone. Therefore, hydrophobic titania particles, with or without surfactant, need more time to diffuse and settle at the surface than the investigated time scale and consequently reaching equilibrium value.

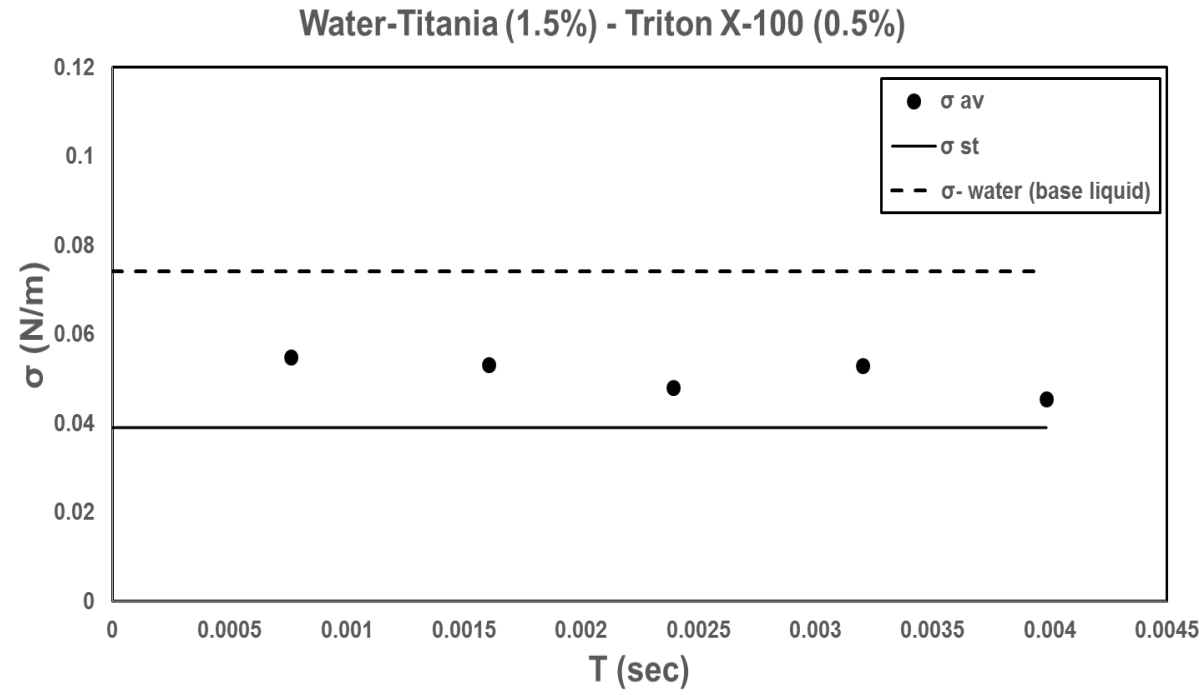

Figure 4-35: Static and average dynamic surface tension σ_{st} and $\sigma_{av}(T)$ for water-1.5% titania particles with a surfactant.

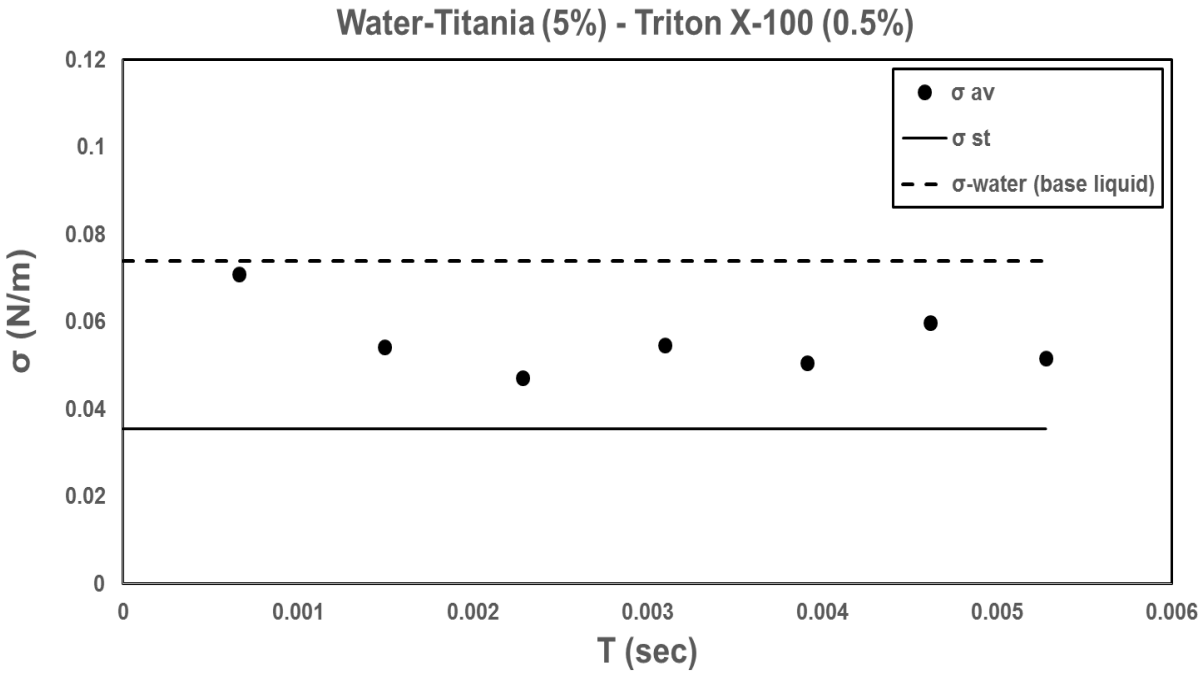

Figure 4-36: Static and average dynamic surface tension σ_{st} and $\sigma_{av}(T)$ for water-5% titania particles with a surfactant.

In summary, the effect of any particle or surfactant molecules on dynamic surface tension in spray conditions will depend strongly on the time scale that needed for molecules or particles to diffuse or migrate from the bulk to the newly created interface. This depends on many factors such as the diffusivity, concentration and type of the particles or surfactant in addition to the size of particles [17]. For analyzing spray droplet formation, which occurs in approximately 0.001 s or less, the dynamic surface tension related to this time should be investigated. From the results, it can be concluded that the effect of the dynamic surface tension of the suspension can be neglected in the time scale of droplet formation for both hydrophilic and hydrophobic particles. Moreover, the surface tension of the base liquid can be used when analyzing the atomization process of suspension liquids and consequently droplet formation.

Chapter 5

Conclusions and Recommendations for Future Work

5.1 Summary and Conclusions

This research can be divided into two main parts that aim to shed light on the suspension atomization process and the suspension properties. In the first part of this study, suspension atomization in a cross flow of air using an effervescent atomizer is investigated experimentally. Two different types of solid particles have been used as suspended particles at different concentrations in distilled water which is the base liquid. The first type is hydrophilic represented by glass particles while the other type is hydrophobic represented by titania particles. The glass particles used are solid soda lime glass microspheres with an average size of 3-6 μm and density equals 2.5 g/cc at concentrations 1.5, 5, and 10% per weight. The titania particles are methicone treated titanium dioxide with an average size of 0.7 μm and density of 3.95 g/cc at concentrations 1.5, 5% per weight. In case of titania particles, the experiments were performed firstly without a

surfactant added to the solution. Then, the experiments were carried out again with addition of a surfactant, Triton X-100, to the mixture.

The experiments were performed inside an open loop subsonic wind tunnel. The tests have been done at different liquid-to-gas momentum flux ratios ranging from 1.73 to11 and gas to liquid ratios ranging from 0 to 7.1%. Flow visualization was carried out on the spray using shadowgraphy. Image processing, such as image averaging, background subtraction and thresholding have been conducted to the images in order to measure the penetration height of the spray. In this study, the penetration height is represented by the windward trajectory of the spray in the crossflow.

From the flow visualization of the non-aerated liquid jets, the breakup regimes are found to change with changing Weber number of the gas cross flow (We_g) which is influenced by liquid surface tension. The solution surface tension can be changed significantly by adding a surfactant. On the other hand, the suspended particles, in range of the present test conditions, did not change the solution surface tension significantly to affect the jet breakup regimes in a cross flow. In addition, the penetration height of non-aerated liquid jets is relatively small. Once, the liquid jet has been aerated, at the same operating conditions, the spray penetration height is visualized to dramatically increase. Furthermore, spray penetration height is increasing by increasing the amount of injected air and consequently GLR. This trend is attributed to the increase of the effective jet to air momentum flux ratio of the aerated liquid jet resulted from increasing liquid film velocity associated to increasing GLR. As a consequence, the spray penetration is deeper into the air cross flow. At low GLR values, the suspension liquid delayed the onset of breakup due to its higher viscosity with respect to the pure water (base liquid). With increasing GLR, the structure of the flow inside the effervescent atomizer changes to the annular flow. Once discharged into the

air cross flow, this high speed annular flow is broken quickly. Therefore, the generated droplets are smaller and the spray is denser compared to that of lower GLRs. It can be concluded that the liquid breakup process in the aerated jets is faster than that of the non-aerated liquid at the same flow conditions.

Generally, the spray penetration height in the case of non-aerated liquid jet is very small compared to the aerated jets with the same liquid flow rate. Based on the experimental results of shadowgraphy, new correlations have been proposed to predict the spray penetration height of suspensions liquids in case of non-aerated liquid jet and for the aerated liquid jet. For non-aerated liquid jets (GLR= 0), the correlation is expressed in terms of liquid-to-gas momentum flux ratio (q), downstream distance (x/d) in addition to the suspended particles concentration (C). For aerated liquid jets (GLR≠0), the correlation is a function of liquid-to-gas momentum flux ratio (q), downstream distance (x/d) and the gas to liquid mass ratio (GLR) in addition to the viscosity ratio (μ_l/μ_w).

In conclusion, a higher penetration height and smaller droplets can be produced by aerating the liquid jet via the effervescent atomizer. Similar behaviors for atomization of pure liquid (water) and suspension liquids are observed. Moreover, the clogging problem is overtaken in spite of the presence of the suspended solid particles. For all of these results, the effervescent atomizer shows a high performance for atomization of a variety of liquids regardless of their rheological properties.

Furthermore, analyzing the properties of suspensions can be a critical factor for understanding suspensions and consequently controlling and predicting the quality of coating. Because the atomization process and droplet formation takes place in a very short timescale, it is necessary to analyze the rapid change of the affecting suspension properties related to this timescale especially surface tension. Therefore, to analyze the spraying process, it is necessary to

analyze the dynamic surface tension than static surface tension. In the second part of this study, the dynamic surface tension of suspension liquid has been investigated experimentally. The elliptical oscillating jet technique combined with a mathematical model has been utilized in measuring the surface tension in the timescale of milliseconds. Shadowgraphy has been used to capture the oscillating jet. Then, image processing is applied to get the jet free surface profiles by a generated code of MATLAB software.

To validate the results of suspension liquids measurements, the methodology is applied first to two sets of liquids. The first set include the liquids with constant surface tension as distilled water and ethanol. As expected, the results showed that the dynamic surface tensions of both are constant and almost equals the static (equilibrium) value. In the second set, liquids with changing surface tensions were tested. Aqueous solutions of a surfactant, Triton X-100, at three concentrations of 0.015, 0.1, and 0.5% by weight were used. The results show that the dynamic surface tension decays faster to the static (equilibrium) value, with increasing the surfactant concentration. These results agree well with the results available in the literature for the same cases.

After validating the results, the methodology is applied to the same suspension liquids used in the effervescent atomization experiment. For hydrophilic glass particles, the dynamic surface tension has shown a more or less constant behavior which is close to the static surface tension of the base liquid (distilled water). This trend is due to the hydrophilicity of the glass particles that lead to slow migration of the particles from the bulk to the surface and consequently affecting surface tension. In spite being hydrophobic, titania particles have shown the same behavior as the hydrophilic glass particles. By adding a surfactant to the titania particles solution, the resultant dynamic surface tension showed a lower reduction rate than that of the surfactant alone. This

demonstrates that even the hydrophobic particles, with or without a surfactant, need more time than the investigated time scale to diffuse and settle at the surface and hence influencing surface tension.

Generally, the effect of any particle on dynamic surface tension in spray conditions depend on the time needed for particles to diffuse or migrate from the bulk to the newly created interface. This is influenced by many factors as the diffusivity, concentration, and particles type and size as well as adding surfactant or not. For investigating droplet formation in the atomization process, which occurs in approximately 0.001 s or less, the dynamic surface tension related to this time should be investigated. From the results, it can be concluded that the dynamic surface tension of the suspension has a negligible effect within the time scale of droplet formation for both hydrophilic and hydrophobic particles. Therefore, the surface tension of the base liquid can be considered when analyzing the atomization process of suspension liquids and consequently droplet formation.

5.2 Recommendations for future work

The present study investigated the effervescent atomization of suspension liquids into a gaseous cross flow. In addition, the effect of the dynamic surface tension of suspension liquid on the droplet formation has been analyzed. In spite of its importance in many industrial applications, the fundamental processes of suspension liquid breakup within atomization are not well characterized. This is attributed to the considerable number of factors affecting its atomization process. Therefore, more experimental and theoretical studies are needed to better understand the physics govern the suspension liquid disintegration. The following suggestions might be taken into consideration for future work to gain a deeper knowledge.

- Investigating the effervescent atomization of suspensions liquids in a cross flow for the following parameters:

  a- Different types of particles.

  b- Different particle size ranges (nano scale).

  c- Higher particle concentrations (more than 10%).

  d- Different types of added surfactants.

  e- Different types of base liquid such as ethanol.

  f- Different types of the gaseous cross flow such as nitrogen.

  g- Using a cross flow at a higher range of velocities.
- Characterization of the spray structure of the suspension liquid droplets using PDPA.
- Performing the effervescent atomization of suspension liquids in plasma conditions.
- Conducting a numerical study to model the effervescent atomization of suspensions liquid in a cross flow of gas.

REFERENCES

1. Pawlowski, L., The science and engineering of thermal spray coatings. *John Wiley & Sons*, (2008).
2. Davis, J.R., Handbook of thermal spray technology. *ASM international*, (2004).
3. Pawlowski, L., Suspension and solution thermal spray coatings. *Surface and Coatings Technology*, **203**(19): p. 2807-2829 (2009).
4. Toma, F.-L., Berger, L.M., Jacquet, D., Wicky, D., Villaluenga, I., de Miguel, Y.R., Lindeløv, J.S., Comparative study on the photocatalytic behaviour of titanium oxide thermal sprayed coatings from powders and suspensions. *Surface and Coatings Technology*, **203**(15): p. 2150-2156 (2009).
5. Jabbari, F., Jadidi, M., Wuthrich, R., Dolatabadi, A., A Numerical Study of Suspension Injection in Plasma-Spraying Process. *Journal of Thermal Spray Technology*, **23**(1-2): p. 3-13 (2014).
6. Farshchi Tabrizi, H., Experimental characterization of effervescent atomization. Concordia University, (2013).
7. Fauchais, P., Etchart-Salas, R., Delbos, C., Tognonvi, M., Rat, V., Coudert, J.-F., Chartier,T., Suspension and solution plasma spraying of finely structured layers: potential application to SOFCs. *Journal of Physics D: Applied Physics*, **40**(8): p. 2394 (2007).
8. Jadidi, M., Moghtadernejad, S., Dolatabadi, A., A Comprehensive Review on Fluid Dynamics and Transport of Suspension/Liquid Droplets and Particles in High-Velocity Oxygen-Fuel (HVOF) Thermal Spray. *Coatings*, **5**(4): p. 576-645 (2015).

9. Esfarjani, S.A., Dolatabadi, A., A 3D simulation of two-phase flow in an effervescent atomizer for suspension plasma spray. *Surface and Coatings Technology*. **203**(15): p. 2074-2080 (2009).

10. Fritsching, U., Mulhem, B., Kurt, O., Schulte, G., Influence of suspended solid particles on suspension atomization processes. in *Twenty first International Conference on Liquid Atomization and Spray Systems*, (2009).

11. Crowe, C.T., Multiphase flow handbook. *CRC Press,* (2005).

12. Amini, G., Instability of Elliptic Liquid Jets. *Concordia University*, (2011).

13. Lefebvre, A., Atomization and sprays. *CRC press,*(1988).

14. Ashgriz, N., Handbook of Atomization and Sprays. *Springer,* (2010).

15. Jobehdar, M.H., Experimental Study of Two-Phase Flow in a Liquid Cross-Flow and an Effervescent Atomizer. *The University of Western Ontario*, (2014).

16. Forest, M., Youssef, N., Zhou, H., The effect of dynamic surface tension on the oscillation of slender elliptical Newtonian jets*, Journal of Applied Mechanics*. 65: p. 1-11 (1998).

17. Gauglitz, P.A., Mahoney, L. A., Blanchard, J., Bamberger, J., Surface Tension Estimates for Droplet Formation in Slurries with Low Concentrations of Hydrophobic Particles*, Polymer Flocculants or Surface-Active Contaminants*: *Pacific Northwest National Laboratory*, (2011).

18. Sirignano, W., Mehring C., Review of theory of distortion and disintegration of liquid streams*. Progress in Energy and Combustion Science*, **26**(4): p. 609-655 (2000).

19. Nguyen, W.H., Measurement of dynamic surface tension on the submillisecond timescale. *The Ohio State University*, (1999).

20. Defay, R., Prigogine I., *Surface tension and adsorption*. *Wiley* (1966).

21. Binks, B.P., Particles as surfactants—similarities and differences. *Current Opinion in Colloid & Interface Science*, **7**(1): p. 21-41 (2002).

22. Alakoc, U., Megaridis, C.M., McNallan, M., Wallace, D.B., Dynamic surface tension measurements with submillisecond resolution using a capillary-jet instability technique. *Journal of colloid and interface science*, **276**(2): p. 379-391 (2004).

23. Kihm, K.D., Deignan, P., Dynamic surface tension of coal-water slurry fuels. *Fuel*. **74**(2): p. 295-300 (1995).

24. Lin, S., Reitz, R., Drop and spray formation from a liquid jet. *Annual Review of Fluid Mechanics*. **30**(1): p. 85-105 (1998).

25. Rayleigh, L., On the capillary phenomena of jets. *Proceedings of the Royal Society of London*. **29**(196-199): p. 71-97 (1879).

26. Reitz, R., Bracco, F., Mechanism of atomization of a liquid jet. *Physics of Fluids*. **25**(10): p. 1730-1742 (1982).

27. Bellofiore, A., Experimental and numerical study of liquid jets injected in high-density air crossflow. *Università degli Studi di Napoli Federico II,* (2007).

28. Wu, P.-K., Kirkendall, K.A., Fuller, R.P.,Nejad, A.S., Breakup processes of liquid jets in subsonic crossflows. *Journal of Propulsion and Power*. **13**(1): p. 64-73 (1997).

29. Becker, J., Hassa, C., Breakup and atomization of a kerosene jet in crossflow at elevated pressure. *Atomization and Sprays*. **12**(1-3) (2002).

30. Sallam, K., Aalburg, C., Faeth G., Breakup of round nonturbulent liquid jets in gaseous crossflow. *AIAA journal*. **42**(12): p. 2529-2540 (2004).

31. Farvardin, E., Biodiesel Spray Characterization*:* A Combined Numerical and Experimental Analysis. *Concordia University*, (2013).

32. Chelko, L.J., Penetration of liquid jets into a high-velocity air stream. *National Advisory Committee for Aeronautics*, (1950).

33. Chen, T., Smith, C., Schommer, D.Nejad, A.S., Multi-zone behavior of transverse liquid jet in high-speed flow. *AIAA paper*. **453**: p. 1993 (1993).

34. Ingebo, R.D., Penetration of drops into high-velocity airstreams. (1964).

35. Stenzler, J.N., Lee, J.G., Santavicca, D.A., Lee, W., Penetration of liquid jets in a cross-flow. *Atomization and Sprays*. **16**(8) (2006).

36. Tambe, S.B., Jeng, S.-M., Mongia, H., Hsiao, G., Liquid jets in subsonic crossflow. in *43rd AIAA Aerospace Sciences Meeting and Exhibit*. (2005).

37. Wu, P.-K., Kirkendall, K.A., Fuller, R.P.,Nejad, A.S., Spray structures of liquid jets atomized in subsonic crossflows. *Journal of Propulsion and Power*. **14**(2): p. 173-182 (1998).

38. Schetz, J.A., Padhye, A., Penetration and breakup of liquids in subsonic airstreams. *AIAA Journal*. **15**(10): p. 1385-1390 (1977).

39. No, S.-Y., A review on empirical correlations for jet/spray trajectory of liquid jet in uniform cross flow. *International Journal of Spray and Combustion Dynamics*. **7**(4): p. 283-314 (2015).

40. Birouk, M., Wang, M., Broumand, M., Liquid Jet Trajectory in a Subsonic Gaseous Cross-flow: An Analysis of Published Correlations. *Atomization and Sprays*. 26(11): (2016).

41. Ashgriz, N., Atomization of a liquid jet in a crossflow. *in the 4th international meeting of advances in thermofluids (IMAT 2011)*. AIP Publishing (2012).

42. Mashayek, A., Jafari, A., Ashgriz, N., Improved model for the penetration of liquid jets in subsonic crossflows. *AIAA journal*. **46**(11): p. 2674-2686 (2008).

43. Eslamian, M., Amighi, A., Ashgriz, N., Atomization of liquid jet in high-pressure and high-temperature subsonic crossflow. *AIAA Journal*. **52**(7): p. 1374-1385 (2014).

44. ELShamy, O.M., Experimental investigations of steady and dynamic behavior of transverse liquid jets. *University of Cincinnati*, (2007).

45. Ingebo, R.D., Aerodynamic effect of combustor inlet air pressure on fuel jet atomization. *Journal of Propulsion and Power*. **1**(2): p. 137-142 (1985).

46. Nejad, A., Schetz, J., Effects of properties and location in the plume on droplet diameter for injection in a supersonic stream. *AIAA Journal*. **21**(7): p. 956-961 (1983).

47. Hautman, D.J., Rosfjord, T.J., Transverse liquid injection studies. in *AIAA, SAE, ASME, and ASEE, 26th Joint Propulsion Conference*. (1990).

48. Inamura, T., Nagai, N., Spray characteristics of liquid jet traversing subsonic airstreams. *Journal of Propulsion and Power*. **13**(2): p. 250-256 (1997).

49. Birouk, M., Azzopardi, B.J., Stäbler, T., Primary Break-up of a Viscous Liquid Jet in a Cross Airflow. *Particle & Particle Systems Characterization*. **20**(4): p. 283-289 (2003).

50. Nejad, A., Schetz, J., Effects of viscosity and surface tension on a jet plume in supersonic crossflow. *AIAA journal*. **22**(4): p. 458-459 (1984).

51. Lefebvre, A., Wang, X., Martin, C., *Spray characteristics of aerated-liquid pressure atomizers.* Journal of Propulsion and Power, 1988. **4**(4): p. 293-298.

52. Sovani, S., Sojka, P., Lefebvre, A., *Effervescent atomization.* Progress in Energy and Combustion Science, 2001. **27**(4): p. 483-521.

53. Qian, L., Lin, J., Modeling on effervescent atomization: A review. *Science China Physics, Mechanics and Astronomy*. **54**(12): p. 2109-2129 (2011).

54. Wang, X., Chin, J., Lefebvre, A., Influence of gas-injector geometry on atomization performance of aerated-liquid nozzles. *International Journal of Turbo and Jet Engines*. **6**(3-4): p. 271-280 (1989).

55. Roesler, T., Lefebvre, A., Studies on aerated-liquid atomization. *International Journal of Turbo and Jet Engines*. **6**(3-4): p. 221-230 (1989).

56. Lefebvre, A., A novel method of atomization with potential gas turbine applications. *Defence Science Journal*. **38**(4): p. 353-362 (2014).

57. Chin, J., Lefebvre, A., A design procedure for effervescent atomizers. in *ASME 1993 International Gas Turbine and Aeroengine Congress and Exposition*. *American Society of Mechanical Engineers,* (1993).

58. Mostafa, A., Fouad, M., Enayet, M., Osman, S., Measurements of spray characteristics produced by effervescent atomizers. *in 40 th AIAA/ASME/SAE/ASEE Joint Propulsion Conference and Exhibit*, (2004).

59. Jedelsky, J., Landsmann, M., Jicha, M., Kuritka, I., Effervescent Atomizer: Influence of the Operation Conditions and Internal Geometry on Spray Structure. *Study Using PIV-PLIF. Proc. ILASS*, (2008).

60. Ghaffar, Z.A., Hamid, A.H., Rashid, M.S., A review on spray characteristics of effervescent atomizer under various geometrical parameters and operating condition. *in The 4th international meeting of advances in thermofluids (IMAT 2011)*. AIP Publishing. (2012).

61. Huang, X., Wang, X., Liao, G., Visualization of two phase flow inside an effervescent atomizer. *Journal of Visualization*. **11**(4): p. 299-308 (2008).

62. Lund, M., Sojka, P. E., Lefebvre, A.,Gosselin, P.G., Effervescent atomization at low mass flow rates. Part I: The influence of surface tension. *Atomization and Sprays.* **3**(1) (1993).

63. Qian, L., Lin, J.,Xiong, H., Chan, T. L., Theoretical investigation of the influence of liquid physical properties on effervescent atomization performance. *Journal of Fluids Engineering*. **133**(10) (2011).

64. Lin, K., Kennedy, P., Jackson, T., Spray structures of aerated-liquid jets in subsonic crossflows. *AIAA paper*, **330**: p. 2001 (2001).

65. Miller, B., Sallam, K., Bingabr, M. G., Lin, K.-C., Carter, C., Breakup of aerated liquid jets in subsonic crossflow. *Journal of Propulsion and Power*. **24**(2): p. 253-258 (2008).

66. Ghenai, C., Sapmaz, H., Lin., C., Characterization of aerated liquid jet in subsonic and supersonic crossflow. *in 41 st AIAA/ASME/SAE/ASEE Joint Propulsion Conference & Exhibit*, (2005).

67. Lin, K.-C., Kennedy, P., Jackson, T., Structures of aerated liquid jets in high speed crossflows. *AIAA paper*. **3178**: p. 2002 (2002).

68. Mulhem, B., Schulte, G., Fritsching, U., Solid–liquid separation in suspension atomization. *Chemical engineering science*. **61**(8): p. 2582-2589 (2006).

69. Ghadimi, A., Saidur, R., Metselaar, H., A review of nanofluid stability properties and characterization in stationary conditions. *International Journal of Heat and Mass Transfer*. **54**(17): p. 4051-4068 (2011).

70. Pabst, W., Fundamental considerations on suspension rheology. *Ceramics Silikaty*. **48**(1): p. 6-13 (2004).

71. Tanvir, S., Qiao, L., Surface tension of Nanofluid-type fuels containing suspended nanomaterials. *Nanoscale research letters*. **7**(1): p. 1-10 (2012).

72. Brian, B., Chen, J., Surface tension of solid-liquid slurries. *AIChE journal*. **33**(2): p. 316-318 (1987).

73. Yuan, K., Chen, L., Wu, C., Study on characteristics of different types of nozzles for coal-water slurry atomization. *Journal of Thermal Science*, **10**(4): p. 331-335 (2001).

74. Son, S., Kihm, K.D., Effect of coal particle size on coal-water slurry (CWS) atomization. *Atomization and Sprays*. **8**(5) (1998).

75. Dombrowski, N., Fraser, R., A photographic investigation into the disintegration of liquid sheets. *Philosophical Transactions of the Royal Society of London. Series A, Mathematical and Physical Sciences*. p. 101-130 (1954).

76. Jedelsky, J., Otahal, J., Jicha, M., Effervescent Atomizer for Atomization of Suspensions Containing Large Particles. *Proc. ILASS*, (2008).

77. Mostafa, A., Khail, A., Measurements of coal water slurry sprays produced by an effervescent atomizer. *in 42nd A IAA/ASME/SAE/ASEE Joint Propulsion Conference & Exhibit*. Sacramento (2006).

78. Mulhem, B., Schulte, G., Effect of solid particle characteristics on suspension atomization. *Atomization and Sprays*. **13**(2) (2003).

79. Ochowiak, M., Broniarz-Press, L., Woziwodzki, S., The analysis of silica suspensions atomization. *International Journal of Heat and Fluid Flow*. **32**(6): p. 1208-1215 (2011).

80. Tropea, C., Yarin, A.L., Foss, J.F., Springer handbook of experimental fluid mechanics. *Springer Science & Business Media*, (2007).

81. Eastoe, J., Dalton, J., Dynamic surface tension and adsorption mechanisms of surfactants at the air–water interface. *Advances in colloid and interface science*, **85**(2): p. 103-144 (2000).

82. Bechtel, S.,Cooper, J, Forest, M.G., Petersson, N.A., Reichard, D.L., Saleh, A., Venkataramanan, V., A new model to determine dynamic surface tension and elongational viscosity using oscillating jet measurements. *Journal of Fluid Mechanics*, **293**: p. 379-403 (1995).

83. Bechtel, S., Koelling, K., Nguyen, W., Tan, G., A new technique for the measurement of the dynamic evolution of surface tension. *Journal of colloid and interface science*. **245**(1): p. 142-162 (2002).

84. Franses, E.I., Basaran, O.A., Chang, C.-H., Techniques to measure dynamic surface tension. *Current Opinion in Colloid & Interface Science*. **1**(2): p. 296-303 (1996).

85. Zhang, X., Harris, M.T., Basaran, O.A., Measurement of dynamic surface tension by a growing drop technique. *Journal of colloid and interface science*. **168**(1): p. 47-60 (1994).

86. Taylor, G., Formation of thin flat sheets of water. *Proceedings of the Royal Society of London. Series A. Mathematical and Physical Sciences*, **259**(1296): p. 1-17 (1960).

87. Amini, G., Dolatabadi, A., Capillary instability of elliptic liquid jets. *Physics of Fluids* . **23**(8) (2011).

88. Rayleigh, L. On the tension of recently formed surfaces. *in Proc R Soc*. (1890).

89. Kasyap, T., Sivakumar, D., Raghunandan, B., Flow and breakup characteristics of elliptical liquid jets. *International journal of multiphase flow*. **35**(1): p. 8-19 (2009).

90. Bohr, N., On the determination of the tension of a recently formed water-surface. *Proceedings of the Royal Society of London. Series A, Containing Papers of a Mathematical and Physical Character*. **84**(572): p. 395-403 (1910).

91. Defay, R., Hommelen, J.R., Measurement of dynamic surface tensions of aqueous solutions by the oscillating jet method. *Journal of Colloid Science*. **13**(6): p. 553-564 (1958).

92. Kochurova, N., Rusanov, A., Dynamic surface properties of water: Surface tension and surface potential. *Journal of Colloid and Interface Science*. **81**(2): p. 297-303 (1981).

93. Bechtel, S., Forest, M.G., Holm, D.D., Lin, K.J., One-dimensional closure models for three-dimensional incompressible viscoelastic free jets: von Kármán flow geometry and elliptical cross-section. *Journal of Fluid Mechanics*. **196**: p. 241-262 (1988).

94. Zakaria, R., Jet fuel spray characterisation using optical methods: an experimental study of high speed fuel injection systems in small rotary engines. *University of Warwick,* (2011).

95. Amini, G., Dolatabadi, A., Axis-switching and breakup of low-speed elliptic liquid jets. *International Journal of Multiphase Flow*. **42**: p. 96-103 (2012).

96. Okubo, T., Surface tension of structured colloidal suspensions of polystyrene and silica spheres at the air-water interface. *Journal of Colloid and Interface Science*. **171**(1): p. 55-62 (1995).

97. Vafaei, S., Purkayastha, A., Jain, A., Ramanath, G.,Borca-Tasciuc, T., The effect of nanoparticles on the liquid–gas surface tension of Bi2Te3 nanofluids. *Nanotechnology*, **20**(18) (2009).